ABSTRACT

SCHIMIZZI, RYAN DONALD. Performance and Reliability Modeling of AlGaN/GaN Hetero-junction Field Effect Transistors. (Under the direction of Dr. Robert J. Trew and Dr. Griff L. Bilbro).

Two independent problem areas in AlGaN/GaN HFETs that affect device performance and reliability are investigated. The first is an investigation into the nonlinear resistance phenomenon present in these devices under high current RF operation. High-voltage microwave AlGaN/GaN HFETs operating under high-power conditions suffer from degraded RF performance and linearity due to a nonlinear resistance effect in the gate-source region. During RF operation, the nonlinear resistance is due to the onset a of space-charge-limited current (SCLC) transport mechanism within the device channel. Under high current injection conditions, SCLC transport can set in and, consequently, the source resistance becomes a function of the injected charge resulting in a rapid increase and limiting device performance. The threshold for SCL current is dependent on the donor-like states on the AlGaN surface which are responsible for supplying electrons to the channel. To understand the effect of nonlinear source resistance we show on an un-gated HFET channel model that the critical current density of space-charge effects and thus the onset of nonlinear source resistance can be reduced or can be shifted above the normal operating current density of the device by modification of the charge on the AlGaN surface.

Secondly, nonlinearities stemming from avalanche breakdown due to high electric field magnitudes in the device channel while operating under high voltage conditions is investigated. A temperature dependent, impact ionization initiated RF breakdown model in the 2DEG channel of AlGaN/GaN HFETs is reported. When operating these devices in RF power amplifier circuits, impact ionization in the channel has a significant effect upon gain saturation, power-added efficiency and output power. An analytical physics-based model of channel breakdown is formulated based on TCAD investigations of the internal device behavior. This model is integrated with an existing physics-based HFET compact model and accurately predicts large-signal device performance. Values of thermal resistance and the breakdown temperature coefficient were extracted from simulations of an industrial HFET and are in agreement with the published measurements as well as an independent model of thermal resistance in AlGaN/GaN HFETs thus validating that the model accurately captures the dominant breakdown mechanism.

Performance and Reliability Modeling of AlGaN/GaN Hetero-junction Field Effect Transistors

by
Ryan D. Schimizzi

A dissertation submitted to the Graduate Faculty of
North Carolina State University
in partial fulfillment of the
requirements for the degree of
Doctor of Philosophy

Electrical Engineering

Raleigh, North Carolina

2012

APPROVED BY:

Dr. Robert J. Trew Committee Chair	Dr. Griff L. Bilbro Committee Co-Chair
Dr. Brian Floyd	Dr. Zhilin Li

DEDICATION

Dedicated to my wife Nikki

BIOGRAPHY

Ryan D. Schimizzi was born in New Kensington, Pennsylvania in May 1978. After graduating high school in 1996 he served a five year enlistment in the United States Marine Corps. In 2003 he enrolled in the North Carolina Community College system 2+2 engineering transfer program. He transferred to North Carolina State University in 2005 to complete his Bachelor of Science in electrical engineering and graduated summa cum laude in August 2007. Starting in 2007 he began working towards a PhD degree in electrical engineering at North Carolina State University in the area of physics-based modeling of AlGaN/GaN HFETs under the supervision of Dr. Robert J. Trew.

ACKNOWLEDGMENTS

I would like to thank my committee chair Dr. Robert Trew for taking me on as a graduate student and supporting and guiding me throughout my research. Thank you for the wonderful opportunity.

I would like to thank Dr. Griff Bilbro for spending considerable time week in and week out discussing and helping me with my research.

Special thanks to Dr. Zhilin Li and Dr. Brian Floyd for serving on my PhD committee. I really appreciate both of you for your valuable time and feedback.

Thanks to fellow students in our research group Danqiong Hou and Arunesh Goswami for their great advice and helpful discussions. I really enjoyed working with you both. I also thank my friends who were past members of our research group: Yueying Liu, Weiwei Kuang, and Hong Yin from whom I learned a great deal from in the short amount of time we all worked together.

Finally I would like to thank all my friends from my time here at NC State and my wife, Nikki, whose love and support made this possible.

TABLE OF CONTENTS

LIST OF TABLES

LIST OF FIGURES

Chapter 1 Introduction

1.1 AlGaN/GaN HFET Device Overview

AlGaN/GaN hetero-junction field effect transistors devices have great potential for RF power applications. The material properties of GaN have enabled the manufacture of high power devices capable of withstanding voltage and currents levels and higher frequencies well beyond that of silicon and gallium-arsenide devices [1]. The large band-gap of GaN enables a large breakdown voltage since the material is able to sustain large electric field magnitudes. High power operation is enabled by the capacity of GaN devices to carry a large channel current in conjunction with the large bias voltages. The AlGaN/GaN material system forms a hetero-junction which results in the establishment of a two-dimensional electron gas (2DEG) channel at the material interface with charge densities near $n_{ss}\approx 1\text{x}10^{13}$ cm^{-2}. The mobility in the channel can range up to $\mu_n\approx 2000$ cm^2/Vs and the electron velocity can reach $v_{sat}\approx 2.5\text{x}10^7$ cm/s leading to a high channel current and the ability to operate at higher frequencies [2].

1.2 Performance and Reliability Issues

While the technology has matured in the last decade and the quality of the materials and devices have improved, there are still areas in which performance and reliability issues remain. The surface of the device in the gate-drain region is of concern due to reliability concerns such as time-dependent degradation of the drain current due to a gate-surface leakage mechanism [3], current collapse due to trapping at the gate edge on the surface and in the AlGaN layer [4], and a non-reversible sudden increase in gate leakage current resulting from physical damage to the AlGaN layer due to the high fields sustained at the gate edge [5]. High voltage and current effects under RF drive such as breakdown in the conducting channel under high-voltage conditions due to impact ionization [6], and a nonlinear source resistance effect under high-current operation due to space-charge-limited current transport in the source access region [7] are areas of performance degradation as well. These issues, illustrated in figure 1, have kept GaN HFETs from being widely adopted for use in RF and microwave systems early on but improvements in device quality and manufacturing techniques in recent years is leading to a greatly expanded market for GaN devices [8].

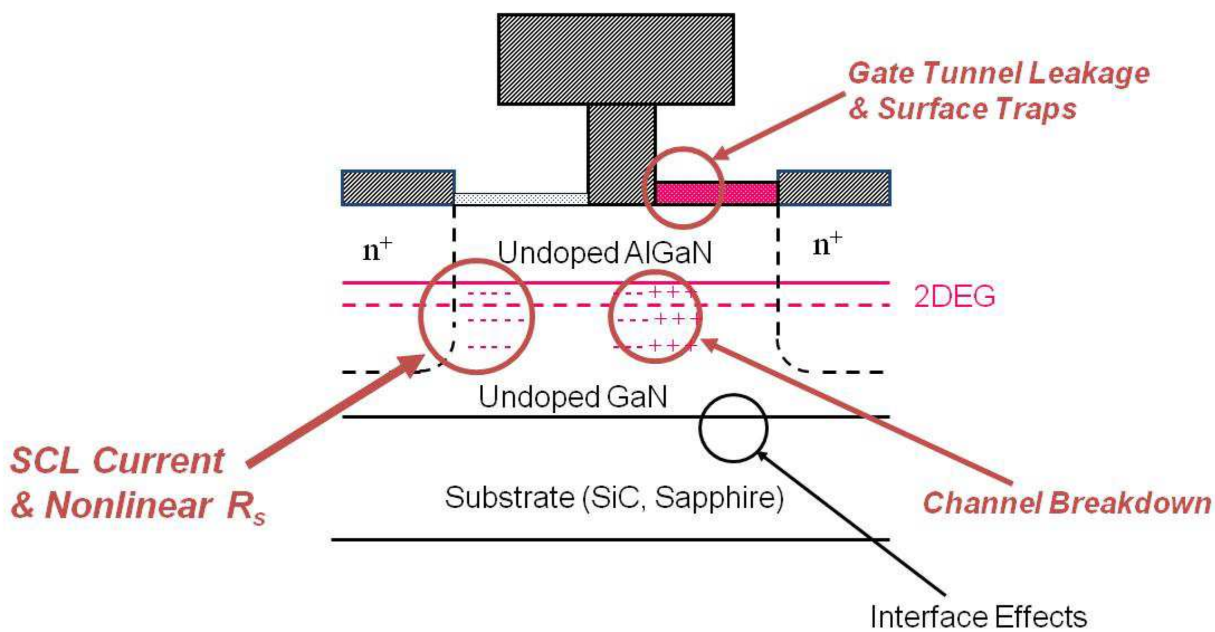

Figure 1.1 Problem areas in AlGaN/GaN HFETs.

1.2.1 High Injection Nonlinearities

Under normal operation of AlGaN/GaN HFETs in RF power amplifier configurations, high magnitude current densities on the order of $Jc \approx 10^6$ -10^7 A/cm^2 can flow in the channel during the low voltage, high current portion of the RF cycle. Trew first established that the high magnitude currents initiated a space-charge-limited conduction current in the source and drain access regions of the HFET leading to a rapidly increasing resistance and premature gain saturation [9]. Later, Palacios *et al.* measured the nonlinear behavior or the source resistance versus drain current and showed the degradation effects on g_m and f_t [10]. Trew *et al.* developed a large-signal model of the nonlinear resistance based on SCL current theory that accurately reproduces RF performance measurements including the sudden change in slope of the gain due to the onset of nonlinear resistance [7]. Recently, Liu showed that the nonlinear resistance effect in the source access region of the HFET can have a significant effect on a devices linearity characteristics which can be mitigated by raising the threshold for SCL current transport [11].

1.2.2 High Field Nonlinearities

At the other extreme, are effects due to large electric field magnitudes developed during the low current, high voltage portion of the RF cycle. Figure 2 illustrates the high fields present at the drain-side gate edge of a device biased at V_{gs}=-6 and V_{ds}=50 volts. The high electric field at the AlGaN surface is known to cause electron tunneling from the gate electrode to the surface causing reliability and performance problems. Electrons tunnel from the gate to available surface states and tend to accumulate creating a virtual gate phenomenon

[12]. The accumulated electrons effectively extend the gate electrode and deplete the channel causing a reduction in the drain current. There have been successful solutions to the leakage problem through surface passivation techniques as well as recessed gate design [13].

As shown in figure 2, the field magnitudes at the drain-side gate edge in the HFET conducting channel are also very large. Under modest drain bias the fields can reach and exceed the critical breakdown field of $E_c \approx 2 \times 10^6$ V/cm.

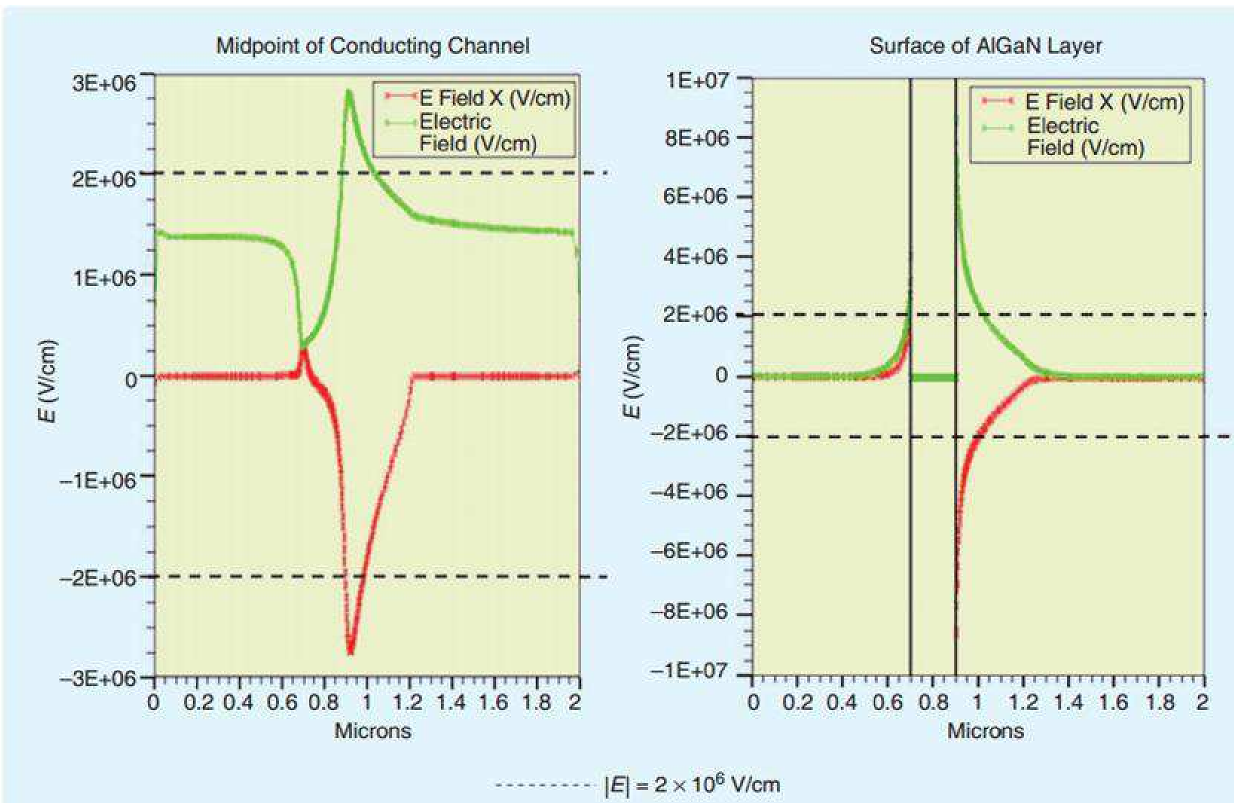

Figure 1.2 TCAD simulation results of the lateral (red) and total (green) electric field profiles along horizontal cutlines through an AlGaN/GaN HFET device for the conducting channel and the AlGaN surface from ref. [3]. **Gate location labeled by horizontal black lines.**

The high field initiates charge generation by impact ionization in the conducting channel during the high-voltage portion of the RF cycle leading to a non-destructive breakdown. This mechanism contributes to voltage saturation and clipping which limits the maximum voltage that can develop at the drain contact and has a significant effect on RF performance [6, 11].

With the advent of field plate technology problems due to the high field at the gate edge have been reduced and increased performance has been achieved. In field-plated devices, an extra piece of metal is deposited above the gate and overhanging into the gate-drain region and is typically connected to the source contact. The electrostatic effect of having this metal above the channel reduces and spreads the field out into the gate-drain region as seen in figure 3. Under this situation, the fields are greatly reduced to allow an even higher drain bias resulting power densities as high as 40 W/mm in S-band operation using a double field plate structure [14].

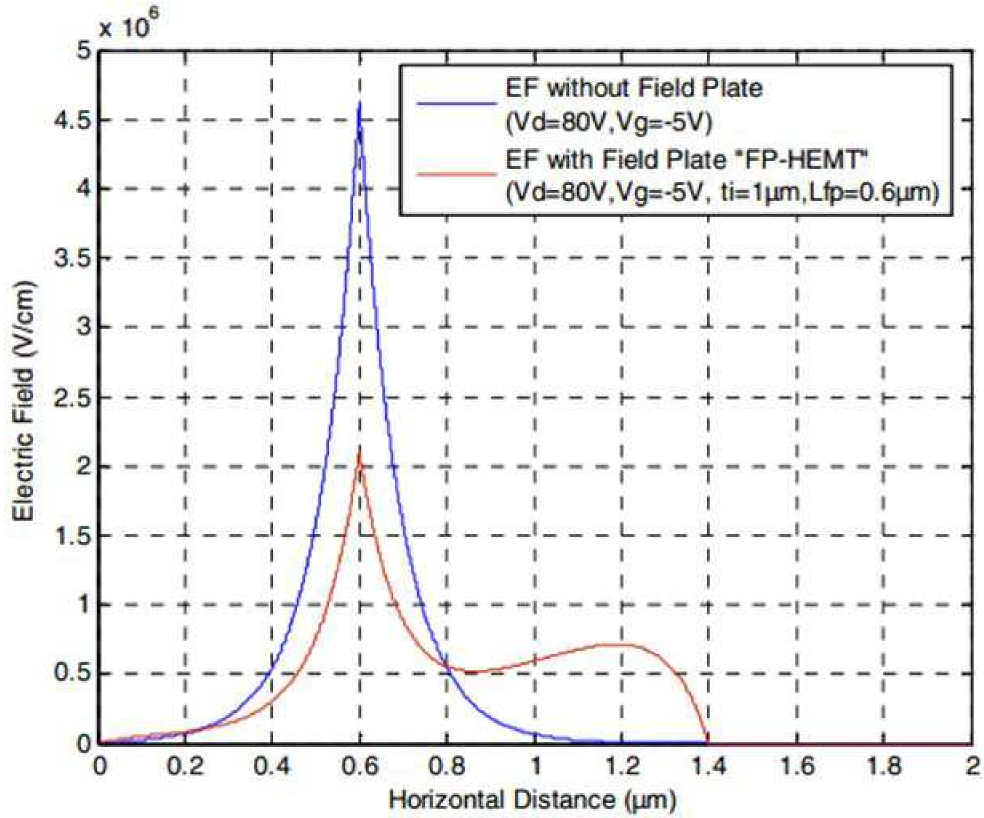

Figure 1.3 Electric field profile along a horizontal cutline through the conducting channel of an AlGaN/GaN HFET. Device without a field plate shown in blue and a device with a field plate shown in red from ref. [15]**.**

However, field plates can add parasitic capacitances that may affect device performance at higher frequencies. Additionally, the difference between the threshold for dc and RF breakdown is not well understood. Farahmand *et al.* show that the RF breakdown is likely higher considering the time it takes the particles to gain energy from the field [16]. Though this effect may be minor for frequencies below around 100 GHz.

1.3 Outline of Thesis

This thesis reports on two distinct problem areas of AlGaN/GaN HFETs. The thesis is divided into two main chapters; each dealing with a different aspect of performance and reliability in these devices.

Chapter 2

The purpose of this work is to gain a better understanding of the mechanisms affecting the threshold of the nonlinear source resistance problem. Through detailed TCAD simulations, an understanding of how the threshold for space-charge-limited current (SCLC) flow varies is established. Background information on the physics of SCL current in semiconductors is presented first. Then the results of TCAD simulations showing the behavior of injected charge and the threshold dependence on background doping density for bulk GaN as well as an AlGaN/GaN hetero-structure. It was found through simulations of a realistic AlGaN/GaN hetero-structure that the threshold for SCLC is quite sensitive to the condition of the AlGaN surface treatment.

Chapter 3

This chapter describes the derivation of a simplified RF breakdown model for AlGaN/GaN HFETs. Guided by TCAD simulations of device behavior, an impact ionization model which is dependent on device temperature was derived that successfully predicts RF performance measurements of an industrial AlGaN/GaN HFET. First an introduction describing experimental evidence of channel breakdown in AlGaN/GaN HFETs is presented. Next a description of the physics behind the impaction ionization process and a report on impact ionization coefficients in GaN is presented. Following that, TCAD simulations are used to narrow down the physical regions and the operating regions in which impact ionization is important. Using this knowledge, a model for channel breakdown is derived that easily integrates into an existing compact physics-based AlGaN/GaN HFET model. Finally, verification of the model against large signal performance measurements is presented as well as a derivation of a temperature dependent ionization coefficient.

Chapter 2 Space Charge Limited Current Transport in AlGaN/GaN HFETs

2.1 Introduction

Microwave HFETs constructed with AlGaN/GaN material system are very promising for high-power applications. High breakdown voltage allows the devices to sustain a large bias and high sheet-charge density, mobility, saturation velocity and good thermal conductivity allows operation at high current levels [2]. However, AlGaN/GaN HFETs suffer from several reliability and performance issues due to these extreme operating conditions.

In this chapter we focus on the problem of nonlinear source resistance. High current injection conditions during RF operation set up conditions for space-charge-limited current (SCLC) transport within the device. Once this threshold is passed, the channel resistivity in the source and drain neutral regions becomes a function of the injected charge which leads to the nonlinear behavior of the source resistance shown in figure 1. The rapid increase in resistance causes premature gain saturation (figure 2), reduces power-added efficiency, and degrades linearity [7].

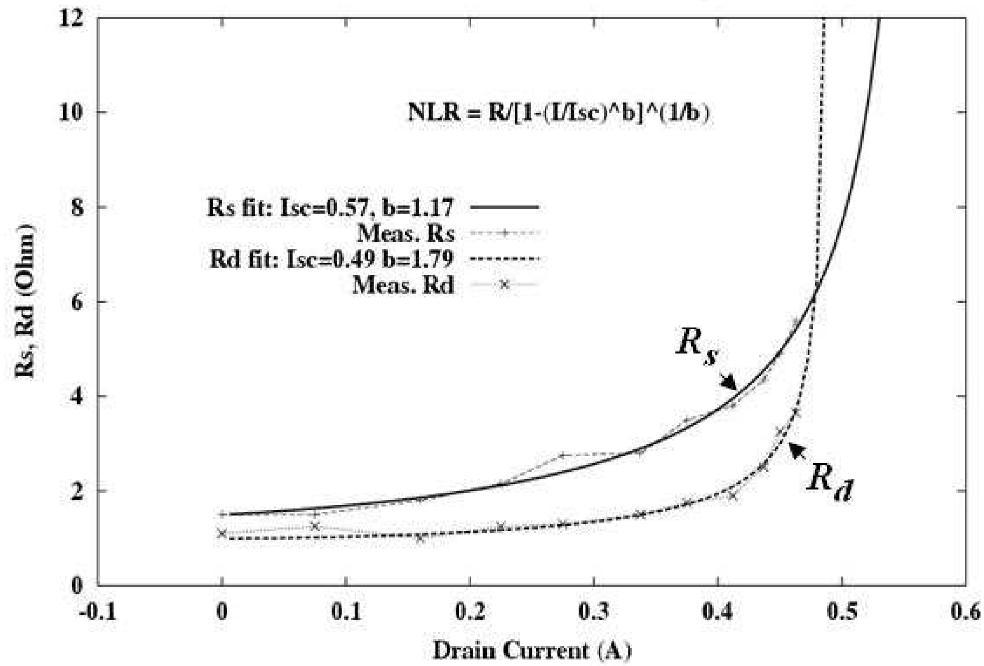

Figure 2.1 Non-linear R_s and R_d measurements from an experimental AlGaN/GaN HFET (Lines). Model from ref. [7] **(Symbols)** [11]**.**

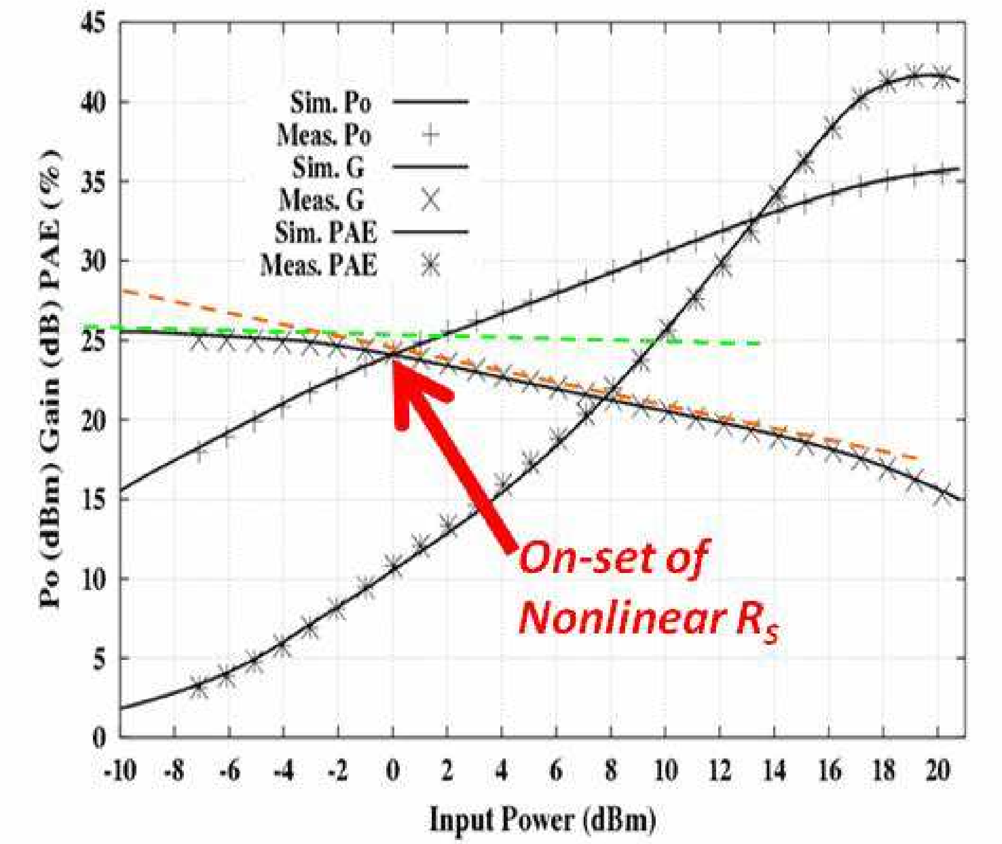

Figure 2.2 Measured and simulated performance of an AlGaN/GaN HFET biased at V_d=48 V, class A-B, 2.14 GHz. Premature gain saturation is visible in the distinct change in slope resulting from a rapid increase in R_s due to the onset of SCLC [11].

Traps and dangling bonds from material defects and processing damage leave the AlGaN surface charged. These donor-like states [17, 18] on the AlGaN surface are of particular interest to the on-set of SCL current and nonlinear source resistance. The electric field due to spontaneous and piezoelectric polarization charges in the AlGaN layer transfers electrons from the surface states to the two-dimensional electron gas (2DEG) at the heterostructure interface [18]. This phenomenon is important to the nonlinear source resistance problem since the threshold for SCLC transport depends on the 2DEG density. The threshold current is given by

$$I_{d,sat} \cong wq\left(N_{surf}t_{pass}\right)v_{sat} \tag{2.1}$$

where w is the device width, q is the electron charge, N_{surf} is the three dimensional surface charge density, t_{pass} is the thickness of the surface charge layer, and v_{sat} is the saturation velocity. The product of $N_{surf}*t_{pass}$ represents the number of electrons in the 2DEG.

In this chapter, an introduction to space-charge-limited current transport in semiconductors is described in the first section. Next, experiments on the space-charge-limited current threshold in AlGaN/GaN HFETs are included in which TCAD is used to model the nonlinear source resistance effect in the HFET channel using the 2-D numerical device simulator Silvaco™ Atlas. First, a simple model of the channel as a block of GaN is simulated with a carrier concentration equivalent to the 2DEG density as was done in reference [7]. Second, to investigate the threshold for space- charge-limited current inside a realistic device 2DEG, the entire AlGaN/GaN heterostructure structure is modelled using typical HFET dimensions and an accurate device charge profile where by including a surface doping density to mimic the donor-like surface states, the polarization field ionizes these states and transfers the electrons to populate the channel.

Results of the numerical simulations verify that modification of the AlGaN surface charge layer can alter the threshold for nonlinear resistance. The quality of the AlGaN surface or type of surface passivation can have a significant effect on the threshold. Specifically, an increase in positive surface charge can shift the nonlinear resistance threshold beyond typical operating conditions and alleviate the degradation in performance and linearity. Additionally, modelling large-signal performance measurements in devices where the nonlinear source resistance effect is significant will allow us to study and understand the AlGaN surface in these devices.

2.2 General SCLC Transport

Space charge limited (SCL) current transport is an important aspect of modern microwave devices. In MESFETs it is a SCL current that flows once the channel is fully depleted. In AlGaN/GaN HFETs the high current density present under large-signal RF operation can exceed the threshold for SCL current and even in MOSFETs space charge effects can be seen with shrinking channel dimensions. The onset of space charge effects can cause changes in the I-V characteristics of a material and have a significant impact on device performance.

In this section the underlying principles leading to SCL current in semiconductors will be discussed. A simple block of semiconductor with ohmic contacts is analyzed to show the criteria used to establish the SCL current mode of operation. Next, an analysis of a semiconductor with shallow traps and then finally a brief look at the deep trap case and the I-V characteristics of each.

2.2.1 Current Injection into a Semiconductor Slab

Although the conditions for SCL current can be established in different devices and materials in different ways, the simplest way to understand the criteria for SCL conditions is to study current flow in a simple slab of semiconductor material.

First we need to consider the basic structure for analysis as well as several approximations that will allow analytical solutions to the problem. Figure 3 below shows a slab of n-type doped semiconductor of length L, sandwiched between two ohmic contacts. The cathode, at $x=0$, is the injecting contact and the anode, at $x=L$, is the blocking contact. Considering only single-carrier (electron) current transport, all electrons are injected at the cathode and exit through the anode. Diffusion currents are neglected near the contacts as well as throughout the slab.

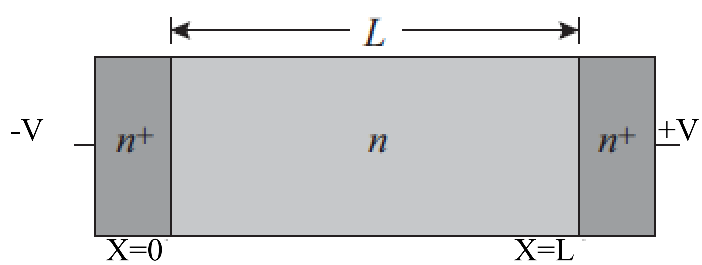

Figure 2.3 Semiconductor slab with ohmic contact.

The simplified current density equation in the slab for single-carrier, electron transport and neglecting diffusion is

$$J = qnv \tag{2.2}$$

For the present discussion, a linear velocity-field dependence is assumed and equation 2.2 can be written as

$$J = qn\mu E \tag{2.3}$$

Poisson's Equation relates the electric field to the charge distribution

$$\frac{dE}{dx} = \frac{q}{\varepsilon}\left(N_d - n_0 - n_{inj}\right) \tag{2.4}$$

Where n_0 is the thermal equilibrium electron density and N_d is the density of ionized donors. Assuming 100% ionization of the donors, $n_0 \approx N_d$, and negligible injected charge, $n_{inj} \approx 0$, electric field across the slab is a constant, and the current density can be simplified to

$$J = qn\mu\frac{V}{L} \tag{2.5}$$

Equation 4 is the familiar ohm's law. Ohm's law holds for 'low-level' injection where a small amount of injected charge is distributed close to the cathode and thus perturbs the electric field very little.

Space-charge effects set in when the injected charge is no longer negligible in Poisson's equation, thus the field distribution becomes a function of the injected charge and is no longer constant and therefore ohm's law is no longer valid. The point at which the injected charge becomes important is related to the dielectric relaxation time of the material. If the dielectric relaxation time, $\tau_R = \varepsilon/\sigma$, is greater than the transit time of electrons in the slab, τ_t, injected charge will exit the anode before it can be relaxed by the background thermal carriers. This process occurs under 'high-level' injection when the injected charge is on the order of the thermal equilibrium density or when $n_{inj} \approx n_0$. In other words, since the transit time in the slab is dependent on the length ($\tau_t = L/v$), the crossover from ohmic current to SCL current can occur just by making the slab short enough. This criteria of $\tau_R > \tau_t$ is also met by materials with a slow relaxation time so device dimensions do not have to be exceedingly small for SCL currents to occur [19, 20].

2.2.2 SCL Current with Traps

In this section the equations and conditions describing ohmic and SCL current flow in semiconductor material are discussed for three different cases. The first is the simplest trap-free case in which all of the injected charge contributes to the current. Next, the cases of shallow traps and deep traps where the current is reduced due to a portion of the injected charges being immobilized in trap states are discussed.

Trap-Free Case

For the trap-free case it is assumed that all charge is injected directly into the conduction band of the semiconductor and that all of this charge contributes to current. It is also assumed that the injecting contact can supply whatever current is necessary for the solution.

The SCL current regime begins when the injected charge is equal to the thermal equilibrium charge density, $n_{inj} \approx n_0$. Now, the current density from 2.2 can be written as

$$J = qn_{inj}(x)v(x) \tag{2.6}$$

And Poisson's equation is no longer equal to zero but instead

(2.7)

Combining these two equations and assuming a linear v-E dependence, $v=\mu E$, and the condition that the electric field must go to zero at x=0 in the slab has the solution

$$J = \left(\frac{9}{8}\right)\varepsilon\mu\frac{V^2}{L^3} \tag{2.8}$$

Equation 2.8 is known as the Mott-Gurney Law, Trap-Free Square Law, or Child's Law for Solids which closely predicts the I-V characteristics of the semiconductor slab [20].

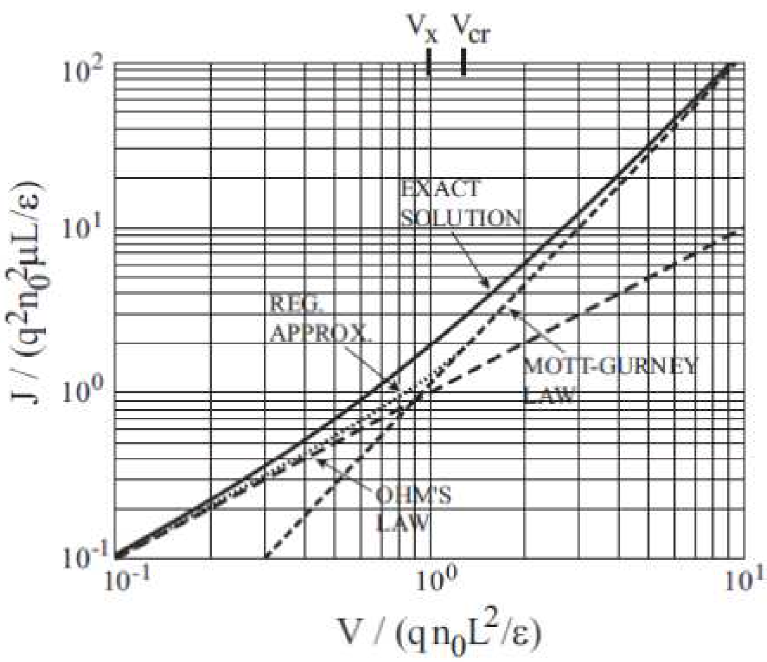

Figure 2.4 I-V Characteristics for the Trap-Free Case [21]**.**

As seen in Figure 4, Ohm's law is valid up to a certain voltage V_x, called the cross-over voltage, at which point the current is space charge limited. V_x can be found from the condition that $Q_{inj}=qn_0L$ and the physical relation $Q_{inj}=\varepsilon V/L$ which is an approximation since V/L describes the average electric field.

$$V_x = \frac{qn_0L^2}{\varepsilon} \tag{2.9}$$

The piecewise solution in Figure 4 of Ohm's law and the Mott-Gurney Law regimes is a good approximation to the exact solution that was evaluated numerically.

Shallow Traps

The SCL current seen in the semiconductor slab can be significantly reduced in the presence of traps [22, 23]. This reduced current can be attributed to the fact that a portion of the injected electrons will fill empty traps, become immobile, and therefore not contribute to current flow in the slab. So the total injected charge can be separated into free and trapped charge.

$$n_{inj}(x) = n_{f,inj}(x) + n_{t,inj}(x) \tag{2.10}$$

Since, to solve for the current, the *free charge* density in necessary and to solve for the potential the *total injected charge* is needed, it is useful to find the ratio of free to trapped injected charge. Consider a semiconductor slab doped with N_d donors partially compensated with N_a acceptors such that the Fermi level is below and doesn't rise above E_d under bias. This situation is shown in Figure 5.

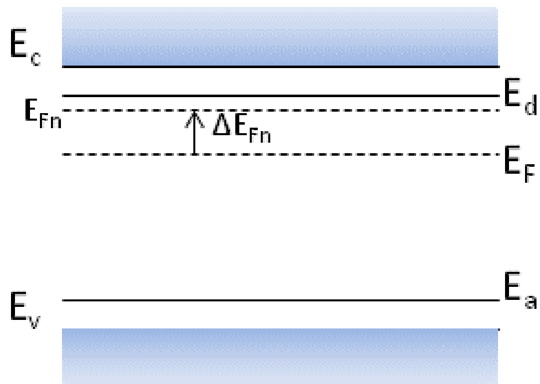

Figure 2.5 Band diagram of the shallow donor case.

The total free charge available for current flow is the sum of the free injected charge, $n_{f,inj}(x)$, and the thermal equilibrium mobile charge concentration n_0. The total trapped charge is equal to the sum of the trapped injected charge, $n_{t,inj}(x)$, and the equilibrium density of electrons in the donor states n_{d0}. The Fermi statistics describing these two quantities are given in Equations 10-11.

$$n(x) = N_C e^{-(E_C - E_{Fn}(x))/kT} \tag{2.11}$$

$$n_d(x) = N_d e^{-(E_d - E_{Fn}(x))/kT} \tag{2.12}$$

The ratio of free to trapped charge can be defined as $\theta = n(x)/n_d(x)$ and thus the quasi-Fermi level, which depends on position, vanishes and the ratio θ is constant throughout the slab such that $\theta = n_{f,inj}(x)/n_{t,inj}(x)$.

Now, just as for the trap-free case, current in the slab will follow Ohm's law up to the point where the *injected free charge* is equal to the thermal equilibrium charge and is then space-charge-limited. The current equation in this case is similar to Equation 5 except that the injected charge is replaced by the free injected charge.

$$J = qn_{f,inj}(x)v(x) \tag{2.13}$$

The effect of the trapped charge shows up in Poisson's equation since it accounts for all charge, mobile or not, within the slab.

$$\frac{dE}{dx} = -\frac{q}{\varepsilon}\left(n_{f,inj}(x) + n_{t,inj}(x)\right) = -\frac{q}{\varepsilon}n_{f,inj}(x)\left[1 + \frac{1}{\theta}\right] \tag{2.14}$$

Finally, the solution to these equations is similar to that of the trap-free case

$$J = \left(\frac{\theta}{\theta + 1}\right)\left(\frac{9}{8}\right)\varepsilon\mu\frac{V^2}{L^3} \tag{2.15}$$

When traps are few, theta is much greater than one and the current approaches the trap-free case. However, if there are many shallow traps, theta becomes much smaller than one and the current is reduced by theta times the trap-free current. The end result is that the current follows Ohm's law beyond then V_x form the trap-free case until it intersects with the new V_x determined by theta, and then follows the approximation in Equation 14.

Deep Traps

Deep traps in the semiconductor slab have a distinct effect on the I-V characteristics as seen in Figure 6.

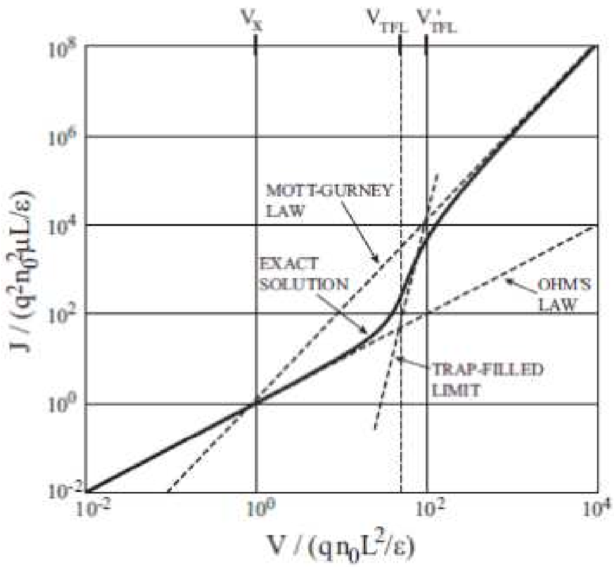

Figure 2.6 I-V Characteristics for the Deep Donor Case [21]**.**

Due to the deep level of the donors in the band-gap and the presence of a partially compensating acceptor concentration, the equilibrium Fermi level will lie just above the donor level leaving less than half ionized. The current follows the Ohm's Law line in Figure 4 until the injected charge equals the thermal equilibrium charge which causes the Fermi level to rise and all donor states to become filled. This is the "Trap-Filled Limit" and once it is reached, the current will begin to rise very fast since all subsequent injected charge in now mobile charge that can contribute to the current [21]: The trap-free limit.

2.2.3 Non-Linear Velocity-Field Dependence

This discussion was focused entirely on a linear *v-E* dependence to simplify the solutions to Poisson's and the current continuity equations. In cases of practical interest fields are high enough that the velocity can saturate and a non-linear *v-E* model must be used in place of *v(x)* in Equation 2.13. The effect of the high field case on the current can be approximated by a piecewise function in which

$$
\begin{aligned}
&v = \mu E \Rightarrow E \leq E_{sat} \\
&v = \mu\sqrt{E_c E} \Rightarrow E_c < E \leq E_{sat} \\
&v = v_{sat} \Rightarrow E > E_{sat}
\end{aligned}
\tag{2.16}
$$

The trap-free case, for example, would have a low-field current density as in the Mott-Gurney Law. For intermediate fields where velocity exceeds some E_c with a square root dependence the current density is give by equation 2.16a

$$J = \left(\frac{2}{3}\right)\left(\frac{5}{3}\right)^{3/2} \varepsilon\mu \frac{V^{3/2}}{L^{5/2}} \tag{2.17}$$

and a high-field current density corresponding to when the velocity is saturated like that of Equation 2.16b

$$J \cong \varepsilon v_{sat} \frac{V}{L^2} \tag{2.18}$$

As shown, the SCL current for the saturated velocity case varies linearly with applied bias and inversely to the square of the length. It should be noted that in order to see Ohm's law cross over to the Mott-Gurney Law, the sample length must be short enough that space charge effects occur prior to velocity saturation [19].

In conclusion it was shown how current in a semiconductor slab can vary greatly from that predicted by Ohm's law. The onset of SCL current was shown to be when $n_{inj} \approx n_0$ which happens to be the point at which the injected charge cannot be relaxed by the background charge before leaving the anode i.e. the dielectric relaxation time is long relative to the transit time of the carriers. It is the bias at this point where the dielectric relaxation time equals the transit time through the sample that is defined as the crossover voltage from the Ohm's Law regime to the SCL current regime. With these methods it is possible to analyze space charge effects in any device to a good approximation.

2.3 TCAD Investigations of SCLC Threshold in AlGaN/GaN HFETs

2.3.1 Bulk GaN Channel Model

We first model the HFET channel as a one-dimensional slab of GaN. Silvaco™ Atlas numerical device simulator was used to solve Poisson's equation and the current density equation on a slab of GaN where L_{SD}=1.5 um long, t_{GaN}=1um thick and w_{Slab}=1 um wide. Contact was made to the source and drain ends of the slab through n^+ doped regions and metal contacts. Transport parameters in the GaN slab mimic those of a typical HFET 2DEG with μ_n=1500 cm^2/Vs, v_{sat}=1.2x10^7 cm/s and a first-order velocity-field relationship given by equation 2.19 [24].

$$v(E) = \frac{\mu|E|}{1 + \frac{|E|}{E_{sat}}} \tag{2.19}$$

To first investigate the threshold for space-charge effects in the slab, we model the sheet charge density with an effective doping N_D. The typical width of an AlGaN/GaN heterojunction 2DEG is approximately t_{2DEG}=2.5 nm [17]. We obtain a sheet-charge density in the range of 10^{12} to 10^{13} of 5.2 x 10^{12} cm^{-2} resulting from an N_D=2.1 x10^{19} cm^{-3}. The critical current for the onset of SCLC can be estimated from the channel saturation current density (eqn. 20).

(2.20)

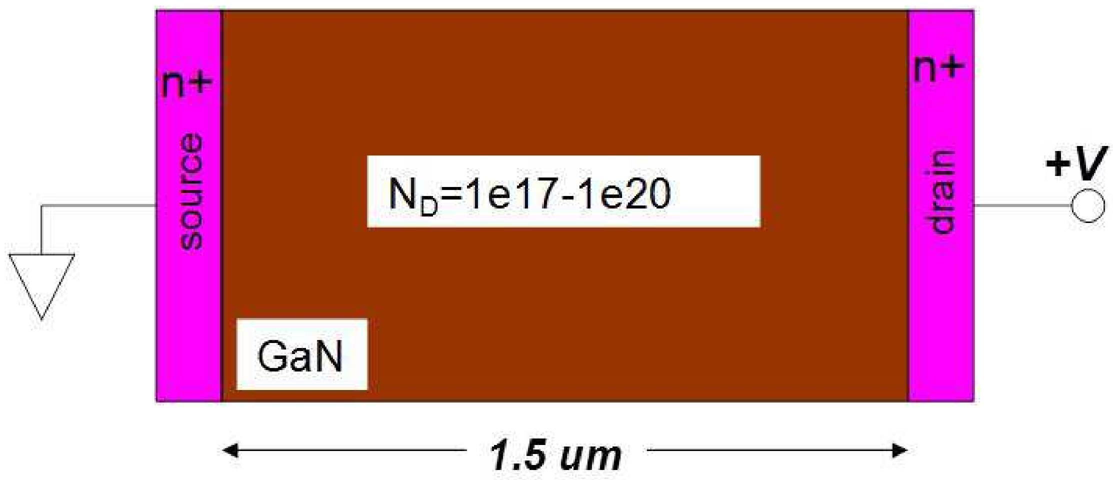

Figure 2.7 TCAD simulation model structure for modeling the AlGaN/GaN HFET conducting channel under high current injection.

Space-charge limited current will become the dominate conduction mechanism when in Poisson's equation, the injected charge becomes comparable to the background thermal equilibrium charge density, N_D [19]. This approximately uniform layer of space charge across the slab is no longer negligible in Poisson's equation and the electric field is driven lower to maintain current continuity in the slab. The electric field and resistivity become a function of the injected charge causing the nonlinear resistance effect [7]. Expected results are confirmed in figure 8 for several simulations of the injected excess charge versus distance along the channel around the saturation current density. For this simulation $I_{d,sat}$≈0.403 A. As seen in figure 8, when the injected current is well below the saturation current, the injected charge is mostly negligible and quickly relaxed so that it is confined to a narrow region next to the source contact. When the current approaches $I_{d,sat}$, the space charge region grows and extends further horizontally into the channel yet still relaxes to the background concentration and can be considered the crossover point form ohmic to SCL current conduction. When $I_{d,sat}$ is met and exceeded, a uniform layer of space charge accumulates along the entire channel and the current is fully space-charge-limited.

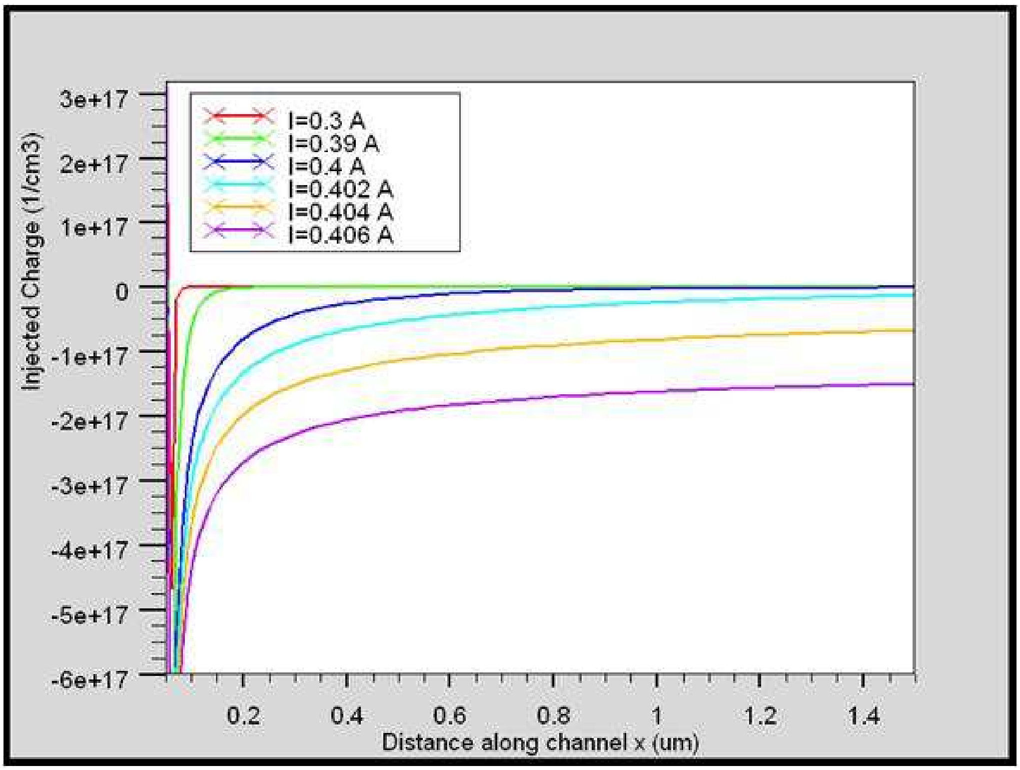

Figure 2.8 Injected charge vs. distance along a horizontal cut-line through the center of the bulk GaN slab. N_D=2.1x10^{19} cm^{-3}.

More insight into the nonlinear source resistance can be obtained by looking at the voltage-current characteristics of the slab. Figure 9 shows several simulations of the slab with doping ranging from N_D=1 x 10^{17}- 1 x 10^{20} cm^{-3} representing a wide range of sheet-charge densities.

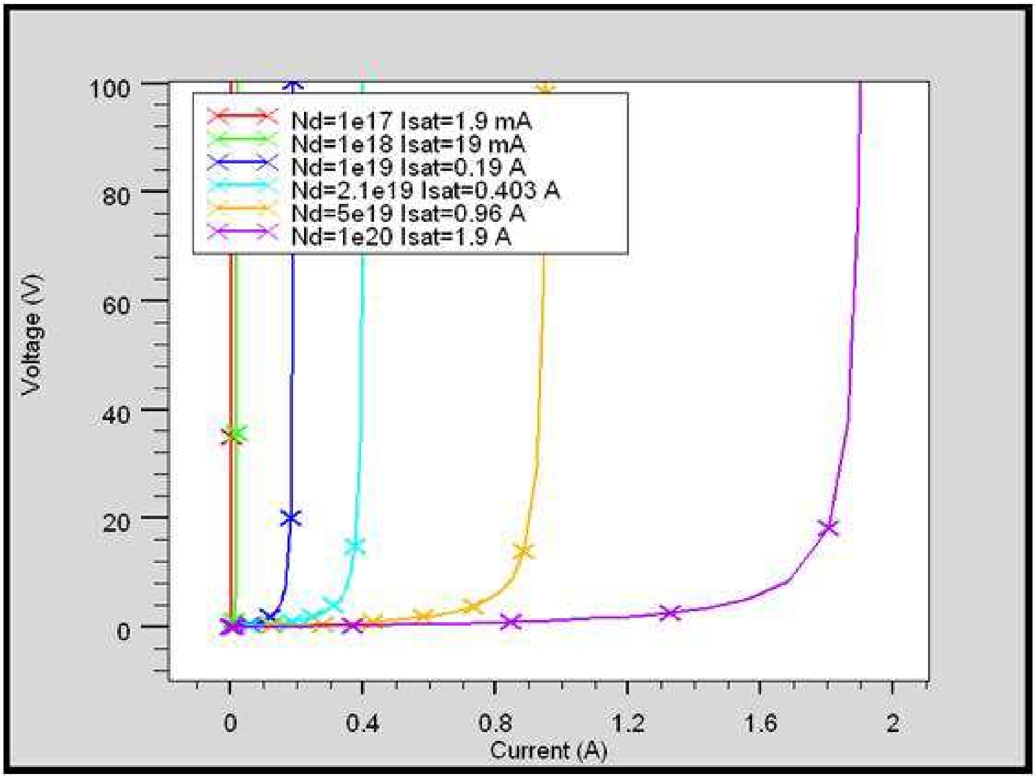

Figure 2.9 Voltage vs. current for the bulk GaN slab. I_{SAT} increases with increasing doping density (sheet-charge density) according to the approximation, $I_{d,sat}=whqN_Dv_{sat}$.

For any particular doping density the threshold for SCLC is clearly visible. Prior to $I_{d,sat}$, the voltage varies linearly with the current (the relationship is somewhat suppressed due to the linear scale) and is essentially ohmic. When the injected current approaches $I_{d,sat}$ space-charge limited current begins to dominate and the voltage-current relationship becomes increasingly nonlinear and consequently so does the resistivity. Figure 9 shows the dependence of SCLC, and thus nonlinear resistance, on the channel sheet-charge density.

2.3.2 AlGaN/GaN Heterostructure Model

The next step was a simulation of a realistic model of the HFET channel to verify the dependence of the threshold for SCLC. The structure is identical to an un-gated AlGaN/GaN HFET of length L_{sd}=0.85 um and an AlGaN barrier layer of thickness t_{AlGaN}=30 nm. The Aluminium content in the AlGaN is 20%. Doping in the AlGaN and GaN is N_D=1x10^{16} and N_D=1x10^{15} cm^{-3} respectively. Transport parameters in the GaN are the same as the slab simulation with μ_n=1500 cm^2/Vs, v_{sat}=1.2x10^7 cm/s and a first-order velocity-field relationship given by equation 2.19.

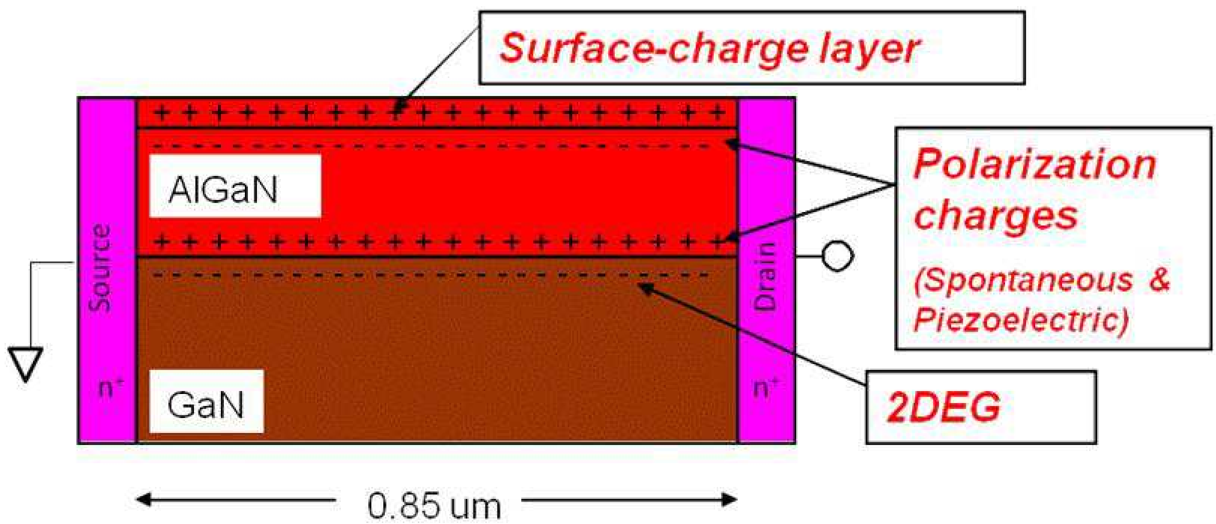

Figure 2.10 AlGaN/GaN heterostructure model used in TCAD simulations to model high injection effects in the gate-source region of and AlGaN/GaN HFET.

A realistic charge profile was used to model the interactions as in an actual HFET. A positive and negative sheet-charge (σ_{pol}=1x10^{13} cm^{-2}) was added at the hetero-junction and at the surface of the AlGaN to model the polarization charges due to both piezoelectric and spontaneous effects. An additional volume charge density was added in the top 1 nm of AlGaN to model surface charges due to defects and processing damage. This surface charge is implemented by a doping, N_D, which models donor-like surface states [18]. These electrons are responsible for filling the 2DEG. The saturated current density in the channel can be written in terms of the surface charge due to passivation (eqn. 21).

$$I_{d,sat} = wq(N_D t_{pass})v_{sat} \tag{2.21}$$

Simulation of the model agrees with the results of the GaN slab channel model. Figure 11 shows multiple simulation results for the injected excess charge in the channel around $I_{d,sat}$=1.9 mA for $N_{D,surf}$=1x10^{20} cm^{-3}.

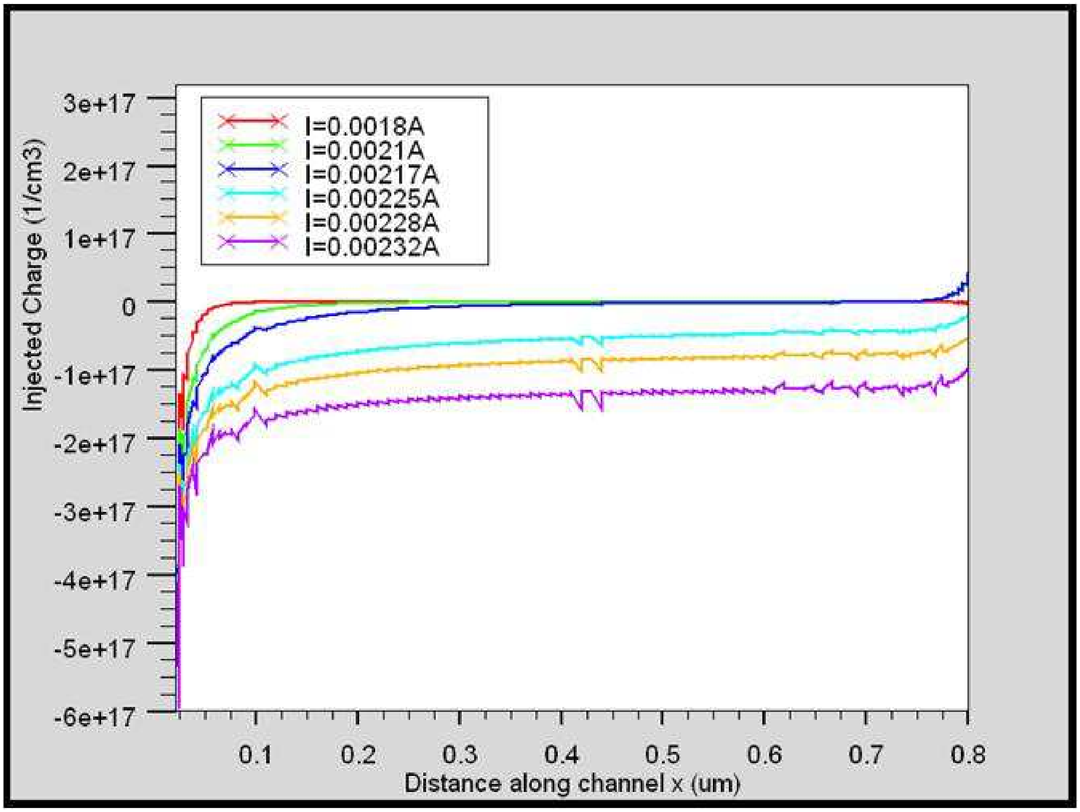

Figure 2.11 Injected charge vs. distance along a horizontal cut-line through the center of the 2DEG for N_D=1x10^{20} cm^{-3}. Net space-charge is accumulating as the current approaches and exceeds $I_{d,sat}$.

A significant uniform layer of space charge is not achieved until the injected current exceeds $I_{d,sat}$, the onset for space-charge-limited current.

Figure 12 shows the voltage-current characteristics for several simulations of the HFET channel in which the doping in the surface layer was increased from 1x10^{18} to 1x10^{20} cm^{-3}. As shown in the figure, when the doping density in the surface layer is increased, representing an increase in positive charge due to ionized donors, the threshold for SCL current is shifted to higher current levels.

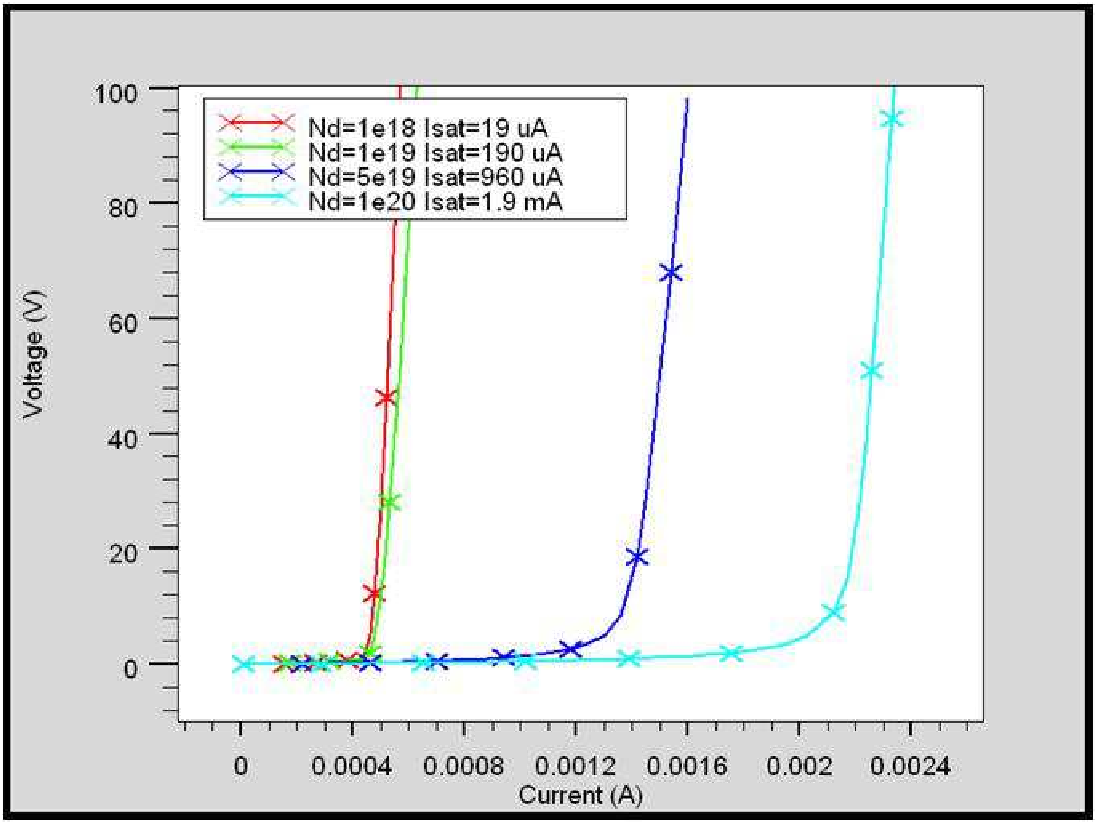

Figure 2.12 Voltage vs. current for an AlGaN/GaN heterostructure. I_{SAT} increases with increasing positive surface charge concentration corresponding to increasing sheet-charge density and is calculated according to $I_{d,sat}=wq(N_D t_{pass})v_{sat}$.

2.4 Conclusion

High power AlGaN/GaN HFETs normally operate under SCL conditions. SCLC conduction in the channel causes a nonlinear resistance effect that degrades device performance and linearity. A simple model of the HFET channel has shown the critical current density for the nonlinear resistance effect is dependent on the channel sheet-charge density. A more exact model of an un-gated HFET has shown that since the 2DEG electrons originate from surface defects, the onset of SCLC is dependent upon the surface charge density. We have shown that an increase in positive charge on the surface can push the SCL threshold beyond normal operating conditions and thus, alleviate the degradation due to nonlinear source resistance.

Chapter 3 RF Channel Breakdown

3.1 Introduction and Experimental Evidence

AlGaN/GaN HFETs are promising devices for RF and microwave power amplifier applications. While there is still work to be done, performance and reliability of AlGaN/GaN HFETs has progressed significantly in recent years to the point where the devices are commercially available and are being inserted into practical systems applications.

AlGaN/GaN HFETs achieve high power densities by means of a large critical breakdown field (E_c >2MV/cm), and the ability to sustain a large channel current. Under normal operation high magnitude electric fields are present within the device at the semiconductor surface near the gate edge and in the conducting channel at the drain-side edge of the gate electrode. The high fields present at the drain-side gate edge in the conducting channel are sufficient for charge generation by impact ionization and subsequent avalanche breakdown. Although the fields on the surface at the gate edge are sufficient to cause an electron tunneling current, gate to drain breakdown usually only occurs for large voltages. While the gate leakage tends to have an effect on reliability [25], breakdown in the channel is the dominant mechanism in performance degradation.

Early experiments investigating impact ionization in the channel of AlGaN/GaN HFETs were done using a method by Hui *et al.* in which the ionization coefficients could be estimated by measuring the increased gate current due to impact generated holes in MESFETs [26]. Dyakonova *et al.* measured DC-HFETs on SiC substrates using Hui's technique across a temperature range of 17-43 ^{o}C. The resulting characteristic electric field of about 2.6 MV/cm agreed well with current Monte Carlo simulations for bulk GaN [27] but may be unreliable since the gate leakage current for these devices was large. However, the measurements did indicate a positive temperature coefficient of the breakdown voltage which confirms that that the impact ionization mechanism is the source of the excess hole current. Kunihiro *et al.* used the same technique to measure the ionization coefficients in AlGaN/GaN HFETs grown on sapphire substrates [28]. The leakage current on these devices was much smaller than the current due to impact ionization generated holes and they were also able to closely approximate the simulation results of Kolnik *et al.* [27]. A few years later, measurements of AlGaN/GaN on sapphire HFETs by Tan *et al.* showed conflicting evidence that the on-state breakdown voltage reduced with increasing temperature indicating a mechanism other than impact ionization [29]. He showed that breakdown likely occurs between the gate and drain due to a thermal runaway mechanism. Brar et al. at the same time showed good evidence of impact ionization in AlGaN/GaN HFETs on SiC by showing a large increase in the 'kink effect' of the drain current with lower temperatures [30]. Although later experiments point to the kink effect can also be explained by the presence of traps [31, 32], Brar's measurements of the gate current of their low leakage devices show an increase in hole current, from impact ionization in the channel, with a positive temperature coefficient. Measurements by Ohno *et al.* on AlGaN/GaN HFETs show evidence of impact ionization through electroluminescence measurements [33]. The region of EL intensity was shown to occur at the drain-side gate edge for devices with Si_3N_4 surface passivation. More recent measurements by Wang and Chen [34], confirm impact ionization is present in the channel of

GaN HFETs measuring breakdown voltage using the drain injection technique [35] for GaN HFETs. And finally, Killat *et al.* provide compelling evidence of impact ionization in GaN HFETs with an InGaN back-barrier shown in figure 1 below. Holes generated by impact ionization are collected at the InGaN layer where they recombine and the large increase in EL intensity at -140 ^{0}C is consistent with the increased mean free path that results in more impact ionization events [36].

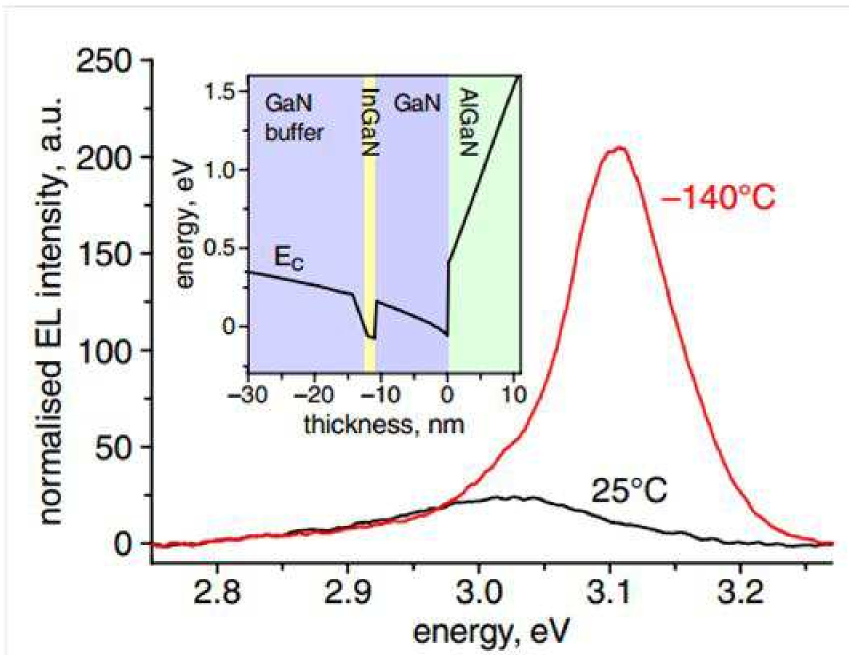

Figure 3.1 Electroluminescence emission from InGaN layer at different temperatures [36]**.**

Measurements of the industrial devices used in this thesis show that impact ionization occurs within the HFET channel and is the dominant breakdown mechanism [6]. Figure 2 shows the results of measurements of multiple devices on the wafer. The devices are biased at pinchoff while the drain to source voltage is swept beyond 70 volts. The gate leakage current (negative-black lines) is small and increases with increasing drain voltage but it never breaks down. However, the drain current does begin to break down starting as low as 30 volts with most device breaking down around 40-50 volts. This experiment shows definitively that channel breakdown has a lower threshold than gate breakdown which can impact device performance even at low drain bias.

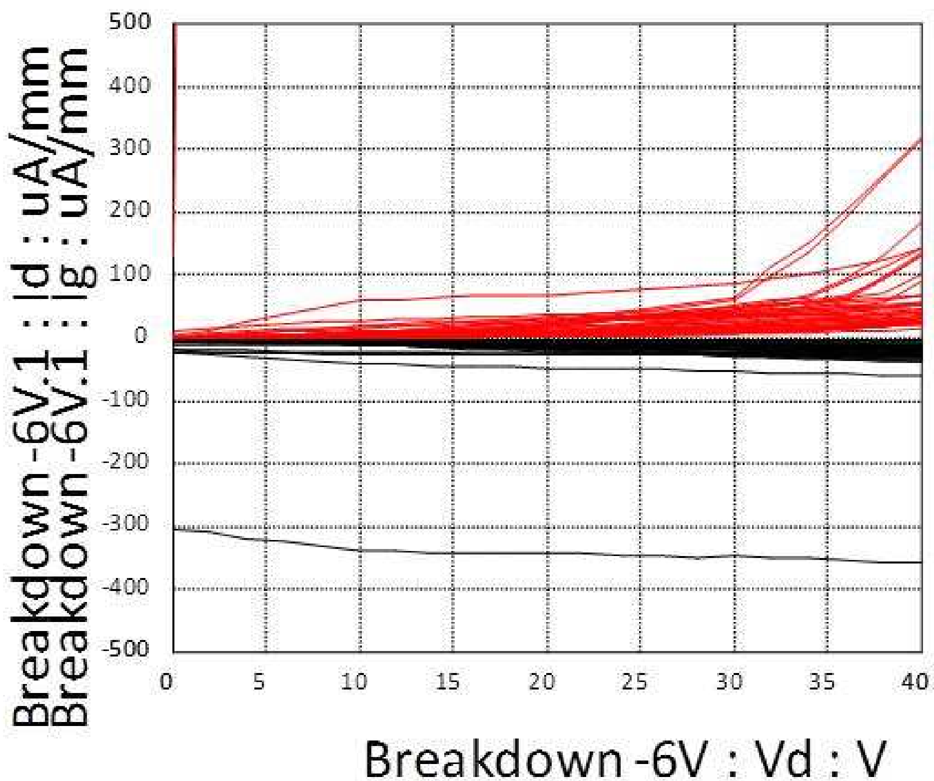

Figure 3.2 Measurements of I_{ds} and I_{gs} vs. V_{ds} for multiple AlGaN/GaN HFET devices from the same wafer.

RF breakdown within the channel results in clipping of the RF voltage [5], as well as impact ionization generated current in the channel. These phenomena limit the RF voltage that can be developed at the drain contact during the peak of the RF cycle, causing the device to saturate and reducing output power, gain, and PAE. Performance of AlGaN/GaN HFETs has been greatly enhanced by the adoption of field plates [37, 38], in which the high field present at the gate edge can be reduced and spread out so that the device can sustain higher voltages without breaking down. However, these plates introduce parasitic capacitances that can effect performance and may not be as useful at higher frequencies [2].

Accurate models of GaN HFETs are necessary for RF circuit design for these devices to be widely used in RF systems. Predictive physical models are also a valuable resource for device research and development. A physical model of the channel breakdown mechanism under large-signal RF operation that is suitable for integration into device simulators has not previously been reported.

Following previously established physical modeling techniques for the large-signal operation of GaAs MESFETs [39], a compact, physics-based, large-signal model of AlGaN/GaN HFETs was developed and has been shown to accurately predict RF performance [40]. In these models, RF breakdown effects are shown to be important and are incorporated within the drain-source circuit using a current generator in the form of a diode with an adjustable reverse breakdown voltage to mimic the effect of avalanche breakdown in the channel. The diode's V_{bd} is used as a fitting parameter to match large-signal measurements. This method, while permitting the models to accurately predict device large-signal operation and provide insight into breakdown behavior, are not predictive and the RF breakdown voltage needs to be extracted from measurement data before the model can be completely defined. Figures 3 and 4 below show the large-signal model employed in these simulations and resulting effect on RF performance.

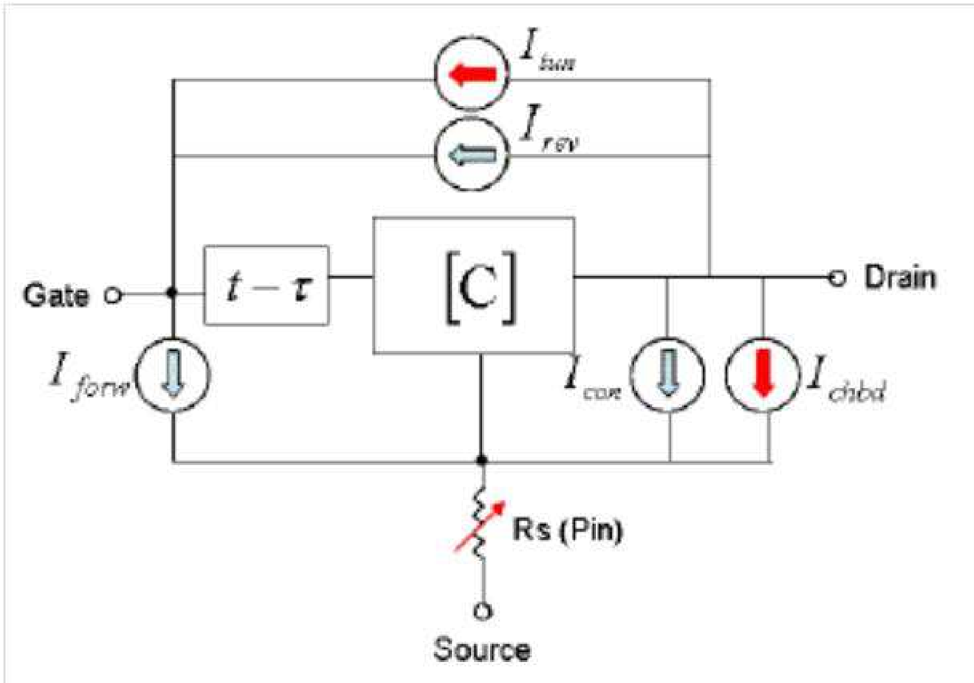

Figure 3.3 Large-signal model including a channel breakdown current generator in the drain-source circuit [6]**.**

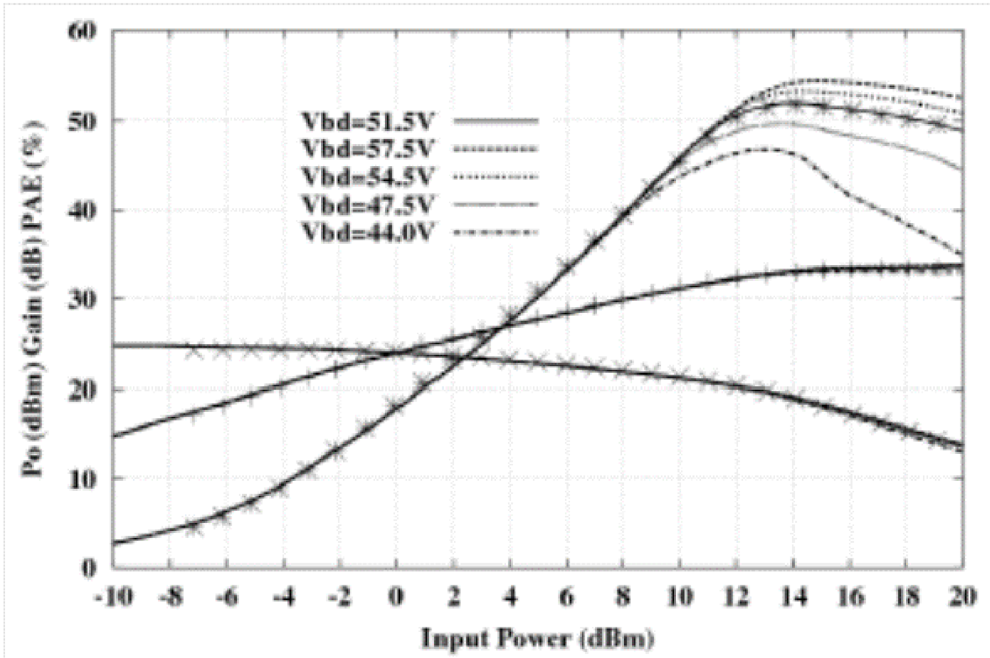

Figure 3.4 Results of varying the breakdown voltage on RF performance measurements.

In this chapter, a physics-based model of channel breakdown is developed and integrated into the previously reported compact model [40]. The model was derived with the help of Silvaco™ TCAD simulations to investigate the internal physics of the HFET. The new model is used to simulate the RF performance of an industrial HFET and excellent agreement is obtained between the simulated and measured RF performance data. In agreement with the measured data the new breakdown model indicates a dependence of RF breakdown voltage on dc drain bias. The breakdown model is further refined to incorporate a temperature dependence of the GaN ionization coefficient. Extracted values for the thermal resistance and temperature coefficient of breakdown verify that the temperature dependence of impact ionization is the dominant mechanism in the breakdown phenomenon.

3.2 Impact Ionization

In modern devices with shrinking dimensions large magnitude electric fields can be established. Under high enough fields electrons (or holes) can become energetic enough where, upon collision with atoms in the semiconductor lattice, an electron-hole pair can be created as the energetic electron caused an ejection of a valence electron from the atom. The original particle and the two newly generated particles can be accelerated again by the field can create more electron-hole pairs through impact ionization. Avalanche breakdown is defined to occur when, on average, every particle that is created from an impact ionization event initiates another separate impact until the current in the circuit reaches some maximum allowable value. In this section an overview of the physical basis for the ionization coefficients will be given followed by a derivation of the ionization integral for calculating avalanche breakdown. Next some background and results for the ionization coefficients in GaN, and finally some approximations that will be used in deriving the breakdown model for AlGaN/GaN HFETs will be explained.

3.2.1 Physical Ionization Coefficients

Speaking in terms of electron initiated impact ionization, for and electron to create an electron-hole pair upon collision with the lattice it must have at least an energy equal to the bandgap, E_g, to promote an electron to the conduction band. This minimum energy is called the threshold energy, E_{th}. However, due to the complicated band structure in semiconductors E_{th} is typically a little larger than E_g.

It is illustrative to derive a simple approximation of the minimum threshold energy to understand the dependencies on the band structure. To determine the minimum energy for an electron to impact ionize we assume parabolic, isotropic, and non-degenerate energy bands. Considering an electron that undergoes a collision with the lattice and creates an electron and a hole we can write the sum of the energies as

$$E_e = \frac{1}{2} m_e \vec{v}_f^{\,2} + \frac{1}{2} m_e \vec{v}_e^{\,2} + \frac{1}{2} m_h \vec{v}_h^{\,2} + E_g \tag{3.1}$$

where E_e is the initial electron energy and is equal to the sum of the final electron energy, the newly created electron and hole energies, and the bandgap energy.

And the momentum as

$$\overrightarrow{P_e} = m_e \overrightarrow{v_f} + m_e \overrightarrow{v_e} + m_h \overrightarrow{v_h} \tag{3.2}$$

If we consider only low energy collisions, which is appropriate since we are looking for the minimum energy, we can assume that the momentum vectors are collinear and thus can be treated as a scalar. Following Wolfe, Holonyak, and Stillman's approach in [41] to find the minimum of E_e, the resulting threshold energy for electron initiated impact ionization is given by

$$E_{th} = E_g \frac{2m_e + m_h}{m_e + m_h} \tag{3.3}$$

which is dependent on the effective masses of electrons and holes and thus the band structure and for holes by

$$E_{ht} = E_g \left[1 + \frac{m_l \left(1 - \Delta / E_g \right)}{2m_h + m_e - m_l} \right] \tag{3.4}$$

where the threshold depends on the light, heavy, split-off bands. In this simple model the electron threshold energy can range from E_g to 2 E_g depending on the ratio of the effective masses. More complicated and realistic band structures need to by analyzed, usually done by Monte Carlo simulations, in order to determine a good number for the threshold energy.

For simple models of devices such as diodes, just knowing the threshold energy can be enough to model the effects of impact ionization. These models would initiate avalanche breakdown as soon as carriers gain the threshold energy from the electric field, the breakdown field [42]. A more accurate way to predict impact ionization is to describe the ionization rate as a function of electric field. This is modeled by an ionization coefficient function $\alpha(F)$ cm^{-1} and $\beta(F)$ cm^{-1} for electrons and holes respectively. These rates, which are calculated using Monte Carlo methods incorporating detailed descriptions of a semiconductors band structure and scattering mechanisms and rates, represent the probability that an electron or hole will undergo an impact ionization event under the influence of an electric field. The reciprocal of this coefficient is equivalent to the minimum average distance the particle must travel to impact ionize. A general form of the ionization coefficient shown by finding the probability that a carrier will gain sufficient energy from the field to reach the threshold energy is given by

$$\alpha(F) = {eF}/{E_{th}} \; P(E_{th}) \tag{3.5}$$

where e is the electronic charge, F is the field seen by the electron, $P(E_{th})$ is the probability that a carrier gains the threshold energy, and E_{th} is the average ionization threshold energy [43]. The probability can be found from the energy distribution function, $f(E_{th})$, which is obtained by solving the Boltzmann transport equation for $f(k)$. Lucky carriers traveling in an electric field where the energy gained between phonon collisions is less than the energy lost in each collision, $eF\lambda \leq E_p$, then the probability that an electron gains the ionization energy without losing its energy in a phonon collision can be written as

$$P(E_{th}) = e^{\left(-E_{th}/eF\lambda\right)} \tag{3.6}$$

so that the ionization rate becomes

$$\alpha(F) = {eF}/{E_{th}} \; e^{\left(-E_{th}/eF\lambda\right)} \tag{3.7}$$

where λ represents the mean free path of the semiconductor. The coefficients are usually extracted and fit from simulations as well as experimental data. At high electric field magnitudes the above expressions are not as accurate and more detailed picture of the scattering mechanisms must be employed [43]. Ionization coefficients determined from simulation or measurements are typically reported in the literature in the form

$$\alpha, \beta = A_{e,h} e^{-\left(F_{e,h}/F\right)^{m_{e,h}}} \tag{3.8}$$

to best approximate the data [28, 44] where $A_{e,h}$ has units of cm^{-1}, F in V/cm.

3.2.2 Avalanche Multiplication

The electron and hole ionization coefficients are important for precisely modeling impact ionization effects in solid-state devices. For predicting breakdown in diodes and FETs a way to accurately model the increase in current due to impact ionization on a macroscopic scale is necessary. Avalanche multiplication in a semiconductor device can be analyzed by relating the ionization coefficients for that material to the multiplication of current flowing due to impact ionization using the basic semiconductor equations. Figure 5 shows a widely accepted model for the derivation of avalanche multiplication across a depletion region [45, 46].

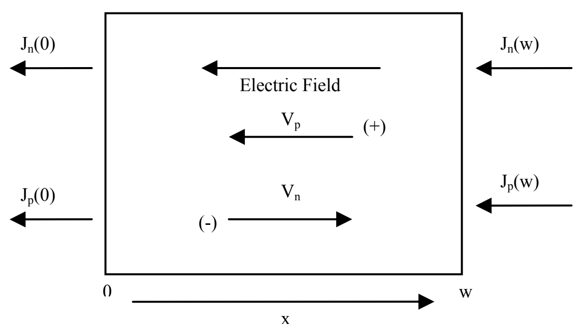

Figure 3.5 One dimensional diagram for a high field region of length *w* showing boundary conditions, electric field, and electron and hole drift velocities.

In this diagram, electrons injected at x=0 travel in the positive x direction and the electron current density increases due to impact ionization multiplication. Likewise holes travel in the negative x direction also increasing in current density due to impact ionization as they approach x=0. The net current is in the direction of the electric field. The differential equation describing this behavior is the Continuity Equation. If it is assumed steady state and the generation term is written in terms of the ionization coefficients

$$G = \alpha_n J_n(x) + \beta_p J_p(x) \tag{3.9}$$

Where α_n and β_p are the ionization coefficients for electrons and holes respectively. Then, for electron initiated avalanche ionization where J is the total constant current, the continuity equation can be written as

$$\frac{dJ_n}{dx} = \alpha_n J_n(x) + \beta_p J_p(x) + \beta_p(x) J \tag{3.10}$$

There is an assumption at this point worth noting that α and β, the measured ionization rates, are the same as those calculated through the distribution function. If we assume that the applied electric field varies slowly in comparison to the average ionization distance so that the carriers can be assumed to be in a spatial steady-state, the assumption that α and β only depends on distance through *E(x)* is a good approximation [43]. Since the total current is constant through the high field region, a multiplication factor, *M*, can be defined as the ratio of two currents; one with avalanche multiplication and one without given by

$$M_n = \frac{J_n(w)}{J_n(0)} \tag{3.11}$$

for electrons. Using this factor and the boundary conditions from figure 5 the differential equation can be solved [45]. In terms of the multiplication factor, the solution for electron initiated avalanche ionization is

(3.12)

The breakdown voltage can be interpreted as the voltage at which the multiplication factor approaches infinity. Breakdown would occur when the integral of the second term in the above equation approaches one. A common assumption used to simplify the second term of the multiplication factor is to consider $\alpha=\beta$. This works in semiconductors where there isn't a large difference between the electron and hole coefficients by defining an effective ionization coefficient, α_{eff}, that best approximates both coefficients [47, 48] seen in figure 6.

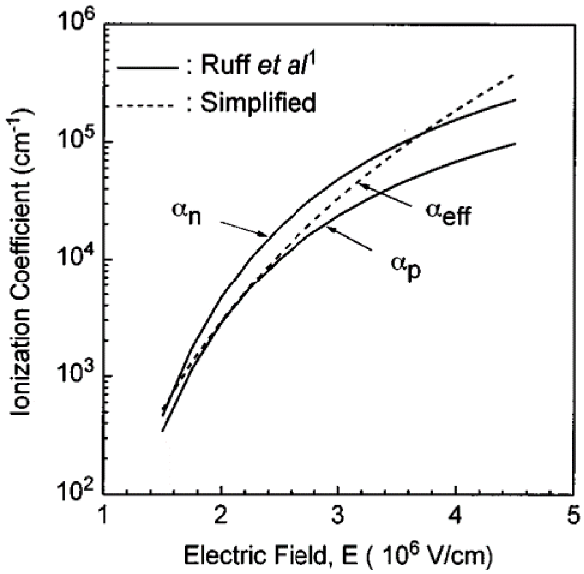

Figure 3.6 Impact ionization coefficients for 6H-SiC. Although the electron and hole coefficients differ somewhat, approximating them with αeff allows a simplified solution to the inoization integral (from [48]**).**

The second term shown above in the multiplication factor is reduced to what is known as the ionization integral and the condition for avalanche breakdown is

$$\int_0^w \alpha_n(x)dx = 1 \tag{3.13}$$

for when the multiplication factor approaches infinity. However, this approximation has its limitations in semiconductors where the electron and hole ionization coefficients are too different. The analytical solution for current multiplication for electrons is given by

$$M_n = \frac{\left[1-\left(\beta_p / \alpha_n\right)\right]\exp\left\{\alpha_n W\left[1-\left(\beta_p / \alpha_n\right)\right]\right\}}{1-\left(\beta_p / \alpha_n\right)\exp\left\{\alpha_n W\left[1-\left(\beta_p / \alpha_n\right)\right]\right\}} \tag{3.14}$$

where the dependency on the coefficients is apparent. At one extreme where $\beta_p=0$ the multiplication factor reduces to

$$M_n = \exp(\alpha_n W) \tag{3.15}$$

where no asymptotic breakdown behavior in the current will occur but will instead increase exponentially. In between $\alpha_n=\beta_p$ and $\beta_p=0$ the current multiplication will behave as

$$M_n = \frac{\exp(\alpha_n W)}{1-\left(\beta_p / \alpha_n\right)\exp(\alpha_n W)} \tag{3.16}$$

in which the predicted current will depend on the ratio of the electron and hole ionization coefficients. For predicting breakdown in devices care must be taken when using the simplifying assumption of $\alpha_n=\beta_p$ so that the valid regions of operation and limits of the model are known.

3.2.3 Ionization Coefficients for GaN

Impact ionization coefficients in gallium nitride have been calculated for both the zinc-blende and wurtzite phases of bulk GaN for electron and hole initiated impact ionization using Monte Carlo techniques [27, 49]. They have also been measured in AlGaN/GaN HFET devices by measuring the impact ionization generated holes that add to the gate current in [28]. More recently they have been measured in bulk GaN epitaxial layers grown on GaN and Sapphire substrates by Ozbek using an Electron Beam Induced Current (EBIC) technique [50]. Additionally Bertazzi et al. have recently calculated more accurate ionization coefficients in wurtzite GaN using a Monte Carlo model that includes band-to-band tunneling effects that become important at high electric fields [44]. His results show an increase in the ionization coefficient which predicts well the breakdown voltage of GaN avalanche photo-detectors [51]. Some measurements and simulation results for wurtzite phase bulk GaN electron initiated ionization coefficients are shown in figure 7 where the increase in the ionization found by Bertazzi et al. is evident.

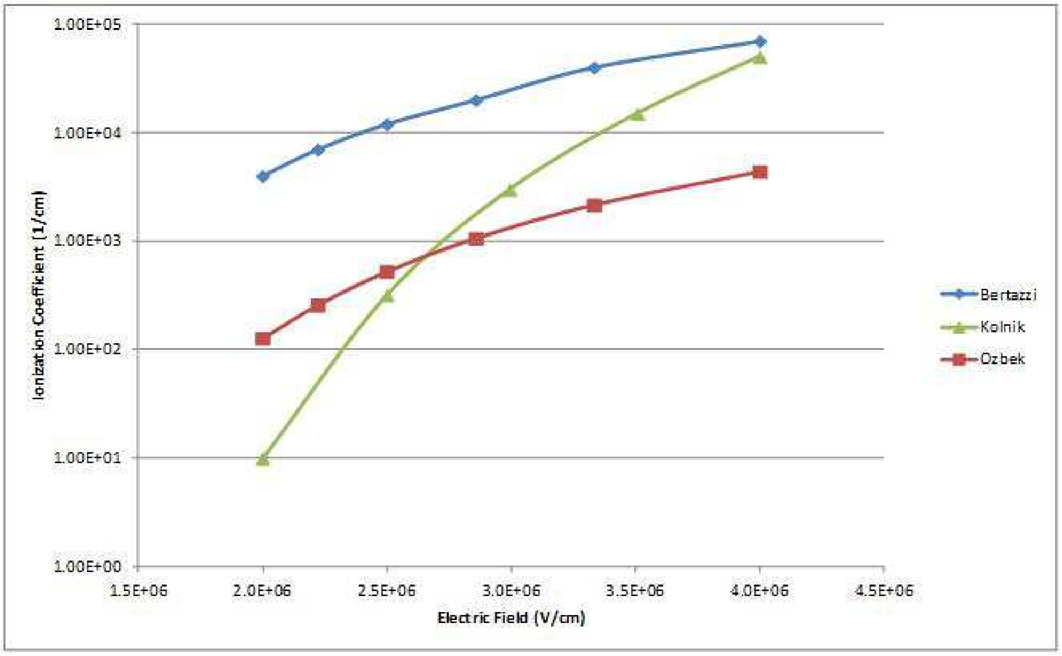

Figure 3.7 Comparison of electron impact ionization coefficients (1/cm) (electron initiated) for wurtzite GaN vs. electric field (V/cm). Data points taken from [27, 44, 50]**.**

For the purposes of modeling breakdown in AlGaN/GaN HFETs electron initiated ionization rates were chosen opposed to hole initiated rates considering that the main transport mechanism is majority charge transport in a 2DEG. The results from reference [44] were used taking into account the improved accuracy of the simulations, the fitting to experimental measurements, as well as inclusion of high-field effects considering the high magnitude electric fields that are typically present in AlGaN/GaN HFETs. The approximation of $\alpha_n = \beta_p$ in GaN is suitable for modeling the impact ionization in AlGaN/GaN HFETs since the electron and hole coefficients are close and increasingly so at higher electric field magnitudes shown in figure 8.

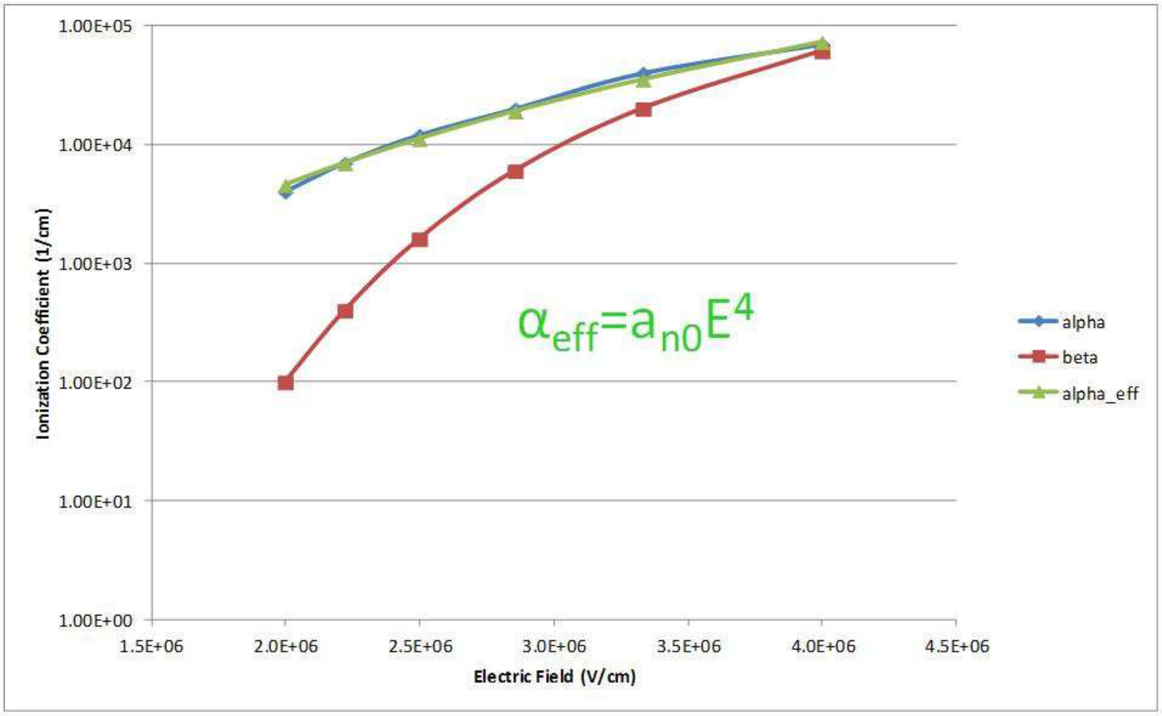

Figure 3.8 Electron initiated ionization coefficients for electrons (blue diamonds) and holes (red squares) in wurtzite GaN from reference [44]**. The effective ionization coefficient (green triangles) is fit as a power function.**

In order to provide analytically tractable solutions to the ionization integral when the expression for the electric field is a function of position within the device a simplification of the effective ionization coefficient is needed. Fulup first approximated the effective ionization coefficient while deriving simple and accurate analytical expressions for avalanche breakdown in silicon p-n junctions [47]. He found that by approximating α_{eff} as

$$\alpha_{eff} = cE^{g}cm^{-1} \tag{3.17}$$

where c and g are constants used to fit the curve, he could derive simple expressions with minimal error. This has become known as the Fulop Approximation and is a widely used method for calculating impact ionization and breakdown in power devices [48, 52, 53].

3.3 TCAD Investigations of Impact Ionization in AlGaN/GaN HFETs

A compact model for avalanche breakdown in the channels of AlGaN/GaN HFETs is derived based on information gleaned from the results of TCAD simulations using Silvaco TCAD software. Performance of the HFET device in specific regions of operation important in breakdown were investigated. The TCAD simulations allow the use of an accurate description of the internal device physics to derive a simplified physical model of impact ionization in the channel.

In this chapter, the physical behavior of conduction in the HFET channel is discussed with respect to the operation of the compact model of [40]. Then, results from TCAD simulations will be presented that show the high-field depletion region in the conducting channel at the drain-side gate edge of the device is where impact ionization initiates.

3.3.1 Brief Overview of Compact Model

In the previous section it was determined that the necessary conditions for avalanche ionization are a sufficiently high electric field magnitude as well as current flow along the same direction as the field. This theory can be applied to the high field region in an AlGaN/GaN HFET channel to calculate impact ionization current and determine the avalanche breakdown voltage. First it is important to define the physical location of the high field regions within the device channel where impact ionization is likely to occur.

We know from experiments that high magnitude electric fields can occur in the conducting channel of AlGaN/GaN HFETs. The lateral electric field magnitude can vary from less than 1 MV/cm to more than 4 MV/cm under different regions of operation with the highest occurring for large negative gate voltages (near pinch-off) and large drain voltages. Under this condition, with the channel above pinch-off yet not fully open, it is instructive to follow the path of 2DEG electrons from source to drain to understand where and why a high field depletion region arises.

A physics-based compact model of AlGaN/GaN HFETs has recently been developed [40]. This model separates the device into five regions or zones in which the dominant operational physics are modeled in a one-dimensional channel. Current continuity is imposed at the boundary of each zone to integrate the various zones into one complete model. An important requirement of the impact ionization model is efficient integration within the existing full HFET compact model. Using the five zone model overlaid on a snapshot of the electron concentration contour from TCAD simulation in Figure 9, we can trace electron conduction through the structure and understand the basic operation of the model.

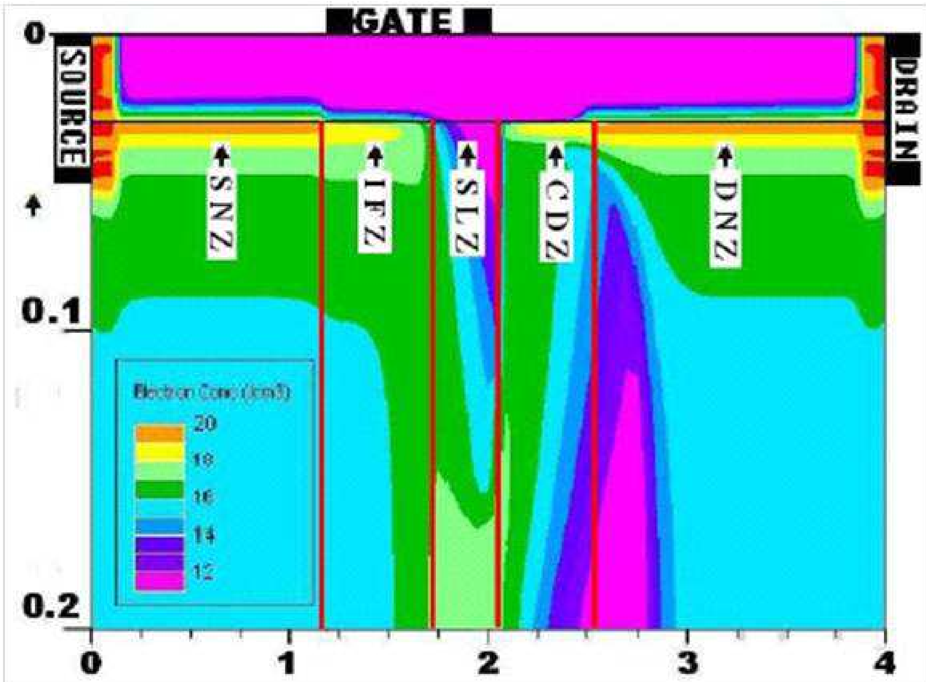

Figure 3.9 Diagram of an AlGaN/GaN HFET structure showing the boundaries of the five zone compact model overlaid on a two-dimensional contour plot of electron concentration from TCAD simulations [54]**.**

Electrons injected from the source into the channel move across the Source Neutral Zone or Zone 1. The 2DEG is completely filled and any vertical slice through the device is charge neutral with the ionized surface donors and the 2DEG electrons balancing the combination of piezo-electric and spontaneous polarization charges in the AlGaN layer. The intrinsic FET zone or zone 2 begins as electrons enter the channel region under the gate. Upon entering zone 2, there is now metal where positive donor-like states once were, the polarization field is thus reduced and the channel is depleted. Travelling further under the gate electrons encounter a narrow region named the Space-Charge Limited Zone or Zone 3 where the drain voltage drop near the gate edge is forcing the junction to a flat band condition. The channel is fully depleted and electrons are being injected into the bulk GaN and driven towards the bottom of the device. In the Charge Deficit Zone or Zone 4, the electrons that were forced into the bulk underneath the gate now rapidly return towards the AlGaN/GaN interface. The channel is reestablished and the 2DEG electrons are partially recovered creating a net space charge where the majority of the drain potential is dropped. The lateral electric field in this region reaches a peak at the gate edge and decreases linearly until the 2DEG fully recovers. In this region, impact ionization is the highest due to the large magnitude lateral electric field and a substantial lateral current flow in the channel. The Drain Neutral Zone or Zone 5 which marks the end of Zone 4 where the lateral electric field becomes constant is similar to Zone 1.

3.3.2 TCAD Simulations Focused on Impact Ionization

Simulations were performed using TCAD software to investigate regions and conditions within an industrial HFET design in which impact ionization may occur. The device structure used in the simulations is shown below in Figure 10. Drift-diffusions transport equations were solved using a field dependent mobility and Shockley-Read-Hall recombination models [24]. Horizontal cut-lines across the entire 4 um width are made at four positions in the device starting at the center of the channel, 10 nm below, 70 nm below, and finally 150 nm below the channel near the bottom of the device. The device under consideration is biased at V_g=-4 volts, and V_d=50 volts. The following parameters are reported to outline where within the device impact ionization is likely to occur; Lateral Electric Field (E_x), Vertical Electric Field (E_y), Lateral Current Density (J_x), Vertical Current Density (J_y). Impact ionization simulations were performed on the same device using the

Selberherr model [24]with ionization parameters taken from the experimental results of Kunihiro et al.[28] in which α_n=2.9x10^8 cm^{-1} and β_n=3.4x10^7 V/cm. The results of the simulation is a two-dimensional contour plot of the Impact Ionization Generation Rate (I_{gen}).

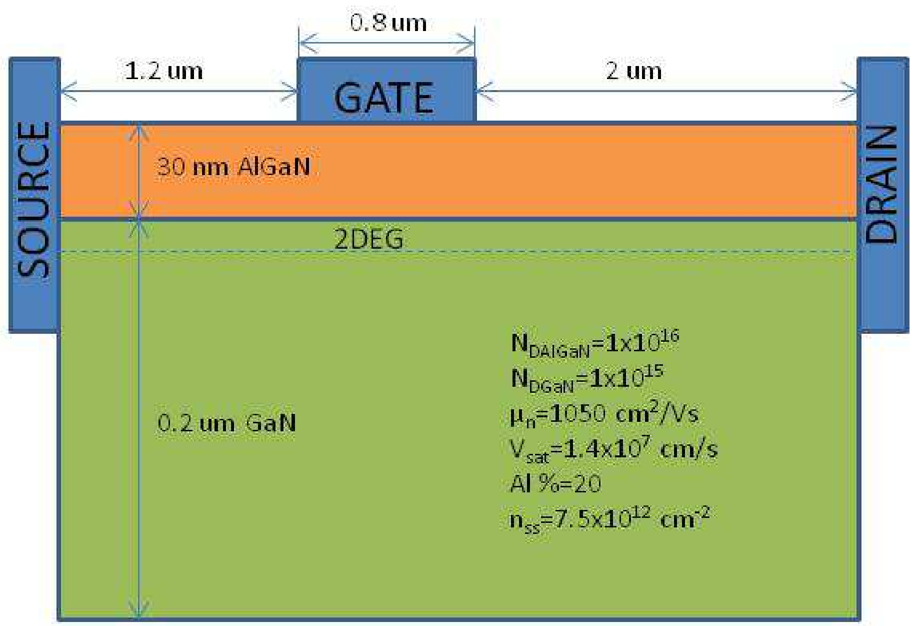

Figure 3.10 Industrial AlGaN/GaN HFET device design used for Silvaco™ TCAD simulations. Dimensions are marked as well as essential parameters used in the simulation.

Impact ionization in AlGaN/GaN HFETs can easily occur due to their ability to sustain high bias voltages. The resulting high magnitude electric field magnitudes developed in the device channel, particularly in the charge-deficit zone, coupled with a large two-dimensional current density in the lateral direction can lead to significant charge generation. The lateral electric field in the gate-drain region is show in Figure 11 below. The peak magnitude of the lateral electric field is found to occur at the drain-side gate-edge of the device. Here the field maximum reaches approximately 3 MV/cm in the channel at the AlGaN/GaN interface and drops off quickly, falling below the critical field for impact ionization of E_{crit}=2 MV/cm approximately 20 nm below the channel. The lateral electric field will always be highest in the channel and can exceed E_{crit} well into the CDZ.

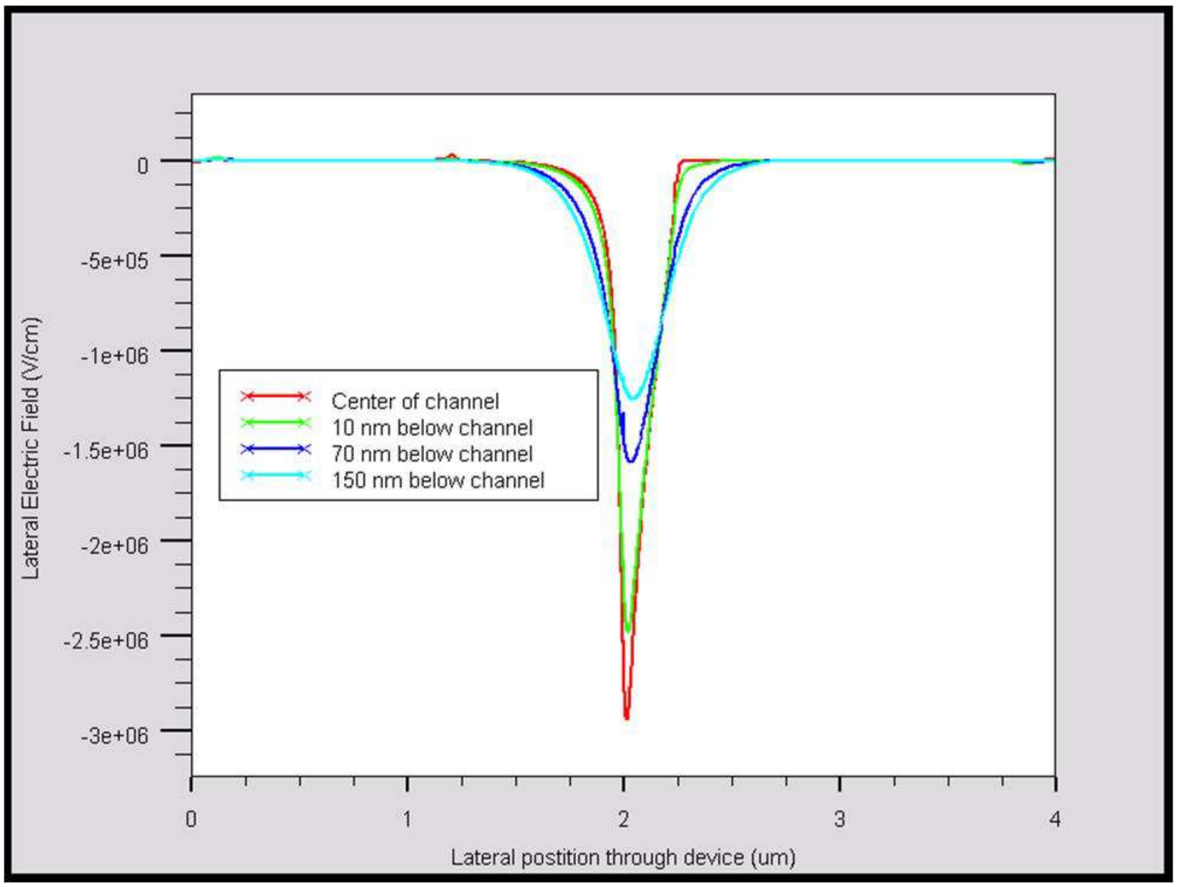

Figure 3.11 Lateral electric field profile (V/cm) along several horizontal cut-lines through the device staring at the center of the 2DEG channel and ending near the GaN/Substrate interface.

Another aspect in determining where impact ionization occurs in the device is to find where current flow is in the same direction as the electric field since we are interested in electrons that are being accelerated by the field as discussed in section 3. Shown in Figure 12, horizontal cut-lines from the same locations as Figure 11 are plotted for the lateral current density. Evident in this plot is that the lateral current density is most significant in the channel region and is increasing rapidly from the gate edge and on into the charge deficit zone towards the drain. The conclusion from the results shown in figures 11 and 12 is that the depletion region starting at the gate edge and ending at the recovery point of the 2DEG is where impact ionization is first initiated and likely dominant. In the drain and source neutral zones where the current density is very large, J_x=-2.4x10^6 A/cm^2 , the magnitude of the lateral electric field is well below 1 MV/cm and is too small to cause significant impact ionization [55]. Starting at the gate edge (x=2 um) and moving toward the source, the lateral electric field decreases rapidly to well below 2 MV/cm within the first 20 nm with the conditions for impact ionization never quite being met. The current is spread out in the bulk. The current density at 150 nm below the channel, which is near the bottom of the GaN buffer, is approximately J_x=-1x10^5 A/cm^2 due to electrons being forced deep into the bulk under the influence of the gate and drain voltages. This region may contribute a small amount to the total charge generated by impact ionization under conditions that allow the field to become sufficiently high.

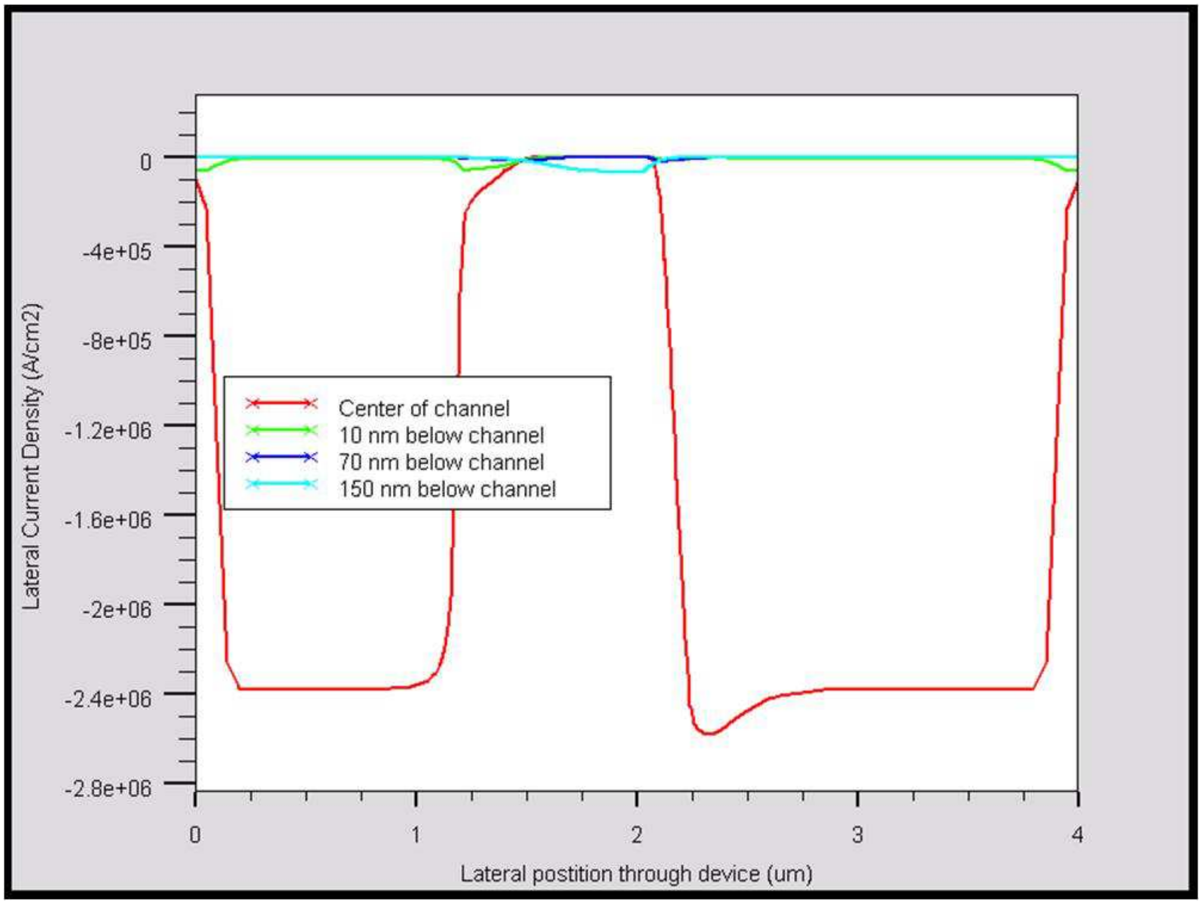

Figure 3.12 Lateral current density (A/cm^2) profile along several horizontal cut-lines through the device staring at the center of the 2DEG channel and ending near the GaN/Substrate interface.

The simulation results for the vertical electric field and vertical current density illustrate a similar structure but with substantially lower magnitudes as shown in figures 13 and 6. In the source and drain access regions, the vertical electric field due to the polarization field across the AlGaN layer is large and nearly constant at approximately E_y=1x10^6 V/cm which is typical for these devices[18]. In these regions the vertical current density is zero with no impact ionization occurring. In the channel under the gate, the net field is reduced and driven negative towards the gate edge as the channel is depleted. The vertical field magnitude is largest in the channel and gets smaller for every point further away in the GaN. The vertical current density behaves opposite with the peak value occurring near the bottom of the GaN layer so that even if the vertical field could meet E_{crit}, significant impact ionization is not likely in the channel.

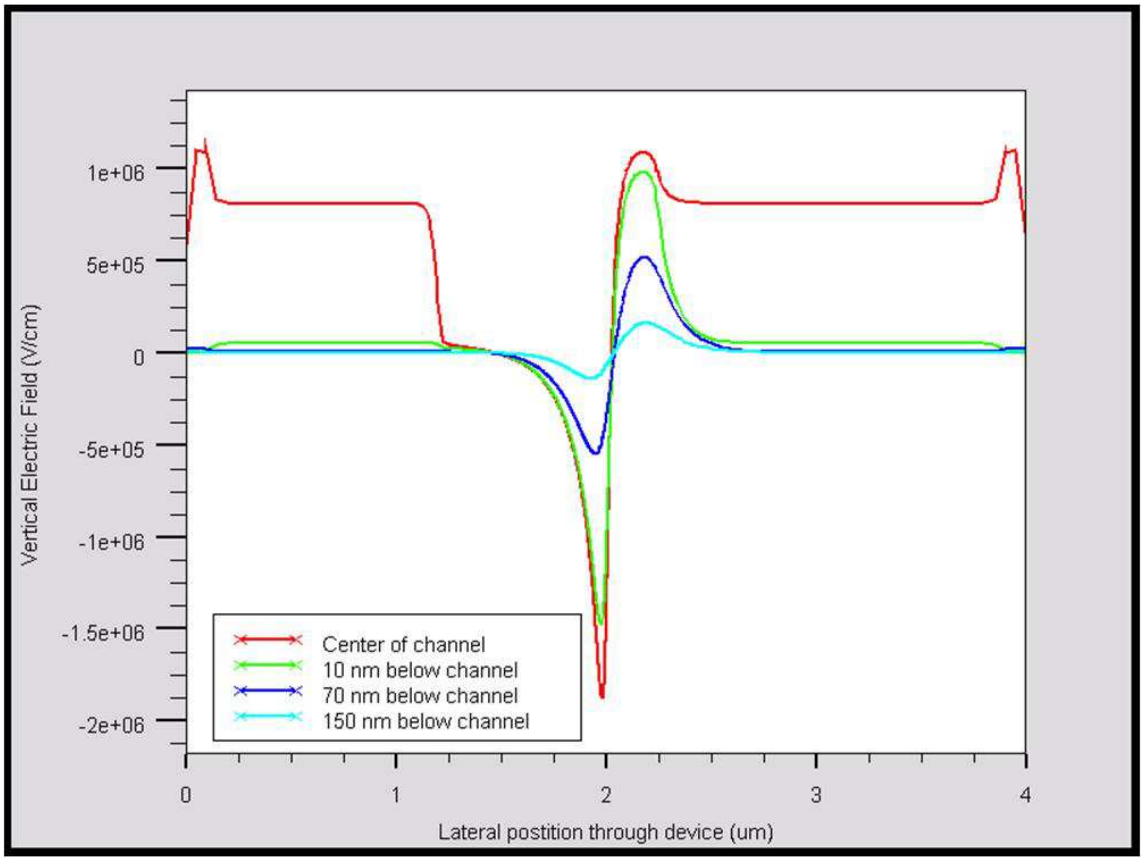

Figure 3.13 Vertical electric field (V/cm) profile along several horizontal cut-lines through the device staring at the center of the 2DEG channel and ending near the GaN/Substrate interface.

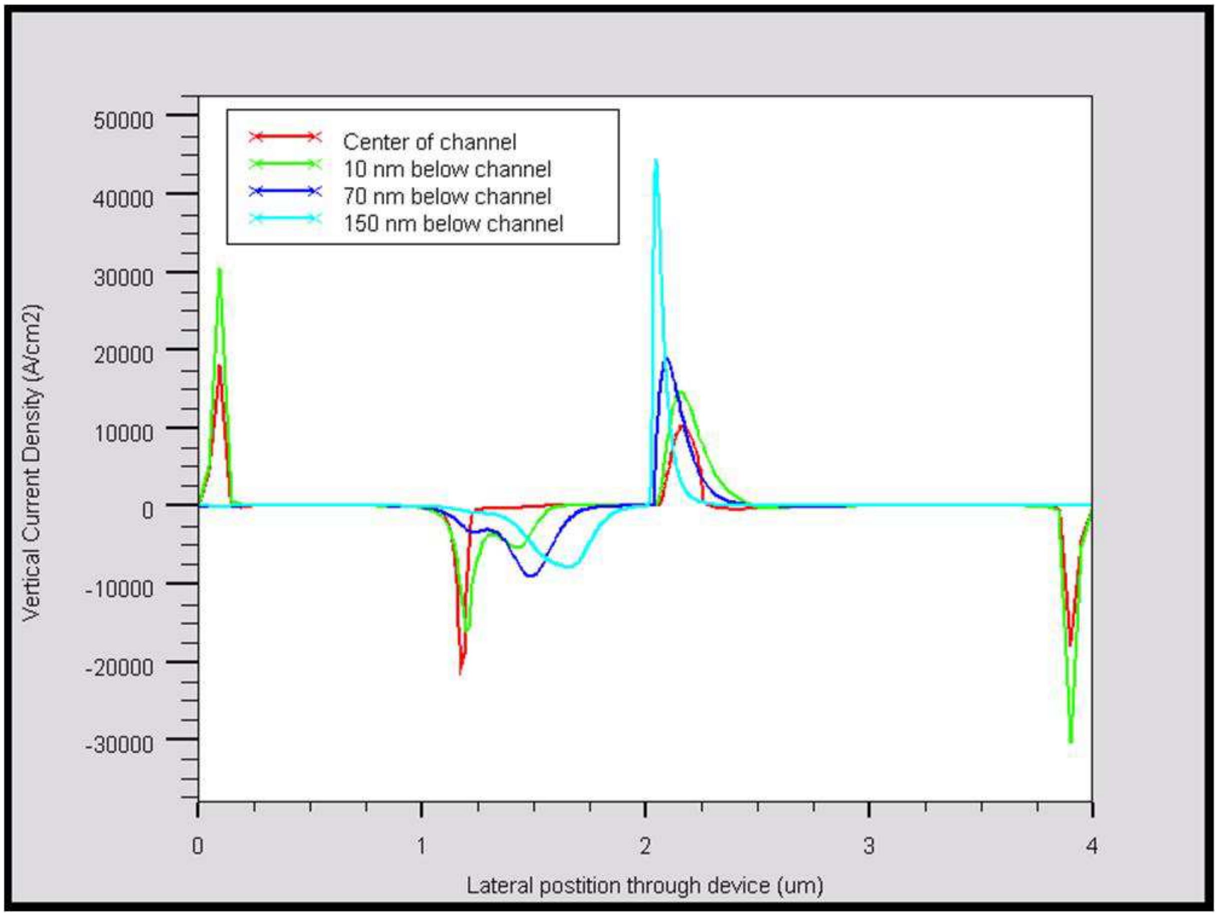

Figure 3.14 Vertical current density (A/cm^2) profile along several horizontal cut-lines through the device staring at the center of the 2DEG channel and ending near the GaN/Substrate interface.

An important result of these simulations is that the impact ionization mechanism prevails in the region immediately adjacent to the drain-side gate edge. The large lateral electric filed and lateral current density that dominate charge generation by impact ionization is most significant in the channel area. This information allows for a simple one-dimensional model of impact ionization in the channel to be developed.

Figure 15 below shows a two-dimensional contour plot of the impact generation rate within the device. The Selberherr impact ionization model was used with ionization coefficients to match those determined experimentally by Kunihiro et al. in [28]. As expected charge generation in the channel at the drain-side gate edge is the most intense reaching values near 10^{25}/cm^{3}s.

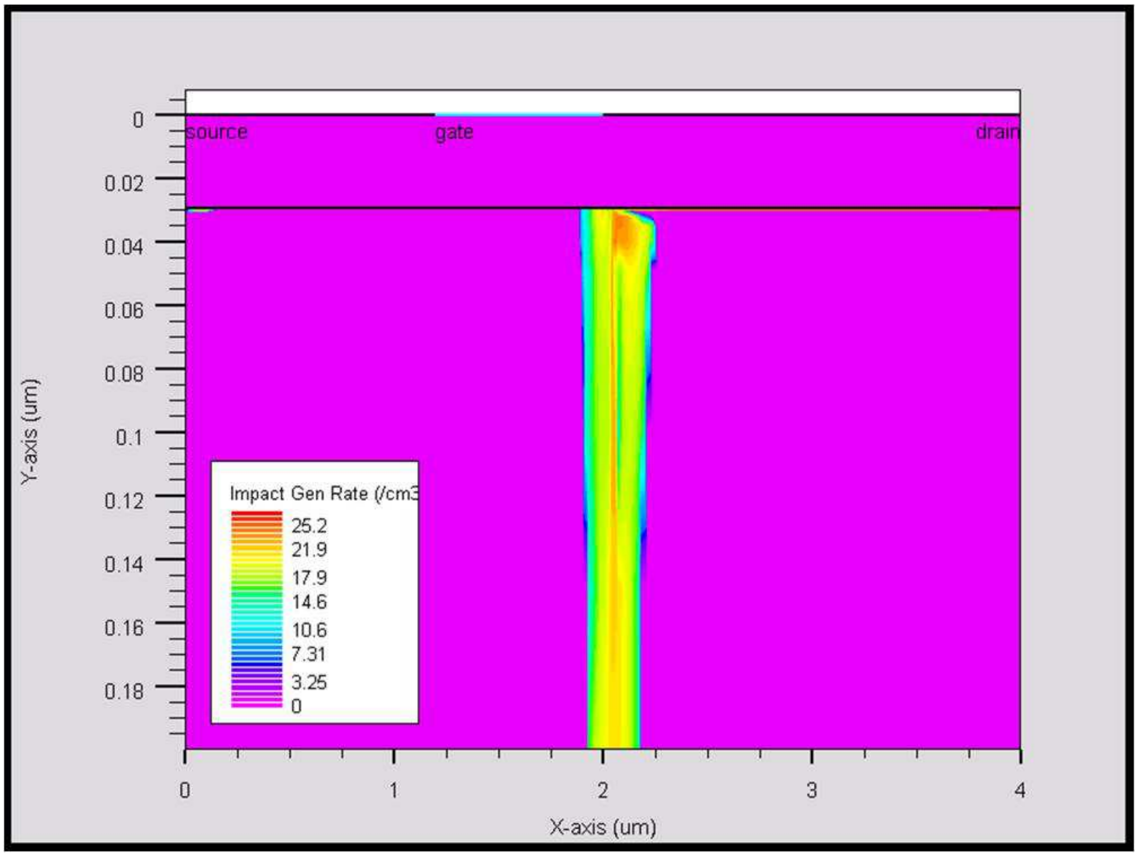

Figure 3.15 Contour plot of the impact generation rate (cm^{-1}s^{-1}) using impact ionization coefficients of α_n=2.9x10^8 cm^{-1} and β_n=3.4x10^7 V/cm from reference [28].

3.4 Breakdown Model

AlGaN/GaN HFETs can operate under some considerably large voltages and currents which can lead to conditions ideal for impact ionization and breakdown in the device channel. In the previous section we discussed these conditions as well as the relevant regions within the device. We also looked at the basics of impact ionization and ionization coefficients from a carrier transport perspective and then went on to relate these coefficients to the multiplication of current flowing through the device. Using this information, a model for avalanche breakdown for AlGaN/GaN HFETs can be derived.

Previous analysis of TCAD simulations has shown that the high field depletion region that begins at the gate edge and ends at some bias dependent point in the drain access region is the location where impact ionization initiates and is the most intense. Using this information and avalanche ionization theory, a model can be proposed of this region on which the generated current can be calculated.

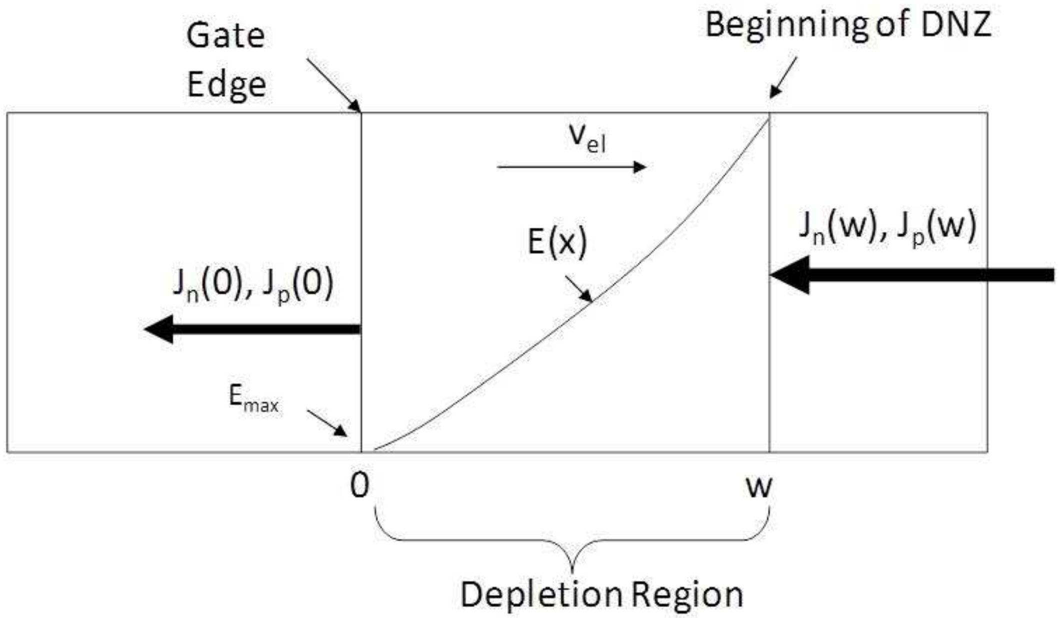

Figure 3.16 Outline of what a one dimensional model of the channel region that could be used to calculate impact ionization.

As shown in figure 16 the depletion region extends from x=0, which is the drain-side gate edge where the maximum of the lateral electric field occurs, E_{max}, to x=W where the 2DEG is fully recovered where the start of the Drain Neutral Zone is defined. Assuming electron initiated impact ionization, it is necessary to find the analytical form of the electric field in the depletion region (shown as some arbitrary function in the diagram) to be able to solve the ionization integral

$$\int_0^w a_n e^{\frac{-b_n}{E}} dx = 1 \tag{3.18}$$

and determine the multiplication factor for the drain current. So, the expression for *E(x)* can be obtained by solving Poisson's equation in the high field region which may be modeled based on TCAD simulations. More simulations and analysis of the device behavior will be needed to come up with an accurate electric field profile in the region especially close to the drain-side gate edge. Then some simplifying assumptions about the ionization coefficients will need to be made to get an analytical solution to the integral.

In this section, the preliminary models of impact ionization and avalanche breakdown for AlGaN/GaN HFETs that were instrumental in developing the final breakdown model, are reported. Guided by 2-D finite-element simulations of the HFET structure using Silvaco™ TCAD software, several approaches to the model were investigated. A simple model was first studied based on analogous behavior of the depletion region width versus voltage behavior and electric field profile to an abrupt P^+-N junction diode. Next, when the abrupt model did not appear to capture the *W(V)* behavior accurately for the proper charge density in the channel, a slightly more complicated model was introduced which modeled the behavior of charge at the drain-side gate edge in the channel as having a hyper-abrupt diode doping profile. The hyper-abrupt model fit the behavior quite well but the simple expression left the model with fitting parameters that would need to be extracted. The final preliminary model presented takes into account a narrow "high-field region" immediately next to the gate edge. This two dimensional model attempts to predict the width of the high-field region by using a simple two-line charge model from electromagnetics. This model can determine where the vertical electric field becomes constant as electrons travel from the bulk GaN back into the device channel. The results of the investigations of these modeling approaches are important for possibly adding increased functionality to the breakdown model or for enhancing the model for different technologies.

3.4.1 Preliminary Modeling Approach and Results

In order to find the excess current due to impact ionization and the avalanche breakdown voltage, an expression for the electric field in the Charge Deficit Zone is necessary. Referring to Figures 11 and 12 in section 4, looking at a horizontal cutline through the center of the channel, current flow is interrupted underneath the gate in the SCL zone and becomes almost completely vertical as electron are pulled down into the bulk and towards the drain under the influence of the gate and drain voltages. Lateral current flow quickly resumes once electrons emerge on the drain side of the gate and the 2DEG is reestablished. This characteristic creates a one dimensional electric field profile through the channel that resembles an abrupt P^+- n junction. Here the drain-side gate edge represents the junction and the depletion region on the lightly doped side is represented by the CDZ with a net positive space charge due to the only partially recovered 2DEG. The CDZ behaves like a reverse biased abrupt junction diode as the depletion region grows with increasing drain voltage and a linear electric field profile. This effect is apparent in figure 17 below which shows the lateral electric field profile in the channel for a constant gate voltage, V_g=-4, and drain voltage ranging from V_d=10 to 80 volts. Compared with the P^+-N abrupt junction diode electric field profile shown in figure 18, where the junction occurs at the gate edge, the behavior is nearly identical. This behavior in the HFET is not due to any type of junction formed within the device channel but rather from an abrupt change in charge densities near to the gate edge that can be likened to a hi-lo structure.

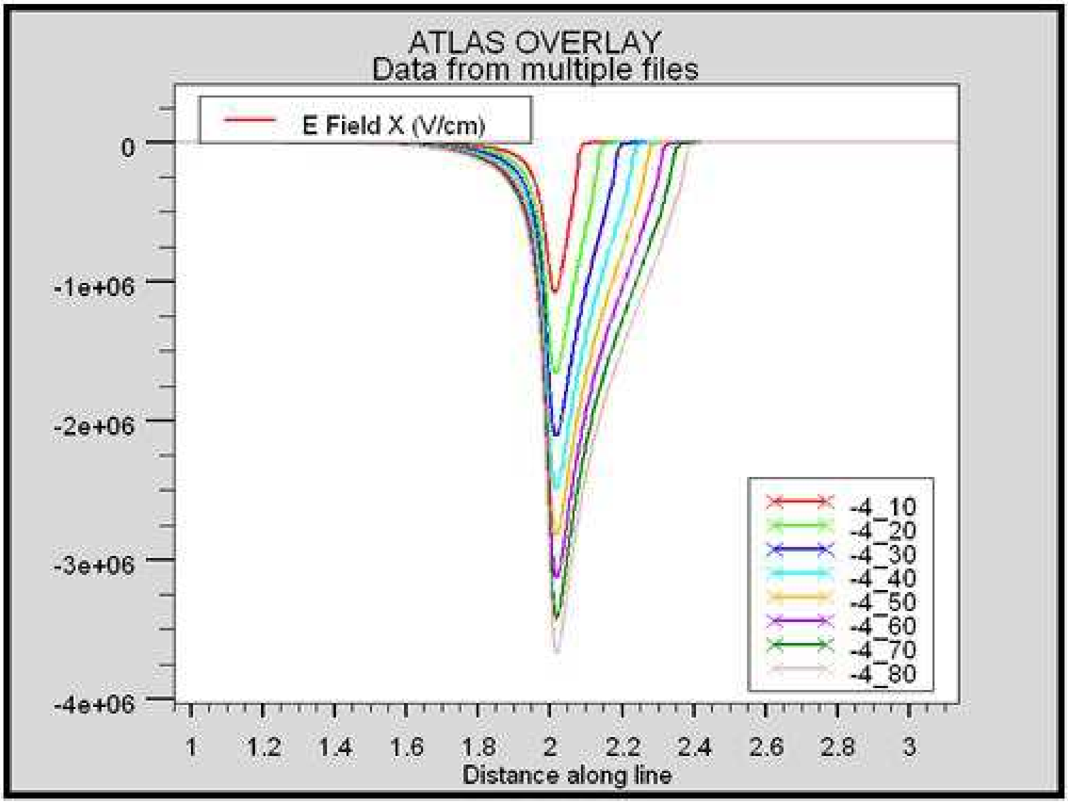

Figure 3.17 Lateral electric field (V/cm) along a cutline through the center of the conducting channel. The gate is biased at pinchoff, Vg=-4 V with drain bias ranging from Vd=10 to 80 V.

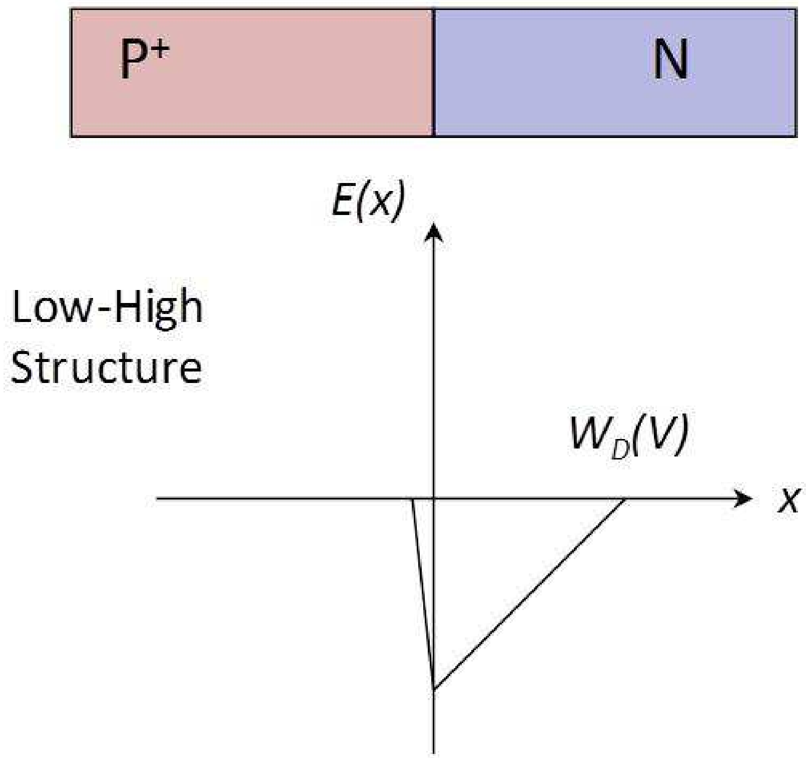

Figure 3.18 Analogous description of the depletion region width of an abrupt junction diode to the Charge Deficit Zone in an AlGaN/GaN HFET.

If the diode analogy is an accurate approximation to the operation of the HFET then the electric field in the CDZ is simply the classic result from Poisson's equation for a one-side abrupt junction diode where the voltage accross the junction is equal to the voltage across the CDZ. Substitution of *E(x)* into the ionization integral will give the width dependent breakdown voltage and the impact ionization generated current.

First the depletion layer width versus applied voltage must be verified to see if the behavior of the HFET CDZ is really analogous to a diode model. To do so, an industrial AlGaN/GaN HFET device was simulated in Silvaco™ ATLAS for various drain biases from 10-100 V. The device was pinched-off such that the peak electric field magnitude was the largest. The width of the CDZ in the HFET was extracted from the results and plotted versus the applied drain bias.

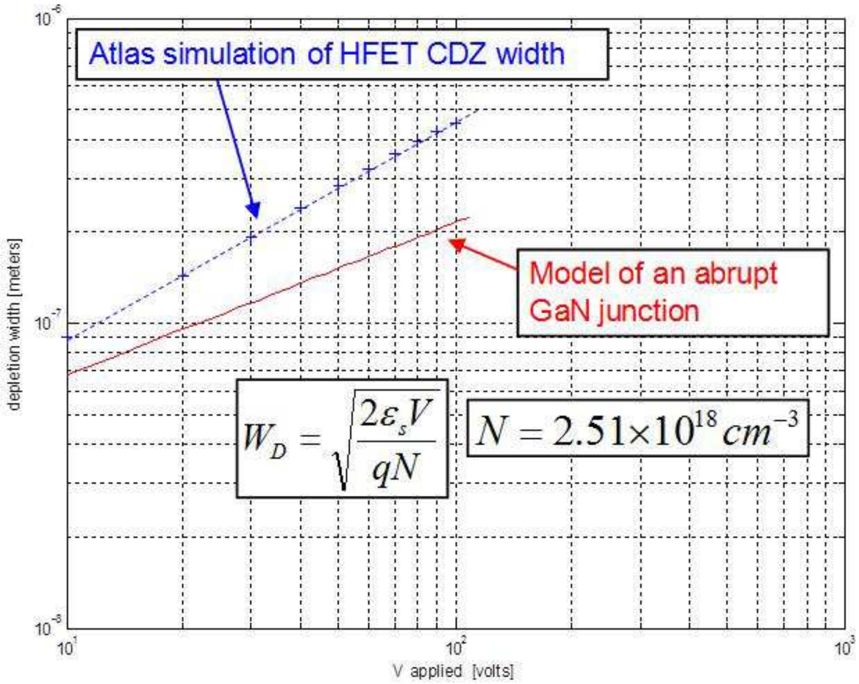

Figure 3.19 Abrupt diode model depletion layer width (red) and simulated HFET CDZ width (blue) versus applied voltage.

In addition to the ATLAS HFET simulation, a P^+- n GaN diode (linearly graded) was simulated and the depletion width versus bias was extracted to confirm model. Figure 19 shows the results of the experiments. The measurements for the HFET and the diode are plotted alongside the *W(V)* model for an abrupt junction. The doping in the N-side of the diode as well as the N in the abrupt model is 2.51 x 10^{18} cm^{-3} which was chosen to match the net positive charge in the HFET CDZ. The abrupt model doesn't quite predict the correct behavior. The CDZ width versus applied voltage for the HFET is incorrect and the functional dependence is not the same indicating that the physical behavior of the HFET cannot be fully captured by the simple abrupt diode model.

In the compact model described in [40, 54, 56], an approximation is made that the CDZ is composed of a constant net space charge that begins at the drain-side gate edge and expands toward the drain with increasing drain bias to accommodate the larger potential. This model has been shown to accurately predict the I-V and performance characteristics of AlGaN/GaN HFET devices [40, 54] as well as to accurately model the lateral electric field in the CDZ [57]. However, the constant net space charge region doesn't exactly begin at the gate edge since there is a finite distance through which the electrons that were originally forced into the bulk GaN need to travel back and partially refill the channel. This transition region is neglected in the compact model for its negligible effect on the predicted drain current but proves to be important for impact ionization calculations which require an accurate description of the peak electric field magnitude at the drain-side gate edge. In figure 20 this effect can clearly be seen in a plot of the electron concentration contours for a cutline though the center of the 2DEG plotted for several drain biases from V_d=10-100 volts with V_g=-4 volts and zoomed in to only show the gate-drain region of the HFET. Clearly, in the diode model of the 1-D channel, the space charge region is less like an abrupt junction and more like a Hyper-abrupt junction.

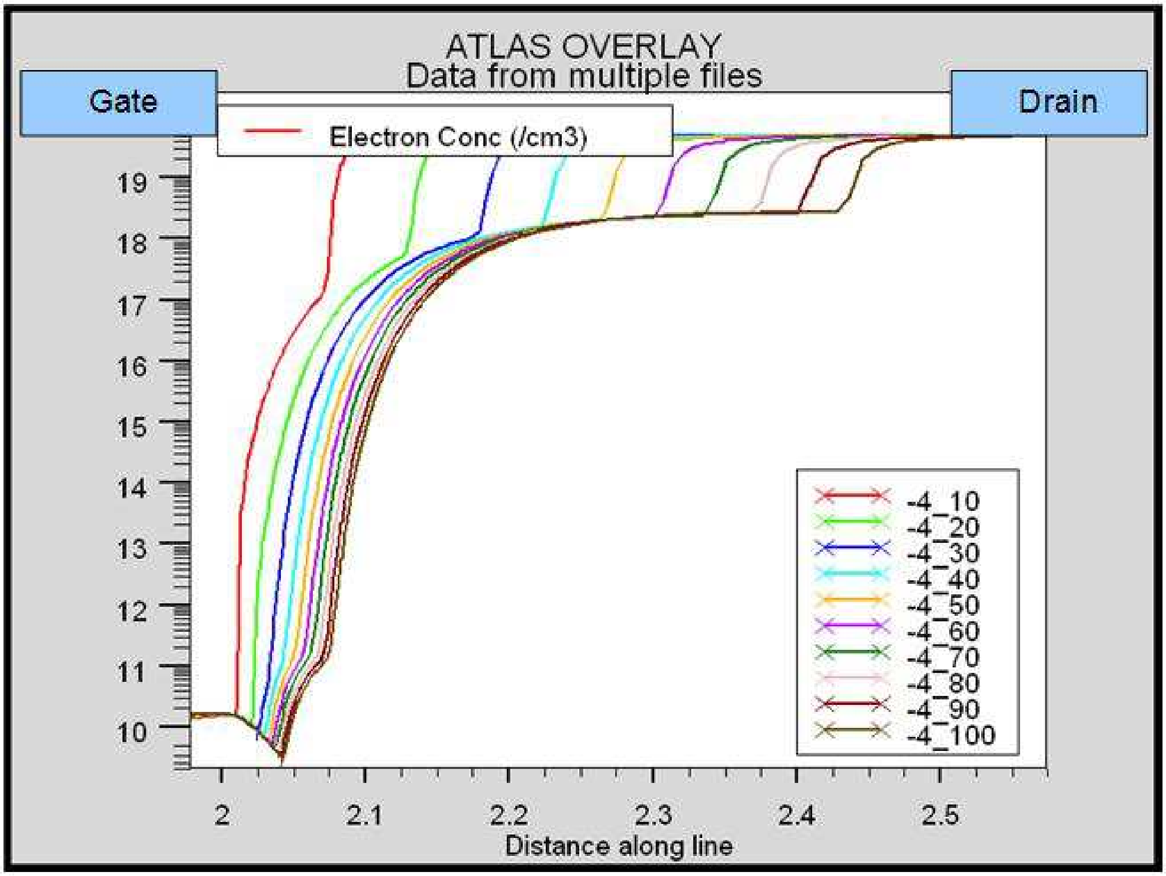

Figure 3.20 ATLAS simulation of a HFET at pinch-off and varying V_D ranging from 10-100 V. The displayed data are the electron concentrations on a cutline through the center of the channel where it is zoomed-in on just the gate-drain region.

Hyper-Abrupt Model

Consider the CDZ starting at the drain-side gate edge to be similar to a one-sided hyper-abrupt junction diode with a doping profile given by

$$N(x) = Bx^{m} \tag{3.19}$$

similar that in figure 21 where *B* and *m* can be used to approximate n(x). Then, the *w(V)* relationship can be found by solving Poisson's equation with the boundary condition that the electric field is zero at *W*, the following expression for the electric field can be obtained.

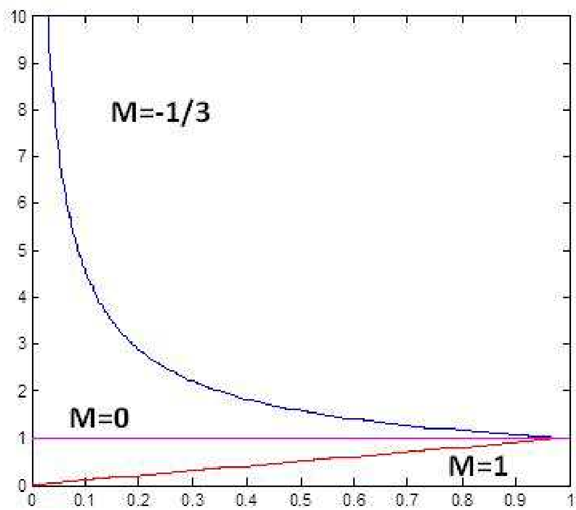

Figure 3.21 Plot of a hyper-abrupt charge profile (blue), abrupt (magenta), and linear (red).

The resulting expression for the electric field is

$$E(x) = -\frac{qB}{\varepsilon}\frac{(x^{m+1} - W^{m+1})}{(m+1)} \tag{3.20}$$

where the potential can be solved for using the boundary condition that *V(0)=0* such that

$$V(x) = -\frac{qB}{\varepsilon(m+1)}\left(\frac{x^{m+2}}{m+2} - W^{m+1}x\right). \tag{3.21}$$

And finally, if the voltage at *W* is $V_{applied}$ an expression for the depletion layer width versus the applied voltage is obtained.

$$W = \left[\frac{\varepsilon(m+2)V}{qB} \right]^{\frac{1}{m+2}} \tag{3.22}$$

Next in figure 22, a plot of the hyper-abrupt model depletion width versus voltage was compared to the HFET CDZ width plot just as in Figure 19. One note on the HFET width is that the measurement from Figure 19 to Figure 22 is different. The measurement in Figure 19 was taken from a simulation of the same device but with much coarser grid spacing that that in Figure 22. The coarse spacing made it difficult to judge where the CDZ actually ended so the simulation with the finer mesh allowed more accurate measurements and the error in the width reading is negligible (on the order of one nanometer).

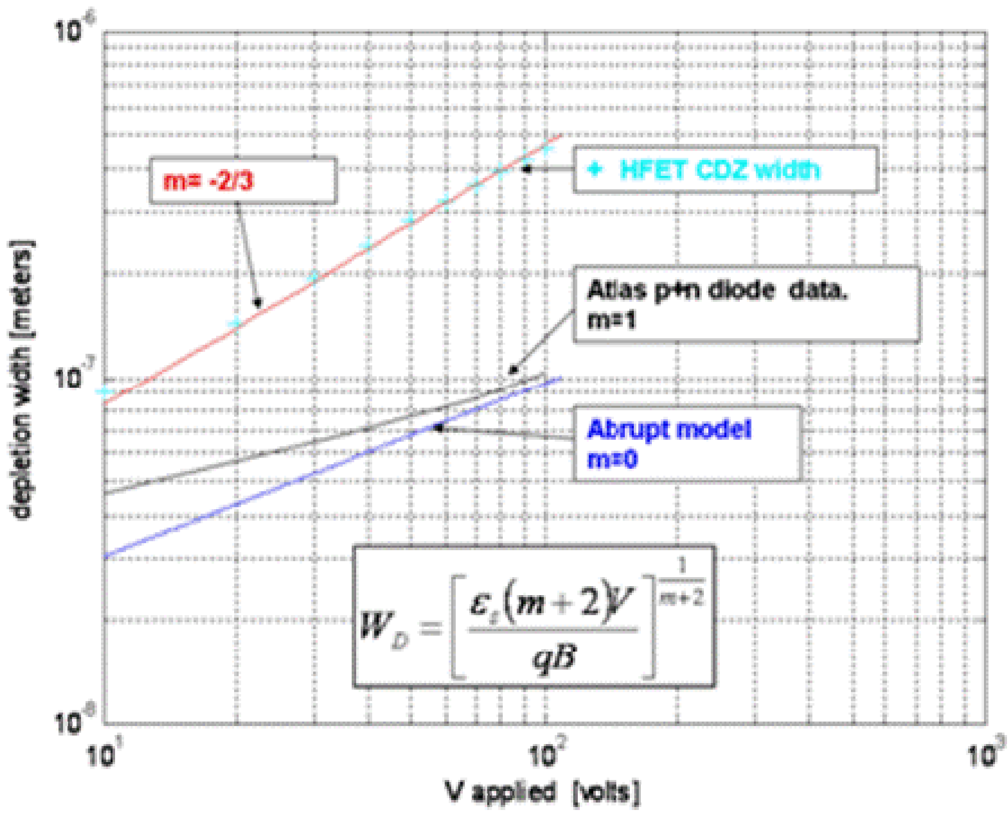

Figure 3.22 W(V) using abrupt junction model (m=0)(blue). W(V) from an atlas simulation of a linearly graded junction diode (m=1) (black). W_{CDZ} (V) from an ATLAS simulation of a GaN HFET (cyan +'s). W(V) using a hyper-abrupt junction model with m=-2/3 (red)

The cyan pluses are the measured data and the solid red line is the model of a hyper-abrupt junction. The value of *m* was adjusted until the slope of the model width matched the measured data. A value of *m=-2/3* was extracted for the charge profile. The value of *B* was adjusted until the graphs were aligned. A way to make a comparison between the model and the HFET is to extract a *B* and *m* from the simulation results for a particular voltage or voltage range and see how close the model is to the HFET. However, this is using *B* and *m* as fitting parameters. To capture the device behavior for any drain bias a physical derivation of $N(x)$ in the high-field transition region would be necessary and a one-dimensional model may not be sufficient. This leads to the need to find a better description of the physics in this region.

Two Dimensional Field Model

The two-dimensional field model is the last preliminary approach to modeling impact ionization that will be discussed. This model is also based on observations from TCAD simulations. Previous models assume that the vertical electric field is constant from the gate edge to drain contact. This assumption ignored the region immediately next to the drain-side gate edge but is fine since, as was determined earlier, the vertical is unlikely to contribute much to impact ionization in the channel. What we found is that there must be a transition region where electrons are attracted back to the channel and beyond the fringing effects from the gate the vertical field is allowed to switch polarity and return to the equilibrium value of the polarization field E_{pol}. A simplified drawing of the situation is depicted in figure 23 below. Simulations show that the high-field transition region in which the slope of the lateral field is sharply increased lasts until the vertical field returns to E_{pol}, This adds some complexity to the lateral field model since the new high-field zone boundary likely depends on V_g, the algan layer width (t_{algan}), as well as the polarization field (E_{pol}).

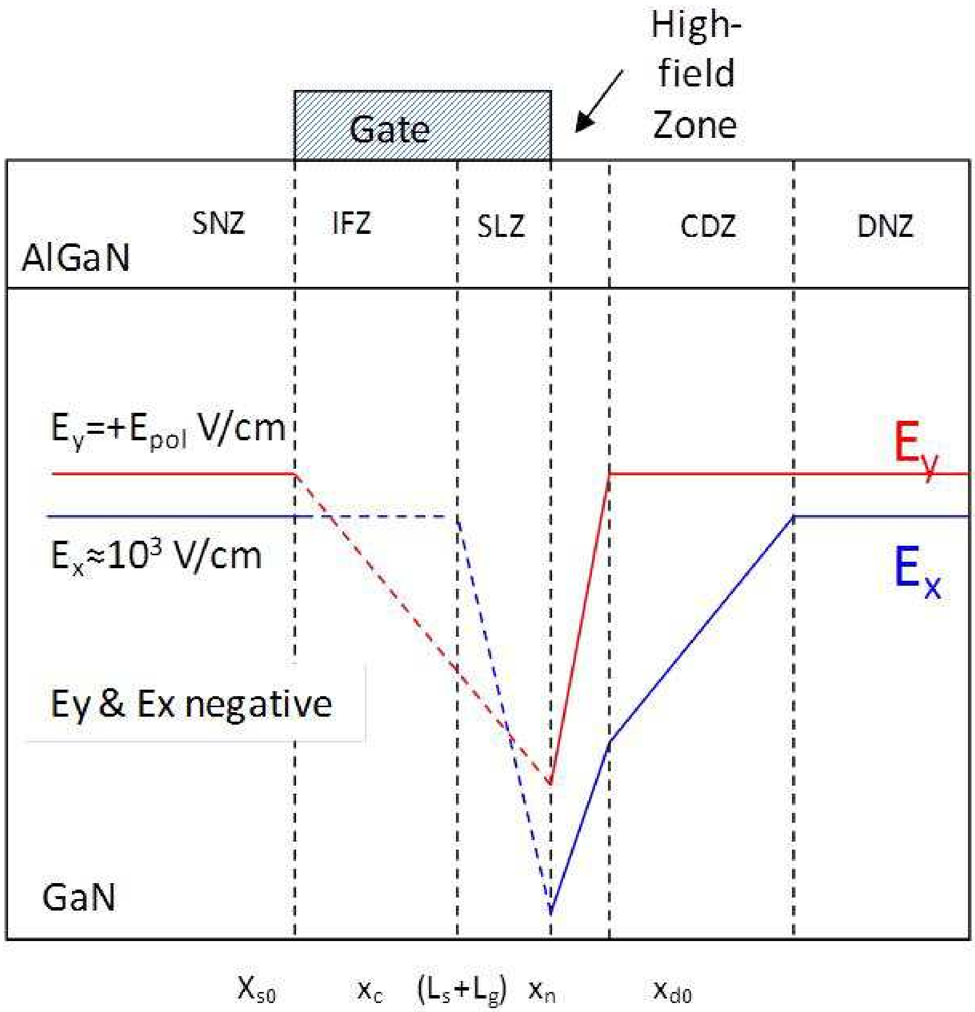

Figure 3.23 Simplified drawing of the vertical (red) and horizontal (blue) electric field profiles in the channel of an AlGaN/GaN HFET. The dashed portion under the gate is an approximation.

So a model that would incorporate the effects of the vertical field due to the gate and drain bias conditions was created as shown in figure 24. Here a two-wire line from electromagnetics is implemented to solve for the line charge. For any given bias, we have a Vg and a V_{34} which is the potential in the channel at the gate edged that is calculated in the compact model [40]. The charge present as a net line charge at the very corner of the gate is given by

$$\rho_l = \frac{\pi\varepsilon(V_g - V_{34})}{2\ln(d/a)} \tag{3.23}$$

which can then be used to calculate its radial field from according to the expression

$$\vec{E}_p = \frac{\rho_l}{2\pi\varepsilon}\frac{1}{r}\hat{r}\,. \tag{3.24}$$

When the y-component becomes negligible such that, the negative vertical field due to the interaction with the gate becomes small so that the vertical polarization filed is once again dominant, this will be the boundary of the high-field zone.

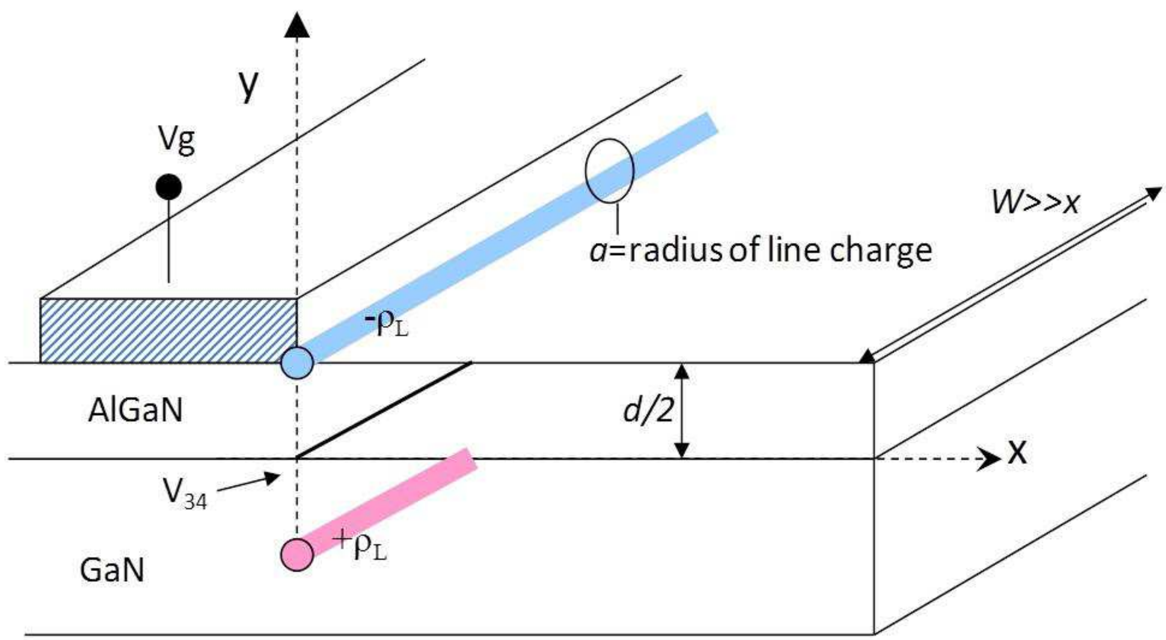

Figure 3.24 Two-line charge model of the 2-D electric field in the high-field region of the HFET.

Preliminary results showed that this was a good estimation of the width of the high-field zone but the model failed to agree with TCAD simulation results of devices of different AlGaN layer thicknesses.

3.4.2 Simplified lateral electric field model

The simple two-piece lateral electric field model was derived based on observations from TCAD simulations of an AlGaN/GaN HFET in addition to results from preliminary modeling attempts. As discussed in the previous section, the high-field zone that fills a narrow region near the drain-side gate edge displays a steeper slope in the lateral electric field profile. Due to an initially higher space charge in this extremely depleted region of the channel, there is a peaking of the lateral electric field when compared to that of the normal charge-deficit zone. A look at figure 25 below in which the lateral and vertical electric fields are plotted along a horizontal cutline through the channel shows the behavior previously described. The vertical field vector rotates from a maximum negative at the drain-side gate edge through zero towards its maximum value beyond the gate, and the lateral electric field is perturbed due to the rapidly increasing charge distribution in the channel.

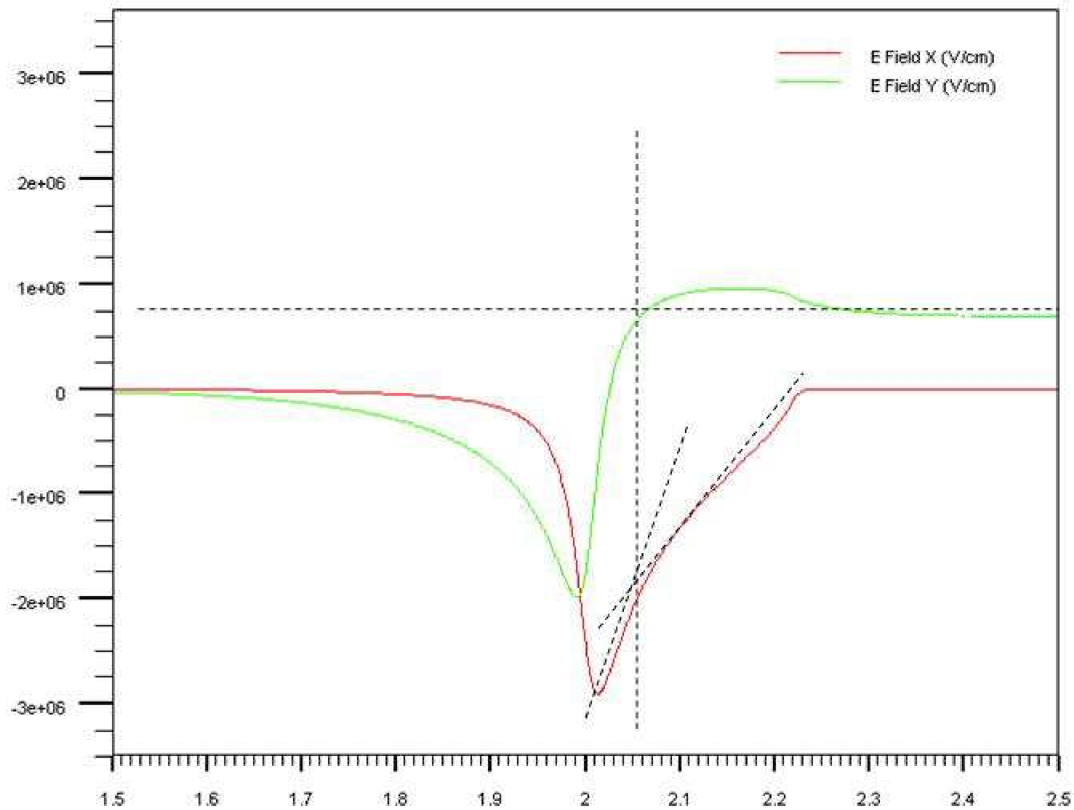

Figure 3.25 Overlay of the lateral (red) and vertical (green) electric field (V/cm) along a horizontal cutline through the conducting channel. Device is 4 um long, but graph is enlarged to show detail. A distinct change of slope of E_x occurs once E_y reaches E_{pol}.

The two sharply defined regions that result in the lateral electric field profile are the basis of the simplified breakdown model. Using TCAD simulations to study the behavior of these regions of the device, some simplifying assumptions can be made about the width of the high-field zone and the magnitude of the maximum lateral electric field at the gate edge. In this section the development of the model will be detailed. The parameters of the piecewise model that are extracted from TCAD simulations will be discussed. The regions of operation and conditions on which the approximations are valid will be presented through the simulation results of various device geometries and device bias conditions.

The channel breakdown model is formulated in order to integrate smoothly within the compact HFET model of [40] in which the HFET channel current is calculated by separating the device into five zones according to the dominant operational physics. Current continuity is imposed to integrate the various zones into a complete model. Of interest for the calculation of impact ionization current is the high electric field charge deficit zone or CDZ (Zone-4 or Z4), which extends from the drain-side gate edge to a bias dependent point in the drain access region where the 2DEG is fully filled and the magnitude of the lateral electric field is reduced to a low value, near zero. This zone contains a high magnitude electric field and the majority of the drain voltage is dropped over this depletion region next to the gate. Electrons are forced from the 2DEG channel by the high magnitude vertical electric field and then return to the 2DEG from the bulk at the edge of the CDZ zone. Simulations show the peak electric field in the channel at the gate edge can exceed a magnitude on the order of 1-3 MV/cm. Under large-signal RF operation and during the high voltage portion of the RF cycle, this peak field can easily exceed the critical electric field for impact ionization, assumed to be approximately 2MV/cm [28]. Note that gate leakage and trapping effects due to the high electric fields at the surface and in the channel, which can be a factor in current collapse, are not considered in the current version of the compact model. However, since the compact model is physics-based, these effects can be included and will be reported in another work.

Although the model of [40] accurately predicts the dc characteristics of the AlGaN/GaN HFET, it neglects the narrow transition region near the gate edge where the lateral electric field peaks to its largest value. The exclusion of the transition region in the compact model has a negligible effect on the device terminal characteristics. The impact ionization mechanism is, however, sensitive to the peak electric field and the original model can underestimate the peak field significantly leading to inaccuracies in circuit simulations where impact ionization is important.

3.4.3 TCAD Simulations Focused on E_x Behavior

The region in the conducting channel under the gate at the drain side edge is almost completely depleted and the lateral electric field magnitude drops off rapidly with distance moving toward the source allowing for only minimal impact ionization and is thus neglected. This effects were seen in detailed simulations in section 4. However, inside the high-field transition region a horizontal current flow is re-established in the channel under a significant lateral electric field so that the directions of the current and the electric field are aligned. Thus this region is where impact ionization initiates. Multiple TCAD simulations were performed to determine the width of the high-field region as well as the behavior of the lateral electric field. Table 1 lists the structure and parameters of the TCAD model. The physics models used in the TCAD simulations were drift-diffusion, field dependent mobility and Shockley-Read-Hall recombination [24]. The TCAD parameters were adjusted to fit the dc IV measurements (those in Table1) of an industrial AlGaN/GaN HFET device. Excellent agreement was obtained as shown in figure 26.

Table 1 TCAD Parameters for HFET Simulation

TCAD Parameter	Value
Electron mobility	1500 $cm^2/V\text{-}s$
Saturation velocity	$1.2x10^7$ cm/s
Al mole fraction	0.2
Gate length	0.8 um
Gate-Source spacing	1.2 um
Gate-Drain spacing	2 um
Gate width	400 um
AlGaN layer thickness	30 nm
GaN layer thickness	0.2 um
Unintentional doping-AlGaN	$1x10^{16} cm^{-3}$
Unintentional doping-GaN	$1x10^{15} cm^{-3}$
Polarization sheet-charge density	$7.04x10^{12} cm^{-2}$
Piezoelectric charge density	$1.04x10^{12} cm^{-2}$

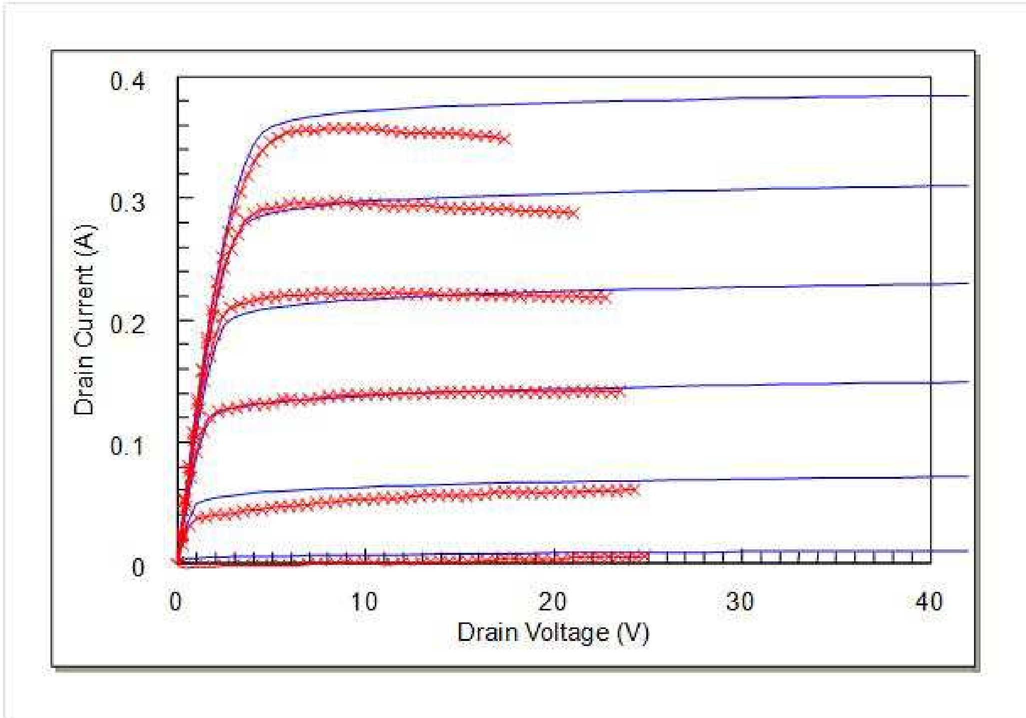

Figure 3.26 Measurements of an industrial AlGaN/GaN HFET device (red symbols) were fit to TCAD simulations (blue lines) for Vg=1 to -4 volts in 1 volts increments.

The width is determined from where the lateral electric field exhibits a distinct change in slope near the gate edge as shown in figure 25. Initial investigations revealed that the width of the high-field zone didn't change across different device dimensions with the exception of the AlGaN layer thickness. Simulations of the device with the parameters in table 1 with the exception of a variable AlGaN thickness showed a dependence of the high-field zone width versus t_{AlGaN}. This was not an accurate picture of a real device since it is know that the polarization field in the AlGaN layer, 2DEG charge density, and 2DEG mobility are all dependent on the AlGaN thickness [18, 58]. The structure was simulated again but this time using a modified and accurate charge profile for AlGaN thickness ranging from 17 to 30 nm.

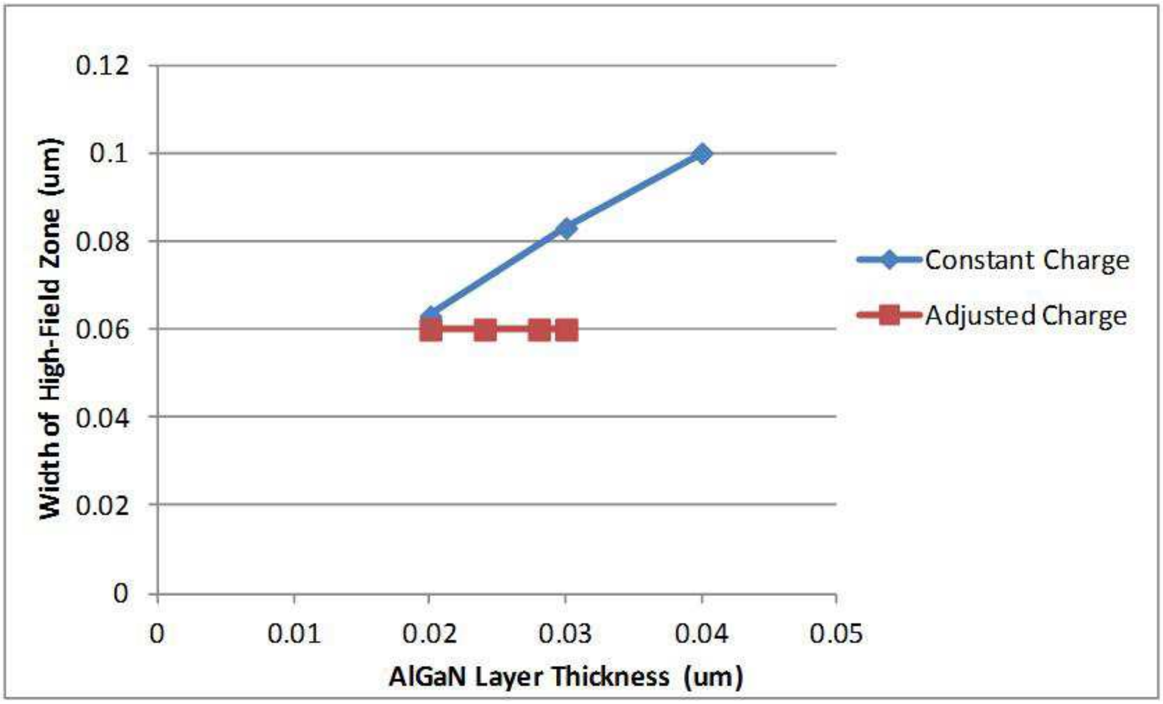

Figure 3.27 High-field zone width versus t_{AlGaN} for device simulations in which the polarization charge was kept constant (blue) and in which the polarization charge was corrected to be physically accurate (red).

Figure 27 shows the results where simulations for AlGaN thicknesses of 20, 24, 28, and 30 nm exhibit a constant width of the high-field region of L_{HF}≈60 nm. Further investigation revealed that the width of the high-field zone is independent of other changes in device geometry. Simulations were performed for gate lengths of L_g=0.5, L_g=0.8, and L_g=1.2 um as well as gate to drain spacing ranging from L_{gd}=1.6 to 2 um. Show below in figure 28 are the results for two different gate lengths L_g=0.5 and L_g=1.6 um in which measurements of L_{HF} were made. These results are indicative of those with different gate to drain spacing in that there is no observed change in the high-field zone width. Measurements of the high-field zone width were performed on simulations of a separate industrial

AlGaN/GaN HFET device with L_g=0.2 um, L_{sg}=0.7 um, L_{gd}=1.1 um, t_{AlGaN}=20 nm, and t_{GaN}=0.5 um also resulting in L_{HF}≈60 nm.

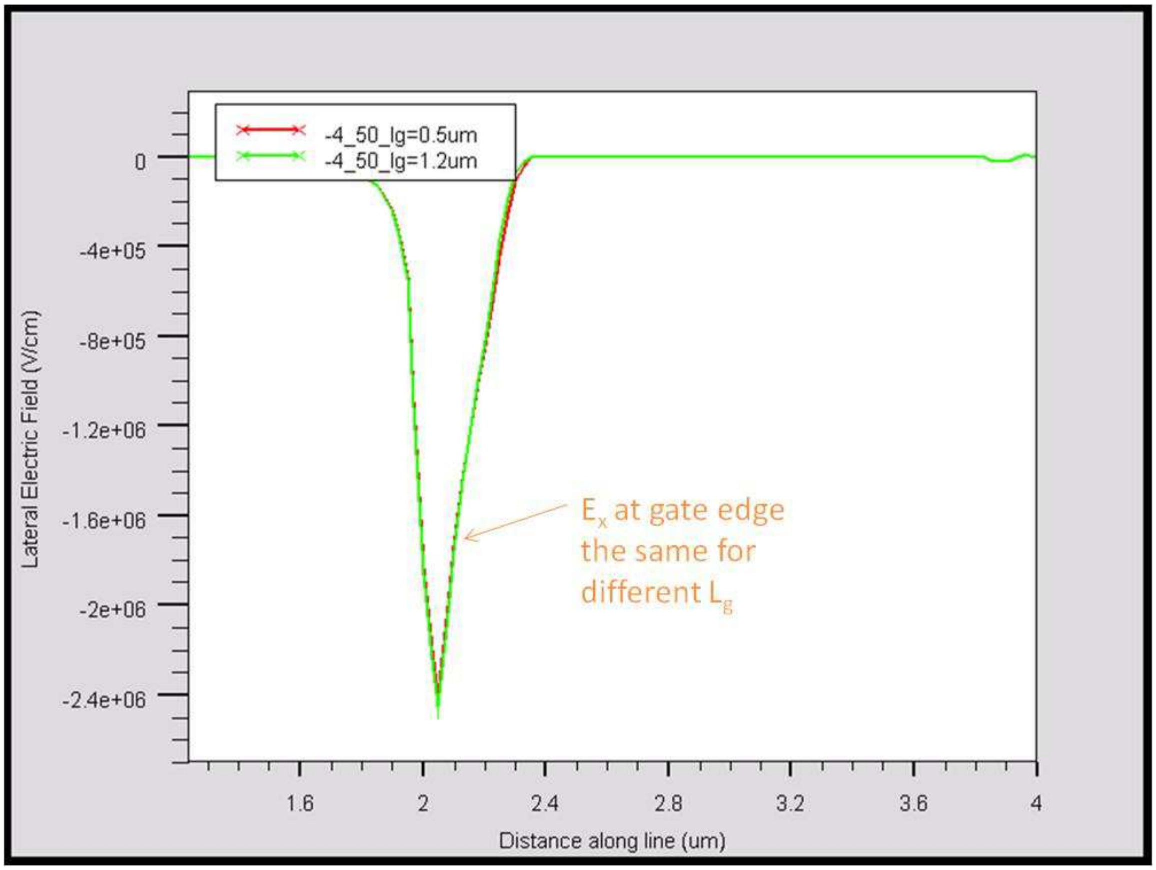

Figure 3.28 Lateral electric field profile along a horizontal cutline through the center of the channel for a device with L_g=0.5 um (red) and L_g=1.2 um (green).

So, changes in the physical structure of the device have shown little to no effect on the width of the high-field region as well as the slope of the field or E_{max}. All of the previous measurements were taken at or near the pinchoff voltage as it is the low current, high voltage region of operation in which the field magnitudes are the largest and breakdown is important [6]. Multiple TCAD simulations were then performed across the full range of the IV plane for the experimental device. The dependence of the high-field region width and the slope of the lateral electric field on both drain and gate voltage was investigated. First, to show the behavior under the highest field magnitudes, figure 29 below includes several lateral electric field cutlines through the channel with the device pinched-off at V_g=-4 volts and the drain voltage ramped from V_d=30 to 100 volts in 10 volt increments. The width of the high-field still remains approximately constant.

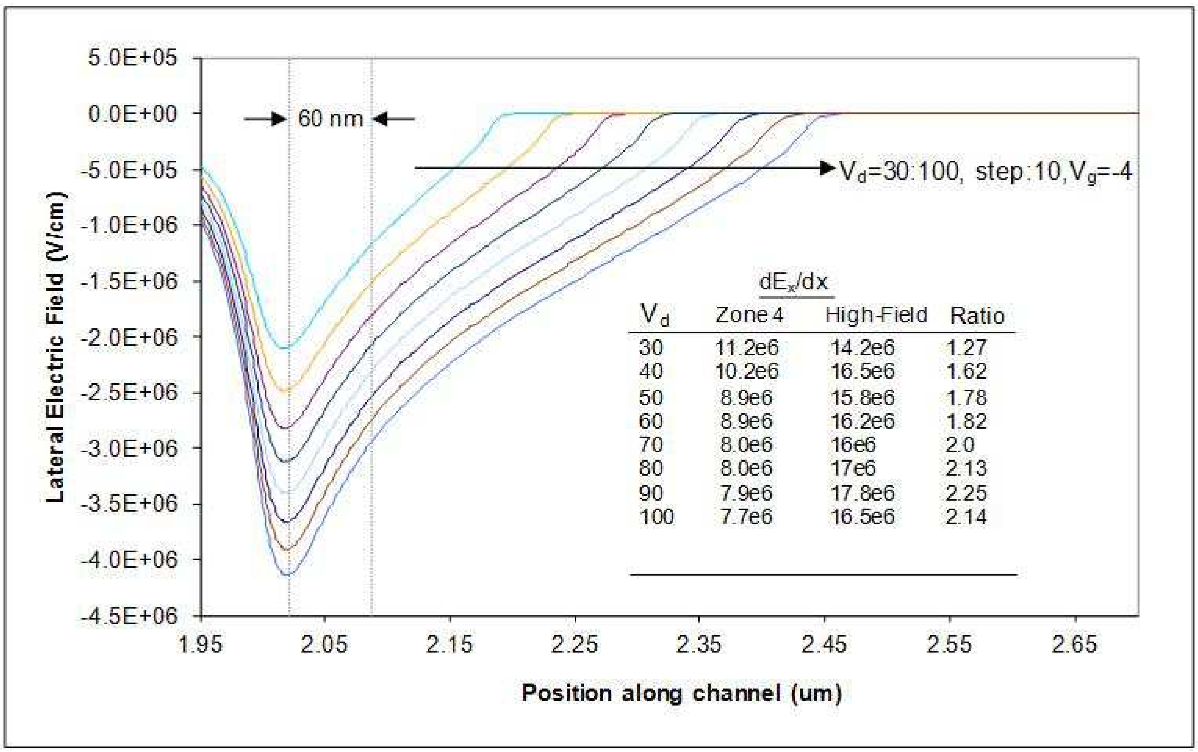

	dE_x/dx		
V_d	Zone 4	High-Field	Ratio
30	11.2e6	14.2e6	1.27
40	10.2e6	16.5e6	1.62
50	8.9e6	15.8e6	1.78
60	8.9e6	16.2e6	1.82
70	8.0e6	16e6	2.0
80	8.0e6	17e6	2.13
90	7.9e6	17.8e6	2.25
100	7.7e6	16.5e6	2.14

Figure 3.29 Lateral electric field distribution in the center of the conducting channel for V_g=-4 volts and V_d=30 to 100 volts in 10V steps. Inset table lists the slope of E_x in zone 4, in the high-field region, and the ratio of the two. Results obtained from TCAD simulations using Table 1 parameters and Drift-Diffusion, Lateral field dependent mobility, and SRH recombination models.

As the drain voltage is increased at a constant gate bias, the area inside the lateral electric field profile must increase accordingly. But, since a constant gate bias is applied and the channel current is (relatively) constant, the charge concentration in the charge deficit zone must remain the same leaving the slope, dEx/dx, approximately the same for varying drain voltages. This same behavior is seen in the high-field region as the peak lateral electric field magnitude at the gate edge increases with drain bias. Inset in figure 29 are the measurements taken from the simulations. The slope of the lateral electric field (V/cm-um) was measured in the high-field zone and the charge deficit zone. The slope of the lateral electric field in the high-field region is approximately two times that of the CDZ ranging from 1.3 times the slope of the CDZ for low voltages to approximately 2 times for drain biases of 40 volts and above.

A similar situation can be observed in simulations of the HFET for a constant drain bias of V_d=50 volts and varying gate bias of V_g=+1 to -4 volts shown in figure 30 below. For a constant drain bias, the slope of the lateral electric field in the charge deficit zone must change to accommodate the change in channel current and hence the 2DEG charge density. The measurements of dE_x/dx (inset in figure 30) for both regions reflect this condition. While the slope in the high-field region varies only a small amount, especially for negative gate biases, the slope in the CDZ can become very flat at high drain currents resulting in significant differences in slope between the zones. However, for increasingly negative values of gate bias, an estimate of the slope in the high-field zone as twice the CDZ becomes a good approximation. This approximation works well for modeling breakdown in these devices since the operating regions with the largest electric field magnitudes are those that are important for impact ionization. Additionally, in this situation of varying gate bias and constant drain bias, the width of the high-field region remains to be approximately unchanged at L_{HF}≈60 nm.

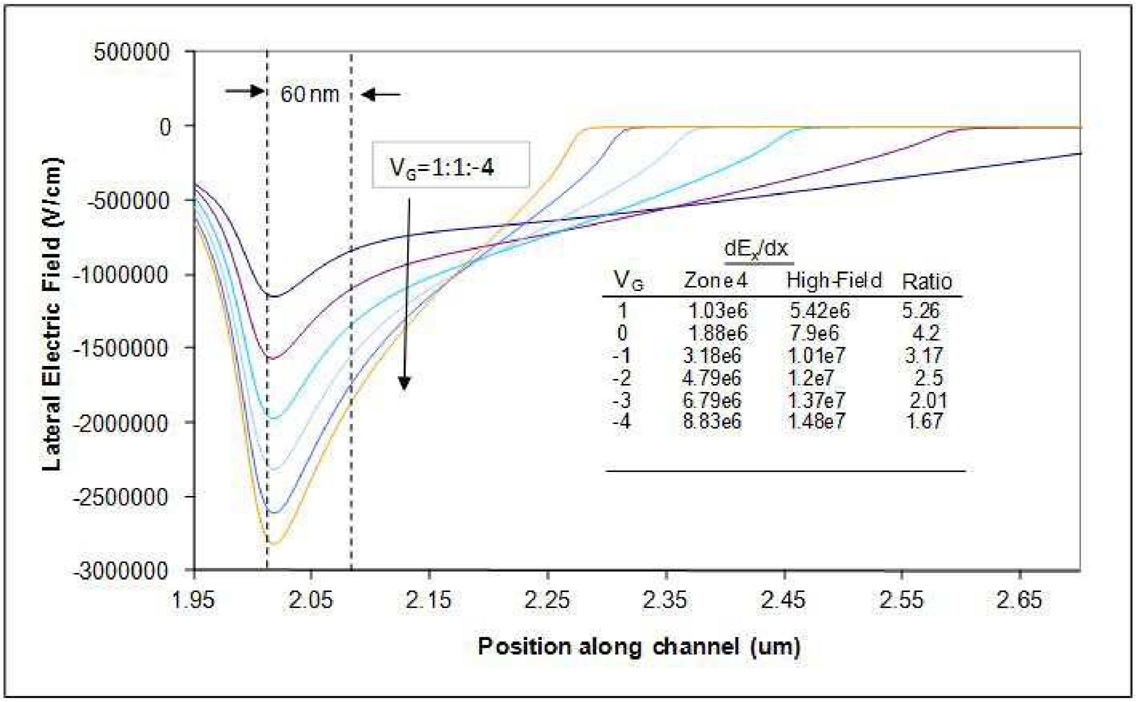

Figure 3.30 Lateral electric field distribution in the center of the conducting channel for V_d=50 volts and V_g=1 to -4 volts in -1V steps. Inset table lists the slope of E_x in zone 4, in the high-field region, and the ratio of the two. Results obtained from TCAD simulations using Table 1 parameters and Drift-Diffusion, Lateral field dependent mobility, and SRH recombination models.

3.4.4 Approximations and integration with compact model

Of interest to the calculation of breakdown of a 2DEG channel current is the charge generation in the direction of current flow. Consequently, the vertical electric field, which is varying and non-zero in the high-field region, is neglected in the calculation of impact ionization. Net electron flow in the vertical direction is negligible, and little current is generated even though the electric field has high magnitude. However, the electric field is at its peak in the high-field region of the high electron density 2DEG channel and a high magnitude current flows in the lateral direction. The high magnitude lateral directed electric field, along with the high electron density in the 2DEG channel, results in charge generation by impact ionization which adds to the existing channel current.

Using the information from the TCAD simulations and a description of the CDZ from [40], an expression for the lateral electric field in the high-field region can be derived. As shown in figure 31, equation 3.25 describes the electric field from the compact model for the charge deficit zone or Z4 of the HFET. E_{34} is the lateral electric field magnitude at the gate edge predicted by the compact model, L_s and L_g are the source-gate distance and gate length respectively, q is the electron charge, n_{ss} is the sheet charge density, ε is permittivity of GaN and t is the GaN thickness, I_d is the drain current, and I_{max} is the maximum current defined as $I_{max}=Wqn_{ss}v_{sat}$ where W is the device width and v_{sat} is the saturated electron velocity. The lateral electric field expression is

$$E(x) = -E_{34} + (x - L_S - L_G) \cdot \frac{qn_{ss}}{\varepsilon t} \frac{I_{max} - I_d}{I_{max}} . \qquad (3.25)$$

Since the value for the zone width, L_{HF}, is known and additionally the slope of the lateral electric field is known to be twice that of the lateral field in the CDZ, the expression for lateral electric field is modified to the following expression where E_{max} is the new realistic peak lateral electric field magnitude at the drain-side gate edge,

$$E(x) = -E_{\max} + 2 \cdot (x - L_S - L_G) \cdot \frac{qn_{ss}}{\varepsilon t} \frac{I_{\max} - I_d}{I_{\max}}. \tag{3.26}$$

The high-field region electric field expression is then inserted into the ionization integral. The ionization coefficients and approximations discussed in section 3 are applied; the electron an hole ionization coefficients are considered equal, impact ionization is electron initiated, and the Fulop approximation of the effective ionization coefficient is used such that

$$\alpha_{eff}(E) = a_n \cdot |E|^4 \tag{3.27}$$

to allow for a nice analytic solution. Applying the boundary condition of the high-field zone width, and the ionization integral is evaluated resulting in the following expression

$$\int^{W} \alpha_{eff}\, dx = \frac{16}{5} a_n k^4 L^5 - 8 a_n E_{\max} k^3 L^4 + 8 a_n E_{\max}^2 k^2 L^3 - 4 a_n E_{\max}^3 k L^2 + a_n E_{\max}^4 L \tag{3.28}$$

where $k=(qn_{ss}/\varepsilon t)((I_{max}-I_d)/I_{max})$. A final drain current including impact ionization generated current in the channel can then be calculated through a multiplication factor [45]

$$M = \frac{1}{1 - \int_0^W \alpha_{eff}\, dx}. \tag{3.29}$$

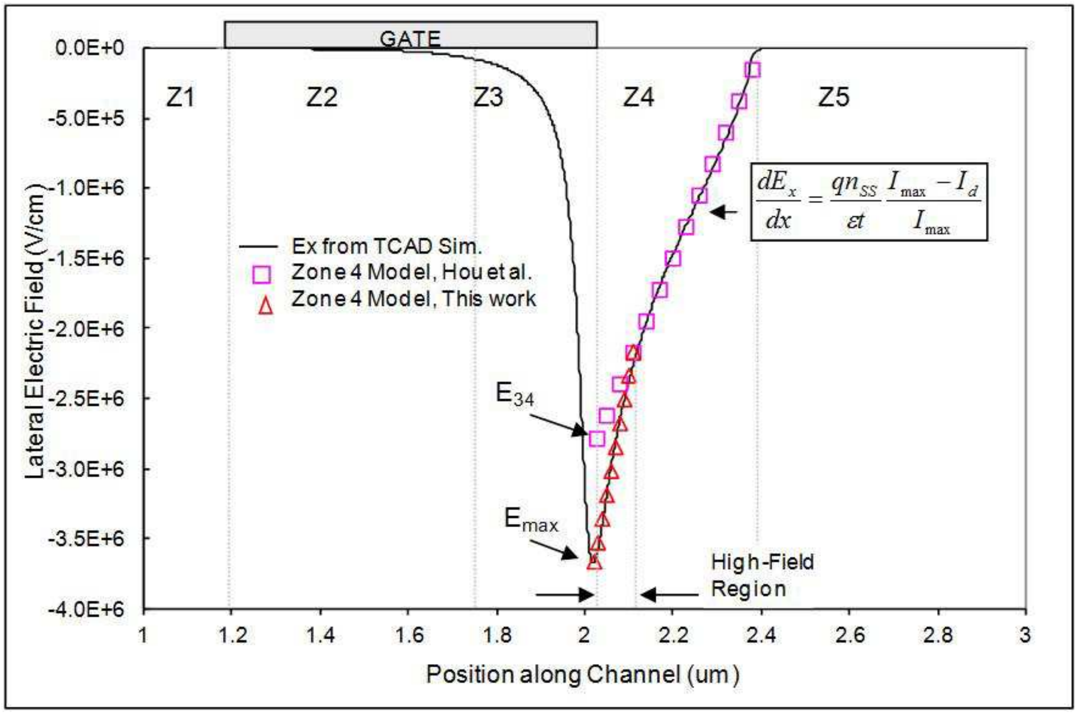

Figure 3.31 Lateral electric field distribution in the center of the conducting channel. The line is E_x from the TCAD simulation using the parameters in Table 1. TCAD models used in the simulation are: Drift-Diffusion, Lateral field dependent mobility, and SRH recombination. The squares show the approximation of E_x in Zone 4 (eqn. 3). The triangles show E_x in high field region (eqn. 4). Beyond the high field region eqn. 3 is valid.

This method of calculating the impact ionization current accounts for the physical behavior of the HFET. Since the model includes the sharp peaking of the field at the gate edge that was previously absent in the compact model a more accurate prediction of impact ionization can be obtained. However, the calculation must be restricted to the regions of operation in which the approximations made in developing the model are valid.

3.5 Verification against Measurements

The HFET compact model of [40] is updated to include the channel breakdown model. The updated Verilog-A^{TM} code was translated and compiled into a user-defined model for use in Micorwave Office^{TM} (MWO) harmonic balance circuit simulator. The compact model first determines the normal drain current for the bias conditions using the standard model in which the CDZ fills the entire depletion region between the gate edge and the drain neutral zone. Once the current is calculated, the breakdown model determines the new maximum field at the gate edge due to the high-field region and then calculates any additional current generated due to impact ionization, depending upon the field description, and the simulator outputs the final drain current. This process works like a current generator from drain to source.

3.5.1 DC IV Measurements

Simulations using the compact model with impact ionization turned off were calibrated to dc IV measurements from an industrial AlGaN/GaN HFET device. The HFET structure, including semiconductor layers thicknesses, impurity doping, and device geometry dimensions were input to the compact model as they were in the TCAD model. Excellent agreement between measurement and simulation data was obtained for the dc I-V characteristics as shown in figure 32. The dc IV characteristics could just as easily be calibrated with the impact ionization model turned on but as discussed in the following paragraph, this will have a slight effect on accuracy. Additionally, it is known that without the breakdown model included, the RF performance simulation has a poor fit to the measurements at large input drive levels [6]. Simulations are therefore performed with the breakdown model turned on and the ionization coefficient is tuned to show excellent agreement with the measurements for the entire range of input power.

The complete model with breakdown included generated the simulated I-V curve at pinch-off which includes the excess current due to impact ionization,

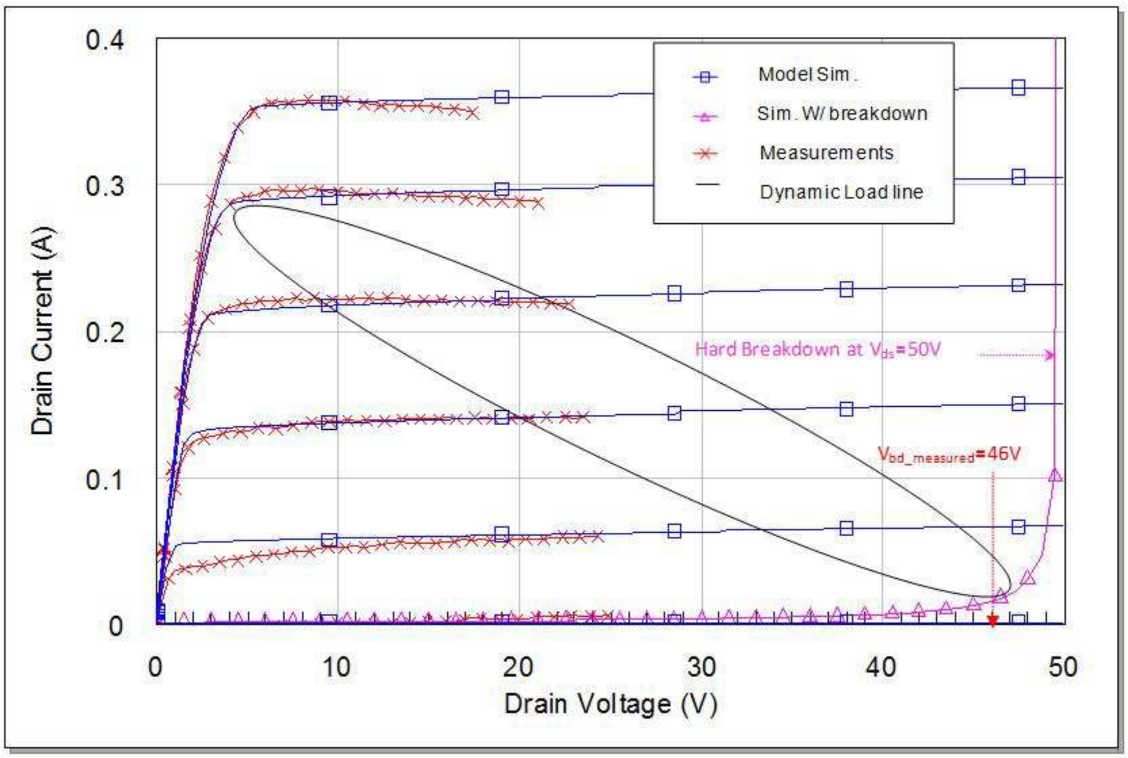

Figure 3.32 Simulations of DC I-V curves for an AlGaN/GaN HFET (Structure same as TCAD model). Red X's are the measurements, Blue squares are the original compact model simulation (impact ionization turned off), and triangles are the compact model including impact ionization for pinch-off. The oval line is an overlay of the dynamic load-line at maximum PAE.

shown in figure 32. Deviations from the dc I-V measurements can occur for other points on the I-V plane where there is a much smaller amount of excess current generated due to impact ionization but where the fields are not sufficient to cause avalanche breakdown. The compact model does not include thermal effects but the calculated increase in current for moderate drain voltages is likely greater than what is actually experienced due to self-heating. Experiments show that avalanche breakdown at the lower right side of the RF load-line is the dominant factor in predicting RF performance measurements [6]. The rate of ionization increases with applied V_{ds} and becomes the most significant where the electric field in the high-field region is at a maximum, i.e. large negative V_{gs} and large V_{ds}. The excess currents elsewhere in the I-V plane have a minor effect on RF performance and it is assumed that self-heating effects will reduce or cancel the increased drain current for all but the lower right corner of the I-V plane where the high voltage, low current portion of the dynamic load-line exists. Under small-signal operation where nonlinearities due to breakdown are not important, the excess current from the impact ionization model has only a minor effect on simulation accuracy. Finally, when biased at pinch-off, the breakdown voltage is defined at the V_{ds} where avalanche breakdown occurs. DC breakdown was measured and simulated at V_{bd}=46 and V_{bd}=45.9 volts respectively for when the current at pinchoff exceeds 10 mA/mm. As indicated in figure 32, hard breakdown occurs for V_{ds}=50 volts.

3.5.2 RF Measurements

RF performance data for an S-band communications amplifier fabricated with an AlGaN/GaN HFET were measured at a frequency of 2.14 GHz HFET for class A-B operation under three different bias voltages of V_{ds}=28V, V_{ds}=38V, and V_{ds}=48V. Initially, the model prediction for the breakdown voltage was inaccurate and underestimated the magnitude of impact ionization current and the model was unable to match the large-signal measurements. This problem could be fixed by fitting the model to the measurements by adjusting the ionization coefficient. The ionization coefficient is the only adjustable parameter in the breakdown model and can be used to fit the measurements though it is still based on a physical mechanism. For each bias point the device model required that the multiplying constant, a_n, of the ionization coefficient be adjusted, thereby modifying the breakdown voltage, until RF output power, gain, and PAE were in agreement with the measured data. The modeled and measured RF performance data for the V_{ds}=28 v bias voltage condition are shown in figure 33, for V_{ds}=38 volts in figure 34, and for V_{ds}=48 volts in figure 35.

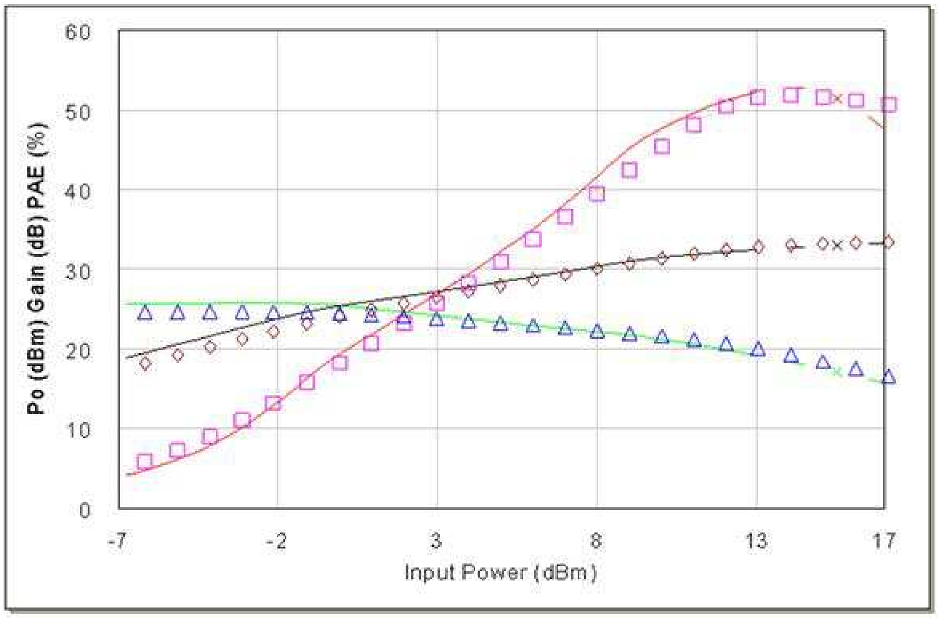

Figure 3.33 RF performance of a 2.14 GHz AlGaN/GaN amplifier operating in class AB and Vds=28V, a_n=6.41x10^{-21}cm^{3}V^{-4}. Impact ionization model is turned on and predicts a breakdown voltage of V_{bd}≈51V.

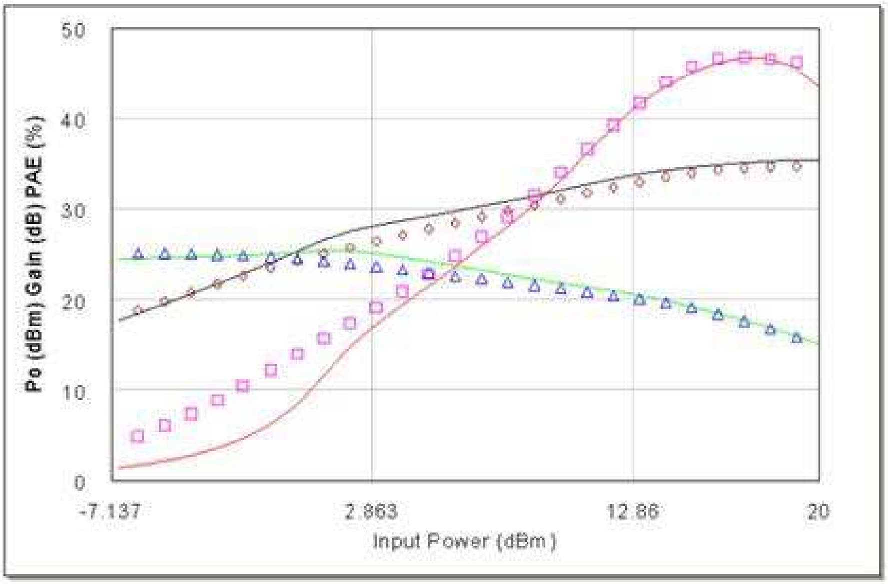

Figure 3.34 RF performance of a 2.14 GHz AlGaN/GaN amplifier operating in class AB and Vds=38V, a_n=4.71x10^{-21}cm^{3}V^{-4}. Impact ionization model is turned on and predicts a breakdown voltage of V_{bd}≈51V.

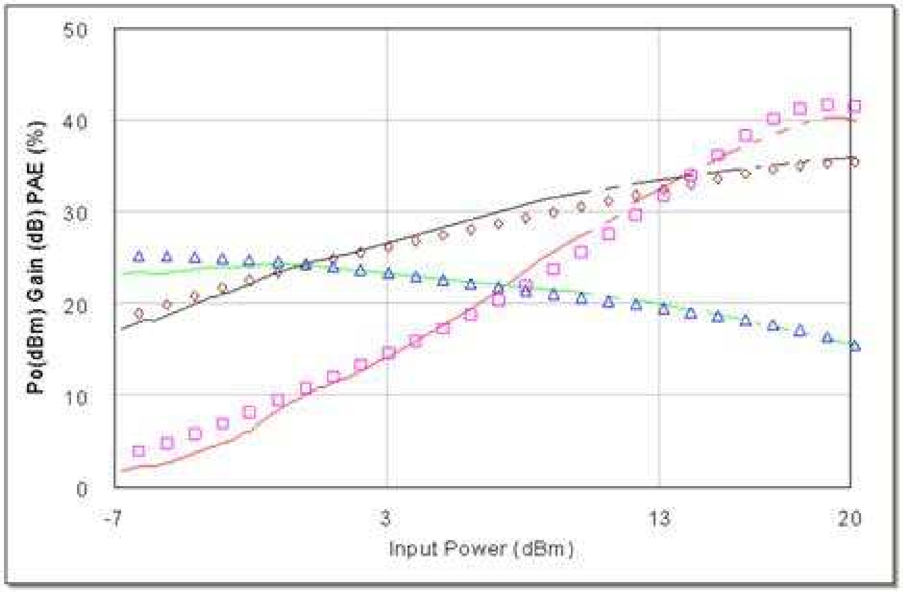

Figure 3.35 RF performance of a 2.14 GHz AlGaN/GaN amplifier operating in class AB and Vds=48V, a_n=3.61x10^{-21}cm^{3}V^{-4}. Impact ionization model is turned on and predicts a breakdown voltage of V_{bd}≈51V.

All three sets of measurements were modeled with good accuracy, in agreement with the measured data using an ionization coefficient in the range of $\alpha_{eff}=3.61\text{x}10^{-21}E^4$ cm^{-1} to $\alpha_{eff}=6.41\text{x}10^{-21}E^4$ cm^{-1}, as shown in figure 36. The extracted a_n is about an order of magnitude greater than that predicted by [44] for bulk GaN. However, avalanche ionization for the HFET is occurring in the 2DEG conducting channel located at the AlGaN/GaN heterointerface, rather than within the bulk GaN semiconductor. Ionization coefficients for an AlGaN/GaN 2DEG have not been reported, but it is likely that the high electron density and mobility in the 2DEG and the large vertical polarization field in the AlGaN layer contributes to an increase in the ionization rate. Thin increased ionization coefficient can be seen in figure 36 below.

3.5.3 Variable Ionization Coefficient

The results of fitting the simulation to the large-signal measurements using the ionization coefficients as an adjustable parameter allows the RF breakdown voltage to be extracted. Results indicate that RF breakdown voltage increases for increasing drain bias. This effect is not predicted by the impact ionization model as evidenced by the necessity to change the ionization coefficient to match the measurements at each V_{ds}. There is no functionality built into the model to account for a changing ionization coefficient. We know that the dc, room temperature measured breakdown voltage for this device shows a V_{bd}=46 volts and that measurements predict an RF breakdown voltage of approximately V_{bd}=51 volts. A increase in V_{bd} must occur for operating points at V_d=38 and V_d=48 volts. Since the voltage at which channel breakdown occurs determines when the device's output voltage saturates, it is expected that the RF breakdown voltage, V_{bd}, will increase with increased drain bias voltage of else the device would be inoperable. This effect is illustrated if you imagine the load-line in figure 32 shifted over for V_d=38 volts drain bias, but with the same breakdown as V_d=28.

Figure 36 shows the predicted ionization coefficients for each bias point as compared to the ionization coefficients predicted for bulk GaN at 300K. As the drain bias increases a smaller value of a_n is necessary to predict V_{bd}. Less excess charge is generated as the class A-B bias point is increased to higher voltages resulting in increased breakdown voltage.

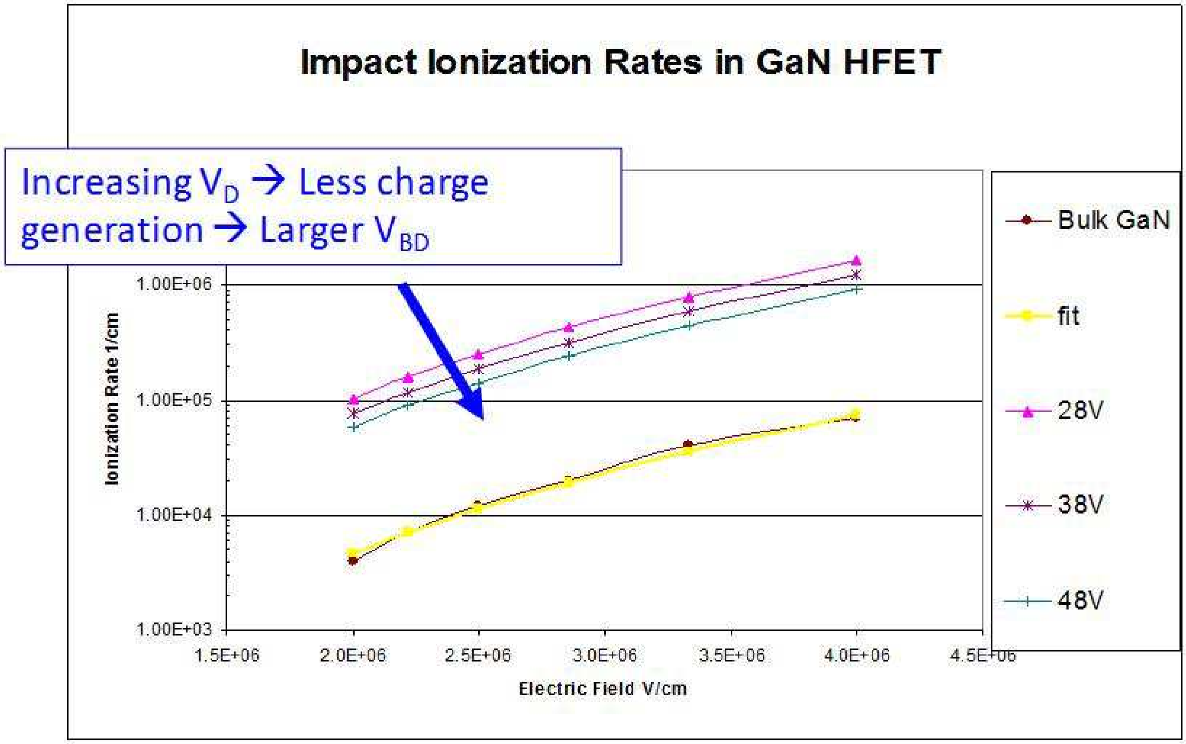

Figure 3.36 Impact ionization coefficients necessary to fit the simulator output to large-signal measurements of a 2.14 GHz. AlGaN/GaN HFET at three separate bias conditions.

3.6 Temperature Dependence of Breakdown

The RF breakdown voltage dependence on bias condition can be explained through the temperature dependence of the impact ionization process. With increased bias voltage there is a subsequent increase in quiescent dissipated power within the device. The resulting increase in temperature reduces the electron mean free path and leads to a reduction in the number of ionizing collisions. The temperature dependence of the electron mean free path is approximately given by

$$\lambda = \lambda_0 \tanh\left(E_p \middle/ 2kT \right) \tag{3.30}$$

where λ_0 is the mean free path at absolute zero and E_p is the average energy lost in a phonon collision [43]. The lower ionization rate means that less excess charge is generated in the high-field region at a higher temperature and the onset of avalanche breakdown is delayed. The positive temperature coefficient, indicated in the experimental data (figure 37), is a signature of impact ionization that has been identified in the breakdown of GaN diodes [59, 60] as well as AlGaN/GaN GaN HFETs [30, 33, 55].

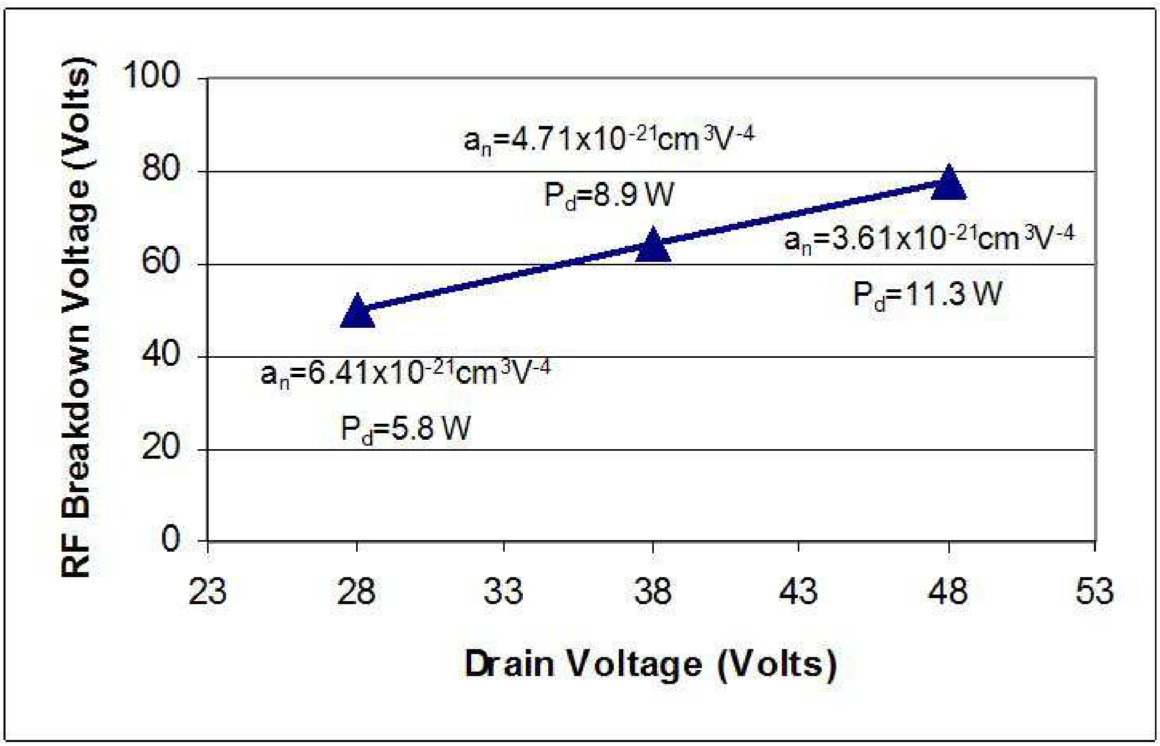

Figure 3.37 RF Breakdown voltage versus drain bias for a 2x200 um 2.14 GHz. AlGaN/GaN PA operating in class AB for Vd=28, 38, 48 volts. Values of V_{bd}, a_n, and P_d were extracted from fitting large-signal performance measurements at each bias point with breakdown model 'on'.

3.6.1 Temperature Dependent Ionization Coefficients

In order for the breakdown model to accurately predict the RF breakdown voltage under varying bias conditions it is necessary to introduce a temperature dependent ionization coefficient that can account for the device heating and adjust the ionization rate accordingly. A measurement based model is proposed. This simple model assumes that the field dependence is constant, $\alpha_{eff} \sim E^4$, and the multiplying factor a_n will change with temperature. Impact ionization coefficients for bulk wurtzite GaN at temperatures of 300 K and 600 K were used from [61] (figure 38).

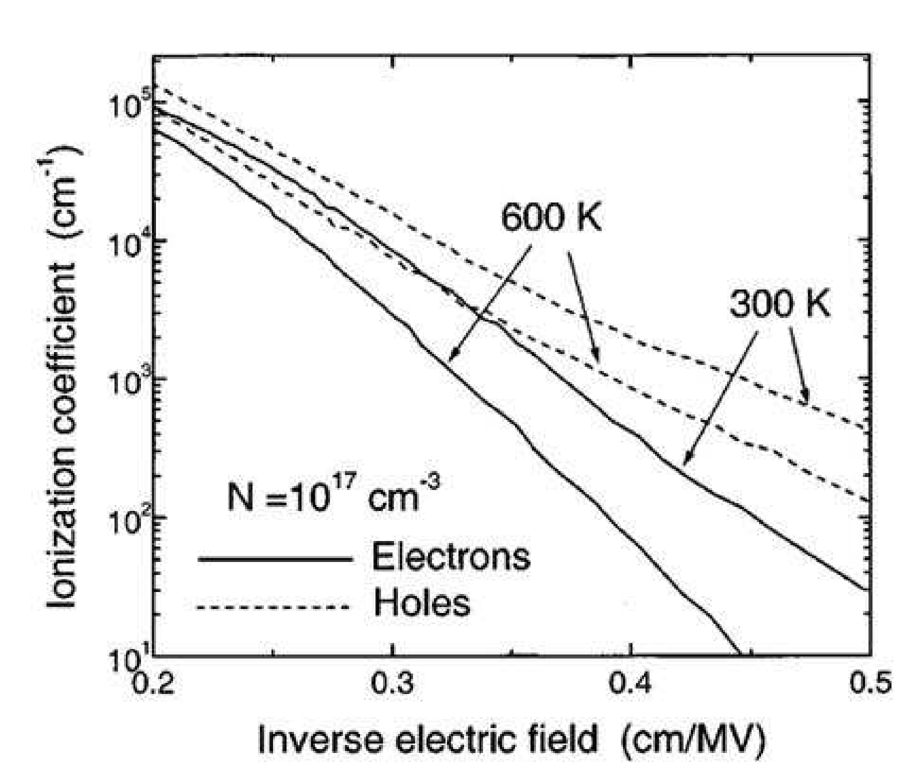

Figure 3.38 Electron and hole ionization coefficients for bulk wurtzite GaN for 300 and 600 K from reference [61].

The temperature sensitivity was extracted from the two curves and then scaled to match ionization coefficient data from [27] at 300 K. The dependency on temperature was extracted using

$$\alpha(E) = \alpha_{300}\left[1 + \frac{1}{\alpha_{300}}\frac{\partial\alpha(E)}{\partial T}(T - 300)\right] . \tag{3.31}$$

Assuming the power approximation for the effective ionization coefficient for different temperatures,

$$\alpha_{eff}(E) = a_n \cdot |E|^4 , \tag{3.32}$$

the coefficient a_n (T) can be described by a linear function using the results of equation 3.31 to get

$$a_n(T) = -3.33\times10^{-25} \cdot T + 3.85\times10^{-22} . \tag{3.33}$$

At this point a simple thermal circuit as that shown in figure 39 can be employed where $\Delta T=P_dR_{th}$ where T_{300} is the ambient temperature, T_{ch} is the channel temperature, P_d is the device dissipated power at a particular operating point, and R_{th} is the device thermal resistance.

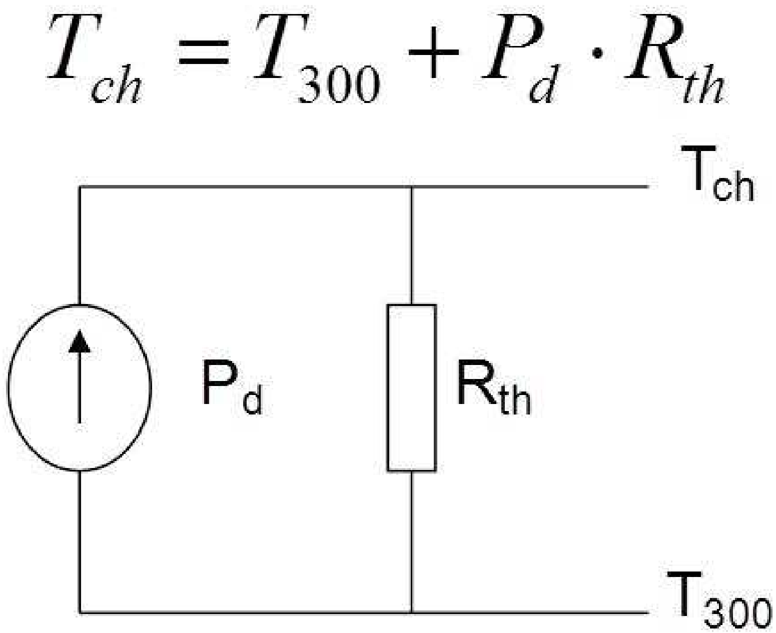

Figure 3.39 Thermal circuit used to calculate temperature rise for a given dissipated power.

The device temperature rise is now linked to the dissipated device power. Using this thermal sub-circuit, the coefficient can be written as

$$a_n(P_d R_{th}) = 2.85\times10^{-22} - 3.33\times10^{-25} \cdot P_d R_{th}. \tag{3.34}$$

P_d and a_n are extracted from the experimental data by comparing the predictions obtained from the model to the RF measured performance data at each bias point as was done in the previous section (Fig. 1). P_d was determined from the RF load line once agreement was obtained. The result of the thermal model is the ability to extract the value for device thermal resistance using equation 3.34.

3.6.2 Temperature Model Verification

Unique to this model is the extraction of a physical parameter, the thermal resistance, that can be compared to the actual value for this device. Extracted R_{th} values range from R_{th}= 5.5 to 7.4 °C/(W/mm) for the HFET used in the simulation which has a 2 x 200 μm device geometry. The extracted thermal resistance values were check against reports of thermal resistance for similar devices and then checked against an analytical model for thermal resistance in AlGaN/GaN HFETs. Measurements by Kuball et al. of multi-finger AlGaN/GaN HFETs on SiC substrates with similar device dimensions using micro-Raman spectroscopy reveal a similar thermal resistance of R_{th}=6.4 °C/(W/mm) for a 1 x 200 μm device and up to R_{th}=12.9 °C/(W/mm) for a 4 x 500 μm HFET [62]. Similar agreement was obtained when comparing the extracted thermal resistance to the results of a separate analytic model [63]. Darwish's compact physical model of the thermal resistance of AlGaN/GaN HFET devices has been verified against measurements and numerical simulations of multiple device designs and substrates. The thermal resistance is given by

$$R_{th} = \frac{1}{\pi W_g k_{GaN}} \ln\left(\frac{4t_1}{\pi L_g}\right) + \frac{1}{\pi W_g k_{Sub}} \cdot \ln\left(\frac{f\left(W_g \big/ 2\rho t_1\right)}{f\left(\sqrt{1+\left(W_g \big/ \sqrt{2}s\right)^2 - \left(\rho t_1 \big/ \sqrt{2}s\right)^2}\right)}\right)$$

$$+ \frac{1}{\pi s k_{Sub}} \cdot \ln\left(\frac{h\left(\left(W_g \big/ \pi t_2\right)^2 - 4\left(\rho t_1 / \pi t_2\right)^2\right)}{h\left(\left(W_g / \sqrt{2}s\right)^2 - 4\left(\rho t_1 / \sqrt{2}\, s\right)^2\right)}\right)$$

(3.35)

where

$$\rho = 4k_{GaN} / \pi^2 k_{Sub} \tag{3.36}$$

$$f(x) = \frac{\sqrt{x+1} + \sqrt{x-1}}{\sqrt{x+1} - \sqrt{x-1}} \tag{3.37}$$

$$h(x) = \sqrt{\frac{\sqrt{x+1}+1}{\sqrt{x+1}-1}} \tag{3.38}$$

and t_1 is the GaN layer thickness, t_2 is the substrate thickness, W_g is the device width, s is the spacing between the gates, L_g is the gate length, and k_{GaN} and k_{Sub} are the thermal conductivities of GaN and substrate respectively and are considered constant. A calculation of the thermal resistance by applying this model to our device's structure and parameters gives a thermal resistance of R_{th}=10 °C/(W/mm).

Another parameter that the thermal model allowed us to extract is the temperature coefficient of breakdown, $dV_{bd}/dT= \eta_{br}$. For this device η_{br}=0.22 VK^{-1}, which is in good agreement with values obtained for AlGaN/GaN HFETs of η_{br}=0.33 VK^{-1} from [55], η_{br}=0.12 and η_{br}=.32 VK^{-1} for non-passivated and passivated surfaces of AlGaN/GaN HFETs from [33].

3.6.3 Flowchart of Extraction and Verification

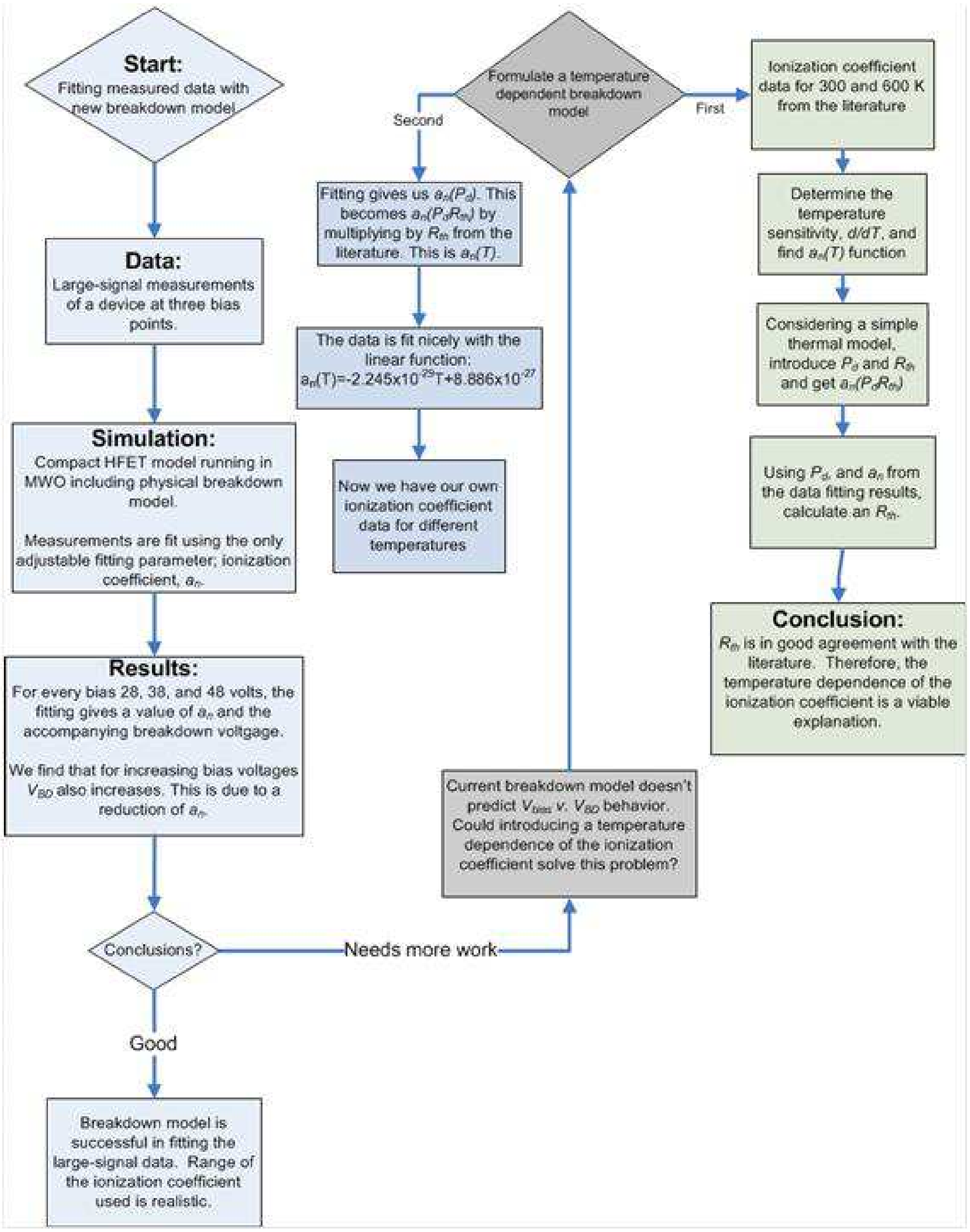

Chapter 4 Conclusions and Future Work

4.1 Conclusion

In this thesis two problem areas of AlGaN/GaN HFETs were addressed. First the nonlinear source resistance phenomenon due to the onset of space-charge-limited current flow in the HFET channel was investigated. Through TCAD simulations the threshold for SCLC transport was studied in two situations. Starting with modeling the 2DEG as a piece of GaN semiconductor, as was used for the derivation of the nonlinear source resistance model, and secondly the source access region was model as a physically accurate AlGaN/GaN hetero-structure. Results of the simulations showed that since the source of the 2DEG electrons are ionized surface states and the threshold for SCLC depends on 2DEG electron concentration, then the condition of the AlGaN surface is an important factor in the threshold. Since the nonlinear source resistance can degrade device performance, understanding how the surface treatment affects the onset of nonlinear resistance is useful.

The second part of this thesis dealt with developing a physical model for the channel breakdown phenomenon that could be integrated with a previously developed physics-based model of AlGaN/GaN HFETs. An existing physics-based compact model of AlGaN/GaN HFETs was modified to include a simplified physical model of impact ionization initiated channel breakdown. The breakdown voltage is determined by calibrating the model to large-signal performance measurements. It was shown that by accounting for breakdown effects, large-signal performance measurements of an industrial AlGaN/GaN HFET device, including power-added efficiency, gain, and output power, can be predicted by using the ionization rate as a fitting parameter. Tuning the model to large-signal performance measurements of other devices may be necessary using the ionization coefficient factor, a_n, due to differences in material quality, process technology as well as the uncertainty of ionization coefficients in AlGaN/GaN channels. But once established for a particular device, the model is completely predictive. The model includes the dependence of breakdown voltage on drain bias and was shown to be an effect of a temperature dependent impact ionization process. This temperature model was verified by the extraction of R_{th} and η_{br} that agree well with published values for similar devices and predictions of R_{th} from an independent analytical thermal resistance model.

4.2 Future Work

In this thesis we derived a simplified model of channel breakdown that is dependent on the physical parameters of the device as well as the bias conditions. However, for this simple model a dependence on frequency is not included. Analysis of the differences of the dc and RF breakdown voltages in these devices is needed. The model is verified on an S-band communications amplifier operated at 2.14 GHz. For this device the dc and RF breakdown voltages are nearly identical. To be able to accurately model channel breakdown at W-band and above some consideration of the frequency effects will likely be necessary. The problem arises when the high magnitude electric field in the device channel changes so fast that electrons cannot fully respond to changes in the field fast enough. Farahmand *et al.* studied this effect in bulk GaN and GaN MESFETs using Monte Carlo analysis [16]. They found that the average electron energy decreases with increasing RF drive frequency. The implication is that for the same drive voltage, the impact ionization coefficient will be reduced and the breakdown voltage of the device will increase with increasing frequency. So in order to accurately model high-frequency devices, this dependency should be introduced to the breakdown model.

Secondly, the accuracy of the breakdown model depends largely on the ionization coefficients used in the calculation. While the approximations applied to this problem are valid, ionization coefficients for bulk GaN are still being used in the model and require some calibration to the measurements. A study to determine the impact ionization coefficients in an AlGaN/GaN two-dimensional electron gas would be useful not only for predicting accurate breakdown voltages but also for deriving a physical model of the temperature dependence of the coefficients as well.

References

[1] R. J. Trew. SiC and GaN transistors - is there one winner for microwave power applications? *Proceedings of the IEEE 90(6),* pp. 1032-1047. 2002.

[2] U. K. Mishra, Shen Likun, T. E. Kazior and Yi-Feng Wu. GaN-based RF power devices and amplifiers. *Proceedings of the IEEE 96(2),* pp. 287-305. 2008.

[3] R. Trew, D. Green and J. Shealy. AlGaN/GaN HFET reliability. *Microwave Magazine, IEEE 10(4),* pp. 116-127. 2009.

[4] A. Koudymov, G. Simin, M. A. Khan, A. Tarakji, R. Gaska and M. S. Shur. Dynamic current-voltage characteristics of III-N HFETs. *Electron Device Letters, IEEE 24(11),* pp. 680-682. 2003.

[5] J. A. del Alamo and J. Joh. GaN HEMT reliability. *Microelectronics Reliability 49(9–11),* pp. 1200-1206. 2009.

[6] R. J. Trew, Y. Liu, W. Kuang, H. Yin, G. L. Bilbro, J. B. Shealy, R. Vetury, P. M. Garber and M. J. Poulton. RF breakdown and large-signal modeling of AlGaN/GaN HFET's. Presented at Microwave Symposium Digest, 2006. IEEE MTT-S International. 2006, .

[7] R. J. Trew, Yueying Liu, L. Bilbro, Weiwei Kuang, R. Vetury and J. B. Shealy. Nonlinear source resistance in high-voltage microwave AlGaN/GaN HFETs. *Microwave Theory and Techniques, IEEE Transactions on 54(5),* pp. 2061-2067. 2006.

[8] D. Yole, "GaN Power Electronics Slow ramp-up but huge expectations..." *I-Micronews,* vol. 2012, pp. 29, .

[9] R. J. Trew. Modeling and limitations of AlGaN/GaN HFETs. Presented at Semiconductor Device Research Symposium, 2001 International. 2001, .

[10] T. Palacios, S. Rajan, A. Chakraborty, S. Heikman, S. Keller, S. P. DenBaars and U. K. Mishra. Influence of the dynamic access resistance in the g_m and f_T linearity of AlGaN/GaN HEMTs. *Electron Devices, IEEE Transactions on 52(10),* pp. 2117-2123. 2005.

[11] Y. Liu 1978-. Analytical physics based AlGaN/GaN HFET large signal model and nonlinearity analysis with nonlinear source resistance [electronic resource]. 2009. Available: http://www2.lib.ncsu.edu/catalog/record/NCSU2215948.

[12] R. Vetury, N. Q. Zhang, S. Keller and U. K. Mishra. The impact of surface states on the DC and RF characteristics of AlGaN/GaN HFETs. *Electron Devices, IEEE Transactions on 48(3),* pp. 560-566. 2001.

[13] L. Shen, R. Coffie, D. Buttari, S. Heikman, A. Chakraborty, A. Chini, S. Keller, S. P. DenBaars and U. K. Mishra. High-power polarization-engineered GaN/AlGaN/GaN HEMTs without surface passivation. *Electron Device Letters, IEEE 25(1),* pp. 7-9. 2004.

[14] Y. -. Wu, M. Moore, A. Saxler, T. Wisleder and P. Parikh. 40-W/mm double field-plated GaN HEMTs. Presented at Device Research Conference, 2006 64th. 2006, .

[15] M. Kaddeche, A. Telia and A. Soltani. Modeling of AlGaN/GaN HEMTs using field-plate technology. Presented at Signals, Circuits and Systems (SCS), 2009 3rd International Conference on. 2009, .

[16] M. Farahmand, K. F. Brennan, E. Gebara, Deukhyoun Heo, Young Suh and J. Laskar. Theoretical study of RF-breakdown in bulk GaN and GaN MESFETs. *Electron Devices, IEEE Transactions on 48(9),* pp. 1844-1849. 2001.

[17] B. Jogai. Influence of surface states on the two-dimensional electron gas in AlGaN/GaN heterojunction field-effect transistors. *J. Appl. Phys. 93(3),* pp. 1631-1635. 2003. Available: http://dx.doi.org/10.1063/1.1530729.

[18] J. P. Ibbetson, P. T. Fini, K. D. Ness, S. P. DenBaars, J. S. Speck and U. K. Mishra. Polarization effects, surface states, and the source of electrons in AlGaN/GaN heterostructure field effect transistors. *Applied Physics Letters 77(2),* pp. 250-252. 2000.

[19] M. A. Lampert 1921-. *Current Injection in Solids* 1970.

[20] M. A. Lampert. Simplified theory of space-charge-limited currents in an insulator with traps. *Phys.Rev. 103(6),* pp. 1648-1656. 1956. Available: http://link.aps.org/doi/10.1103/PhysRev.103.1648.

[21] I. Ben-Yaacov and U. K. Mishra, "Unipolar Space Charge Limited Transport," vol. 2008, pp. 21, 2004.

[22] A. Rose. Space-charge-limited currents in solids. *Phys.Rev. 97(6),* pp. 1538-1544. 1955. Available: http://link.aps.org/doi/10.1103/PhysRev.97.1538.

[23] G. T. Wright. Mechanisms of space-charge-limited current in solids. *Solid-State Electronics 2(2–3),* pp. 165-189. 1961.

[24] I. Silvaco, *ATLAS User's Manual Device Simulation Software.* Santa Clara, CA: 2010.

[25] R.J. Trew, Y. Liu, W.W. Kuang and G.L. Bilbro. The physics of reliability for high voltage AlGaN/GaN HFET's. Presented at Compound Semiconductor Integrated Circuit Symposium, 2006. CSIC 2006. IEEE. 2006, .

[26] K. Hui, C. Hu, P. George and P. K. Ko. Impact ionization in GaAs MESFETs. *Electron Device Letters, IEEE 11(3),* pp. 113-115. 1990.

[27] J. Kolnı k, I. s. H. Oguzman, K. F. Brennan, R. Wang and P. P. Ruden. Monte carlo calculation of electron initiated impact ionization in bulk zinc-blende and wurtzite GaN. *Journal of Applied Physics 81(2),* pp. 726-733. 1997.

[28] K. Kunihiro, K. Kasahara, Y. Takahashi and Y. Ohno. Experimental evaluation of impact ionization coefficients in GaN. *Electron Device Letters, IEEE 20(12),* pp. 608-610. 1999.

[29] W. S. Tan, P. A. Houston, P. J. Parbrook, D. A. Wood, G. Hill and C. R. Whitehouse. Gate leakage effects and breakdown voltage in metalorganic vapor phase epitaxy AlGaN/GaN heterostructure field-effect transistors. *Appl. Phys. Lett. 80(17),* pp. 3207-3209. 2002. Available: http://link.aip.org/link/?APL/80/3207/1.

[30] B. Brar, K. Boutros, R. E. DeWarnes, V. Tilak, R. Shealy and L. Eastman. Impact ionization in high performance AlGaN/GaN HEMTs. Presented at High Performance Devices, 2002. Proceedings. IEEE Lester Eastman Conference on. 2002, .

[31] R. Cuerdo, Y. Pei, Z. Chen, S. Keller, S. P. DenBaars, F. Calle and U. K. Mishra. The kink effect at cryogenic temperatures in deep submicron AlGaN/GaN HEMTs. *Electron Device Letters, IEEE 30(3),* pp. 209-212. 2009.

[32] G. Meneghesso, F. Zanon, M. J. Uren and E. Zanoni. Anomalous kink effect in GaN high electron mobility transistors. *Electron Device Letters, IEEE 30(2),* pp. 100-102. 2009.

[33] Y. Ohno, T. Nakao, S. Kishimoto, K. Maezawa and T. Mizutani. Effects of surface passivation on breakdown of AlGaN/GaN high-electron-mobility transistors. *Appl. Phys. Lett. 84(12),* pp. 2184-2186. 2004. Available: http://link.aip.org/link/?APL/84/2184/1.

[34] Maojun Wang and K. J. Chen. Off-state breakdown characterization in AlGaN/GaN HEMT using drain injection technique. *Electron Devices, IEEE Transactions on 57(7),* pp. 1492-1496. 2010.

[35] S. R. Bahl and J. A. del Alamo. A new drain-current injection technique for the measurement of off-state breakdown voltage in FETs. *Electron Devices, IEEE Transactions on 40(8),* pp. 1558-1560. 1993.

[36] N. Killat, M. Ťapajna, M. Faqir, T. Palacios and M. Kuball. Evidence for impact ionisation in AlGaN/GaN HEMTs with InGaN back-barrier. *Electronics Letters 47(6),* pp. 405-406. 2011.

[37] A. Chini, D. Buttari, R. Coffie, S. Heikman, S. Keller and U. K. Mishra. 12 W/mm power density AlGaN/GaN HEMTs on sapphire substrate. *Electronics Letters 40(1),* pp. 73-74. 2004.

[38] Y. Ando, Y. Okamoto, H. Miyamoto, T. Nakayama, T. Inoue and M. Kuzuhara. 10-W/mm AlGaN-GaN HFET with a field modulating plate. *Electron Device Letters, IEEE 24(5),* pp. 289-291. 2003.

[39] M. A. Khatibzadeh and R. J. Trew. A large-signal, analytic model for the GaAs MESFET. *Microwave Theory and Techniques, IEEE Transactions on 36(2),* pp. 231-238. 1988.

[40] D. Hou, G. L. Bilbro and R. J. Trew. Analytic model for conduction current in AlGaN/GaN HFETs/HEMTs. *Active and Passive Electronic Components 2012*pp. 11. 2012. Available: http://dx.doi.org/10.1155/2012/806253.

[41] C. Wolfe, J. Holonyak Nick and G. Stillman, *Physical Properties of Semiconductors.* Englewood Cliffs, New Jersey: Prentice Hall, 1989.

[42] M. Levinshtein, J. Kostamovaara and S. Vainshtein, Eds., *Selected Topic in Electronics and Systems: Breakdown Phenomena in Semiconductors and Semiconductor Devices.* World Scientific Publishing Co., 2005.

[43] W. T. Tsang. *Semiconductors and Semimetals, Volume 22 Lightwave Communications Technology, Part D Photodetectors.*1985*(Physics of Avalanche Photodiodes, Federico Capasso).*

[44] F. Bertazzi, M. Moresco and E. Bellotti. Theory of high field carrier transport and impact ionization in wurtzite GaN. part I: A full band monte carlo model. *Journal of Applied Physics 106(6),* pp. 063718-063718-12. 2009.

[45] R. K. Willardson and A. C. Beer, Eds., *Semiconductors and Semimetals, Volume 12, Infrared Detectors II.* New York: Academic Press, Inc., 1977.

[46] S. M. Sze 1936-. *Physics of Semiconductor Devices* 2007[Located in Duke: Perkins/Bostock Library (Call Number: TK7871.85 .S988 2007); Located in NCSU: D.H. Hill Library (Call Number: TK7871.85 .S988 2007)]. Available: http://www2.lib.ncsu.edu/catalog/record/NCSU1945577.

[47] W. Fulop. Calculation of avalanche breakdown voltages of silicon p-n junctions. *Solid-State Electronics 10(1),* pp. 39. 1967. Available: http://www.sciencedirect.com/science/article/pii/0038110167901116.

[48] D. Byeon, M. Han and Y. Choi. Analytical solution of the breakdown voltage for 6H-silicon carbide p[sup +]n junction. *J. Appl. Phys. 79(5),* pp. 2796-2797. 1996. Available: http://dx.doi.org/10.1063/1.361113.

[49] I. H. Oguzman, E. Bellotti, K. F. Brennan, J. Kolnik, R. Wang and P. P. Ruden. Theory of hole initiated impact ionization in bulk zincblende and wurtzite GaN. *J. Appl. Phys. 81(12),* pp. 7827-7834. 1997. Available: http://link.aip.org/link/?JAP/81/7827/1.

[50] Özbek, Ayse Merve, 1983- author. Measurement of impact ionization coefficients in GaN. 2012. Available: http://www2.lib.ncsu.edu/catalog/record/NCSU2641950.

[51] M. Moresco, F. Bertazzi and E. Bellotti. Theory of high field carrier transport and impact ionization in wurtzite GaN. part II: Application to avalanche photodetectors. *J. Appl. Phys. 106(6),* pp. 063719. 2009. Available: http://link.aip.org/link/?JAP/106/063719/1.

[52] B. J. Baliga, *Modern Power Devices.* John Wiley & Sons, 1987.

[53] Y. S. Lee, W. O. Lee, M. K. Han and Y. I. Choi. The analytic models for temperature dependence of the breakdown voltage of 6H- and 4H-SiC rectifiers. Presented at Power Electronics and Motion Control Conference, 2000. Proceedings. IPEMC 2000. the Third International. 2000, .

[54] Hong Yin, Danqiong Hou, G. L. Bilbro and R. J. Trew. Harmonic balance simulation of a new physics based model of the AlGaN/GaN HFET. Presented at Microwave Symposium Digest, 2008 IEEE MTT-S International. 2008, .

[55] N. Dyakonova, A. Dickens, M. S. Shur, R. Gaska and J. W. Yang. Temperature dependence of impact ionization in AlGaN–GaN heterostructure field effect transistors. *Applied Physics Letters 72(20),* pp. 2562-2564. 1998.

[56] G. L. Bilbro, D. Hou, H. Yin and R. J. Trew. Predicting the performance of a power amplifier using large-signal circuit simulations of an AlGaN/GaN HFET model. 2009, Available: http://dx.doi.org/10.1117/12.803348.

[57] H. Yin 1982-. A physics-based large-signal analytical model for AlGaN/GaN HFETs [electronic resource]. 2008. Available: http://www2.lib.ncsu.edu/catalog/record/NCSU2169374.

[58] L. Hsu and W. Walukiewicz. Effect of polarization fields on transport properties in AlGaN/GaN heterostructures. *J. Appl. Phys. 89(3),* pp. 1783-1789. 2001. Available: http://dx.doi.org/10.1063/1.1339858.

[59] R. L. Aggarwal, I. Melngailis, S. Verghese, R. J. Molnar, M. W. Geis and L. J. Mahoney. Temperature dependence of the breakdown voltage for reverse-biased GaN p–n–n+ diodes. *Solid State Commun. 117(9),* pp. 549-553. 2001.

[60] V. A. Dmitriev, K. G. Irvine, C. H. Carter, N. I. Kuznetsov and E. V. Kalinina. Electric breakdown in GaN p-n junctions. *Applied Physics Letters 68(2),* pp. 229-231. 1996.

[61] A. Reklaitis and L. Reggiani. Monte carlo study of hot-carrier transport in bulk wurtzite GaN and modeling of a near-terahertz impact avalanche transit time diode. *J. Appl. Phys. 95(12),* pp. 7925-7935. 2004. Available: http://dx.doi.org/10.1063/1.1702144.

[62] M. Kuball, S. Rajasingam, A. Sarua, M. J. Uren, T. Martin, B. T. Hughes, K. P. Hilton and R. S. Balmer. Measurement of temperature distribution in multifinger AlGaN/GaN heterostructure field-effect transistors using micro-raman spectroscopy. *Appl. Phys. Lett. 82(1),* pp. 124-126. 2003. Available: http://dx.doi.org/10.1063/1.1534935.

[63] A. M. Darwish, A. J. Bayba and H. A. Hung. Thermal resistance calculation of AlGaN-GaN devices. *Microwave Theory and Techniques, IEEE Transactions on 52(11),* pp. 2611-2620. 2004.

APPENDICES

Appendix A TCAD Input Deck For HFET Simulation

```
go atlas

Title HFET

# MESH DEFINITION
mesh width=400
x.mesh loc=0.0  spac=0.05
x.mesh loc=0.8  spac=0.05
x.mesh loc=1.0  spac=0.02
x.mesh loc=1.2  spac=0.01
x.mesh loc=2.0  spac=0.001
x.mesh loc=2.2  spac=0.006
x.mesh loc=2.5  spac=0.05
x.mesh loc=4.0  spac=0.05

y.mesh loc=0.0      spac=0.01
y.mesh loc=0.02     spac=0.005
y.mesh loc=0.0297   spac=0.0001
y.mesh loc=0.04     spac=0.005
y.mesh loc=0.1      spac=0.05
y.mesh loc=0.2      spac=0.05

# REGIONS AND ELECTRODES
region    num=1  material=GaN y.min=0.0297
region    num=2  material=AlGaN y.max=0.0297 x.composition=0.2
elec      num=1  name=source x.min=0.0 x.max=0.0 y.min=0.0 y.max=0.05
elec      num=2  name=gate   x.min=1.2 x.max=2.0 y.min=0.0 y.max=0.0
elec      num=3  name=drain  x.min=4.0 x.max=4.0 y.min=0.0 y.max=0.05
# DEVICE DOPING
doping    uniform region=1 n.type conc=1.e15
doping    uniform region=2 n.type conc=1.e16
doping    uniform x.min=0.0 x.max=0.1 y.min=0.0 y.max=0.05 n.type conc=5.e19
doping    uniform x.min=3.9 x.max=4.0 y.min=0.0 y.max=0.05 n.type conc=5.e19

material material=AlGaN  affinity=3.8 mun=600 mup=10 vsatn=1E6 nc300=2.07e18
material material=GaN  affinity=4.4 permitti=10.1 nc300=1.07e18
mobility material=GaN mun=1050 mup=10 betan=1.5 vsatn=1.4e7
contact name=gate workfun=5.39
#contact name=source con.resistance=.5e-7
#contact name=drain  con.resistance=.5e-7
```

```
interface x.min=0 x.max=4.0 y.min=0.0297 y.max=0.0297 charge=8.4e12 S.S
interface x.min=0 x.max=4.0 y.min=0 y.max=0 charge=-0.9e12 S.X
model material=AlGaN fldmob evsatmod=0 srh print
model material=GaN fldmob evsatmod=0 srh print

#trap e.level=0.59 acceptor density=1.5E16 degen=1 sign=1E-14 sigp=1E-14
#impact region=1 selb E.DIR egran=.4e6 an1=2.9e8 bn1=3.4e7 ap1=2.9e8 bp1=3.4e7
an2=1.9e6 bn2=3.4e7 ap2=1.9e6 bp2=3.4e7

# SOLUTIONS

method newton trap itlim=35  maxtrap=10   carriers=2
solve vgate=0 outf=hfet_vgate0.bin
solve vgate=0.001
solve vgate=0.002
solve vgate=1 outf=hfet_vgate1.bin
solve vgate=-1 outf=hfet_vgate-1.bin
solve vgate=-2 outf=hfet_vgate-2.bin
solve vgate=-3 outf=hfet_vgate-3.bin
solve vgate=-4 outf=hfet_vgate-4.bin

load infile=hfet_vgate0.bin
log outf=hfet_vd_sweep_vgate0.log
solve name=drain vdrain=0
solve name=drain vdrain=0.001
solve name=drain vdrain=0.002
solve name=drain vdrain=0.5 vfinal=5 vstep=0.5
solve name=drain vdrain=6 vfinal=11 vstep=1
solve name=drain vdrain=12 vfinal=50 vstep=2
save outf=hfet_Vg0Vd50.str

load infile=hfet_vgate1.bin
log outf=hfet_vd_sweep_vgate1.log
solve prev
solve name=drain vdrain=0.0001
solve name=drain vdrain=0.002
solve name=drain vdrain=0.5 vfinal=5 vstep=0.5
solve name=drain vdrain=6 vfinal=11 vstep=1
solve name=drain vdrain=12 vfinal=50 vstep=2
save outf=hfet_Vg1Vd50.str

load infile=hfet_vgate-1.bin
log outf=hfet_vd_sweep_vgate-1.log
```

```
solve prev
solve name=drain vdrain=0.0001
solve name=drain vdrain=0.002
solve name=drain vdrain=0.5 vfinal=5 vstep=0.5
solve name=drain vdrain=6 vfinal=11 vstep=1
solve name=drain vdrain=12 vfinal=50 vstep=2
save outf=hfet_Vg-1Vd50.str

load infile=hfet_vgate-2.bin
log outf=hfet_vd_sweep_vgate-2.log
solve prev
solve name=drain vdrain=0.0001
solve name=drain vdrain=0.002
solve name=drain vdrain=0.5 vfinal=5 vstep=0.5
solve name=drain vdrain=6 vfinal=11 vstep=1
solve name=drain vdrain=12 vfinal=50 vstep=2
save outf=hfet_Vg-2Vd50.str

load infile=hfet_vgate-3.bin
log outf=hfet_vd_sweep_vgate-3.log
solve prev
solve name=drain vdrain=0.0001
solve name=drain vdrain=0.002
solve name=drain vdrain=0.5 vfinal=5 vstep=0.5
solve name=drain vdrain=6 vfinal=11 vstep=1
solve name=drain vdrain=12 vfinal=50 vstep=2
save outf=hfet_Vg-3Vd50.str

load infile=hfet_vgate-4.bin
log outf=hfet_vd_sweep_vgate-4.log
solve prev
solve name=drain vdrain=0.0001
solve name=drain vdrain=0.002
solve name=drain vdrain=0.5 vfinal=5 vstep=0.5
solve name=drain vdrain=6 vfinal=11 vstep=1
solve name=drain vdrain=12 vfinal=50 vstep=1
#solve name=drain vdrain=53.1 vfinal=54 vstep=.1
save outf=hfet_Vg-4Vd50.str

output	j.electron j.hole impact j.conduc j.total e.velocity ex.velocity ey.velocity ex.field 
ey.field \
	flowlines e.mobility h.mobility e.temp h.temp con.band val.band qfn j.disp photogen qss 
charge
```

```
tonyplot -overlay hfet_vd_sweep_vgate1.log hfet_vd_sweep_vgate0.log
hfetRFMD_vd_sweep_vgate-1.log hfet_vd_sweep_vgate-2.log \
        hfet_vd_sweep_vgate-3.log hfet_vd_sweep_vgate-4.log meas_vgate1.log
meas_vgate0.log meas_vgate-1.log meas_vgate-2.log \
        meas_vgate-3.log meas_vgate-4.log

quit
```

Appendix B TCAD Input Deck for Ungated Heterostructure

```
go atlas
#
Title new_device
#
# SECTION 1: Mesh input

mesh
x.mesh loc=0.0        spac=0.003
x.mesh loc=0.09       spac=0.007
x.mesh loc=0.11       spac=0.01
x.mesh loc=0.6        spac=0.01
x.mesh loc=0.73       spac=0.007
x.mesh loc=0.85       spac=0.003

y.mesh loc=0.0     spac=0.001
y.mesh loc=0.02    spac=0.001
y.mesh loc=0.0297  spac=0.0005
y.mesh loc=0.04    spac=0.0009
y.mesh loc=0.045      spac=0.001
y.mesh loc=0.05    spac=0.001
#y.mesh loc=0.2     spac=0.02
#y.mesh loc=0.3       spac=0.05
#y.mesh loc=0.4       spac=0.08

# SECTION 2: Structure Specification
#
region    num=1  material=GaN y.min=0.0297 y.max=0.05
region    num=2  material=AlGaN y.min=0 y.max=0.0297 x.composition=0.2
#
elec      num=1  name=source x.min=0.0 x.max=0.0 y.min=0 y.max=0.05
elec      num=2  name=drain  x.min=0.85 x.max=0.85 y.min=0 y.max=0.05

# SECTION 3: Doping Definition
# n-bulk
doping    uniform region=1 n.type conc=1.e15
doping    uniform region=2 n.type conc=1.e16
doping    uniform x.min=0.0 x.max=0.02 y.min=0 y.max=0.05 \
  n.type conc=5.e19
doping    uniform x.min=0.83 x.max=0.85 y.min=0 y.max=0.05 \
  n.type conc=5.e19
```

```
doping     uniform x.min=0 x.max=0.85 y.min=0 y.max=0.001 n.type conc=6e19

interface x.min=0 x.max=5.0 y.min=0 y.max=0 charge=-1.02e13 S.X
interface x.min=0 x.max=5.0 y.min=.0297 y.max=0.0297 charge=1.02e13 S.S
# SECTION 4: Material & Models Definitions
mobility material=GaN vsatn=1.2E7 betan=1.0
mobility material=AlGaN vsatn=1E6
material material=AlGaN affinity=2.6 mun=300 mup=10 nc300=2.07e18
material material=GaN affinity=3.6 mun=1500.0 mup=10 nc300=1.07e18
model fldmob srh print
model material=GaN fldmob srh print
#quantum

contact name=source
contact name=drain current

# SECTION 5: Id-Vd calculation

log outf=Nd_5e19.log master
method newton trap itlim=35  maxtrap=10   carriers=1 elect
solve init
#solve qfactor=0.0
#solve qfactor=0.0000001
#solve qfactor=0.000001
#solve qfactor=0.00001
#solve qfactor=0.0001
#solve qfactor=0.001
#solve qfactor=0.01
#solve qfactor=0.1
#solve qfactor=1
solve idrain=0.00001
solve idrain=0.0001
solve idrain=0.0008
solve idrain=0.00085
solve idrain=0.001
#solve idrain=0.0015
#solve idrain=0.0018
#solve idrain=0.004
#solve idrain=0.005
solve electrode=2 idrain=.001 nstep=25 ifinal=.00151

output  impact j.electron j.hole j.conduc j.total e.velocity ex.velocity ey.velocity ex.field
ey.field \
```

flowlines e.mobility h.mobility e.temp h.temp con.band qfn j.disp photogen qss val.band charge
save outf=Nd_5e19.str

quit

Appendix C TCAD Input Deck for Bulk GaN

```
go atlas
#
Title simple GaN Slab
#
# SECTION 1: Mesh Input
#
mesh
x.m     l=0.0   spac=0.02
x.m     l=0.05   spac=0.01
x.m     l=0.175  spac=0.01
x.m     l=0.45  spac=0.03
x.m     l=1.2   spac=0.03
x.m     l=1.4   spac=0.01
x.m     l=1.55   spac=0.01
x.m     l=1.6   spac=0.02
#
y.m     l=0.0   spac=0.01
y.m     l=1.0   spac=0.01
#
#
# SECTION 2: Regions & Electrodes
#
region    num=1   material=GaN x.min=0.0  x.max=1.6
#
elec     num=1 name=cathode y.min=0 y.max=1 x.min=0.0     x.max=0.0
elec     num=2 name=anode  y.min=0 y.max=1 x.min=1.6  x.max=1.6


contact name=cathode
contact name=anode current

# SECTION 3: Doping Definition
# n-bulk
doping    region=1  uniform conc=5e19 n.type

doping    uniform x.min=0.0 x.max=0.05 y.min=0.0 y.max=1.0 \
  n.type conc=5.e20
doping    uniform x.min=1.55 x.max=1.6 y.min=0.0 y.max=1.0 \
  n.type conc=5.e20

#
# SECTION 4: Material & Models Definitions
```

```
mobility material=GaN betan=1 vsatn=1.2e7
material material=GaN mun=1500.0 affinity=3.3 mup=10 nc300=1.07e18
models fldmob srh print
#
#
# SECTION 5: Id-Vd calculation

method newton carriers=2 trap itlim=35  maxtrap=10
log outf=GaNSlab_Nd_5e19_.962A.log master
solve init
solve ianode=0.00001
solve ianode=0.0001
solve ianode=0.001
solve ianode=0.002
solve ianode=0.003
solve ianode=0.004
solve ianode=0.005
solve ianode=0.006
solve ianode=0.01
solve electrode=2 ianode=.01 nstep=25 ifinal=.962
#solve electrode=2 vanode=0 nstep=50 vfinal=5
#
output     j.electron j.hole j.conduc j.total ex.velocity ey.velocity e.velocity ex.field ey.field \
      flowlines e.mobility h.mobility e.temp h.temp con.band qfn qss charge j.disp \
      photogen impact

save outf=GaNSlab_Nd_5e19_.962A.str


#
quit
```

Appendix D MWO Script

```
' Code Module
Option Explicit

Sub Main
Debug.Clear
        Dim Rth As Double
        Dim T1 As Double
        Dim T2 As Double
        Dim Pdc As Double
        Dim Pd As Double
        Dim An As Double
        Dim i As Double
        Dim j As Double
        Dim Pin As Double
        Dim p As Double
        Dim delT As Double
        Dim P_out() As Double
        Dim PAE_() As Double
        Dim Gain_()As Double
        Dim pstart As Double
        Dim pstop As Double
        Dim pstep As Double
        Dim pskip() As Double
        Dim Tcrit As Double
        Dim g As Graph
        Dim PAE As Measurement
        Dim Pout As Measurement
        Dim Gain As Measurement
        Dim hfet As Element
        Dim PinSwp As Element
        Dim schem As Schematic
        Dim d As DataFile
        Dim errornumber As Long

        Rth=getRthermal()
        Debug.Print "Rth= ";Rth
        'Rth=16
        createDataFiles("Sim_PAE_28")
        createDataFiles("Sim_Pout_28")
        createDataFiles("Sim_Gain_28")
```

```
	Set schem = Project.Schematics("HB_28")
	Set hfet  = schem.Elements("Lib_HFETNCSUD.X1")
	Set PinSwp = schem.Elements("SWPVAR.SWP1")
	Set g = Project.Graphs("LSmatch_28v")
	""initialize some varialbes"""
	i = 0
	j = 0
	delT=10
	T2 = 26.85
	An = -3.18e-29 * T2 + 10.17e-27
	'An = -5.086e-29 * T2 + 1.0687e-26

	Begin Dialog UserDialog 400,203 ' %GRID:10,7,1,1
		OKButton 90,168,90,28
		CancelButton 250,168,90,28
		Text 50,63,110,14,"Power Start:",.Text1,2
		Text 50,98,110,14,"Power Step:",.Text2,2
		Text 50,133,110,14,"Power Stop:",.Text3,2
		TextBox 210,63,120,21,.TextBox1
		TextBox 210,98,120,21,.TextBox2
		TextBox 210,133,120,21,.TextBox3
		Text 40,14,310,21,"Enter power sweep parameters (dBm)",.Text4,2
	End Dialog
	Dim dlg As UserDialog
	dlg.TextBox1 = "-7"
	dlg.TextBox2 = "1"
	dlg.TextBox3 = "17"
	'Dialog dlg

	errornumber = Dialog(dlg)
	If (errornumber = 0) Then
		MsgBox ("Simulation Ended","End Simulation")
		End
	End If
	pstart = CStr(dlg.TextBox1)
	pstep = CStr(dlg.TextBox2)
	pstop = CStr(dlg.TextBox3)
	checkInputs(pstart,pstep,pstop)
	Tcrit = .1			'delta T threshold
	Debug.Print
"_Pin_";vbTab;"_Pout_(mw)";vbTab;vbTab;vbTab;"_PAE_";vbTab;vbTab;vbTab;"_Gain_"

For p = pstart To pstop Step pstep	'loop to sweep Pin
```

```
        i = i + 1                                                        'tracking power value for plotting
        ReDim Preserve P_out(i) As Double 'grow arrays eh iteration to store outputs for
plotting
        ReDim Preserve PAE_(i) As Double '
        ReDim Preserve Gain_(i) As Double '

                Do                           'inner loop to reconcile temperature at each Pin
                        T1=T2
                        PinSwp.Parameters("Values").ValueAsDouble = p   'set the power
level
                        Project.Simulator.Analyze                                'run the simulator
                        Set PAE =
g.Measurements("HB_28.AP_HB:PAE(PORT_1,PORT_2)[1,X]") 'get the simulation results
                        Set Pout = g.Measurements("HB_28.AP_HB:PT(PORT_2)[1,X]")
                        Set Gain =
g.Measurements("HB_28.AP_HB:PGain(PORT_1,PORT_2)[1,X]")
                ''''calculations to determine T and An''''''
                        Pin = Pout.YValue(1,1)/Gain.YValue(1,1)
                        Pdc = (Pout.YValue(1,1)-Pin)/(PAE.YValue(1,1)*.01)
                        Pd = Pdc + (Pout.YValue(1,1) - Pin)
                        If Pd > 10000 Then
                        j = j+1
                        ReDim Preserve pskip(j) As Double
                        pskip(j) = p
                        GoTo nextP
                        End If
                        T2 = 26.85 + Pd*Rth                      'next temp and 'an' based on
results
                        An = -2.245e-29 * T2 + 8.886e-27
                        'An = -5.086e-29 * T2 + 1.0687e-26
                        hfet.Parameters("an").ValueAsDouble = An  ''set new value for 'an'
                        delT = Abs(T2 - T1)
                        'Debug.Print "Pin=";Pin;" Pd=";Pd;" T1=";T1;" T2=";T2;" delT";delT
                Loop Until delT < Tcrit         'loop until temps match
        '''save output values in arrays for plotting
        P_out(i) = 1000*Pout.YValue(1,1)
        PAE_(i) = PAE.YValue(1,1)
        Gain_(i) = Gain.YValue(1,1)
        Debug.Print p; vbTab;  P_out(i);vbTab;  PAE_(i);vbTab;  Gain_(i)
nextP:
Next p
''''''Saving the simulation data for plotting''''''''''''''''
```

```
Set d = Project.DataFiles("Sim_PAE_28")
saveData(d, PAE_(), pstart, pstop, pstep,j, pskip())
Set d = Project.DataFiles("Sim_Gain_28")
saveData(d, Gain_(), pstart, pstop, pstep, j, pskip())
Set d = Project.DataFiles("Sim_Pout_28")
saveData(d, P_out(), pstart, pstop, pstep, j, pskip())
Project.Simulator.Analyze    '''display simulation data
End Sub
Function checkInputs(pstart As Double, pstep As Double, pstop As Double)
        If pstart>pstop Then
        MsgBox ("'Power Stop' must be less than 'Power Start'","Error")
        End
        End If
        If pstep <=0 Then
        MsgBox ("'Power Step' must be greater than zero","Error")
        End
        End If

End Function

Function createDataFiles(filename As String)
        If Project.DataFiles.Exists(filename) Then
        Project.DataFiles.Remove(filename)
        Project.DataFiles.AddNew(filename, mwDFT_TXT)
        Else
        Project.DataFiles.AddNew(filename, mwDFT_TXT)
        End If
        MWOffice.Windows.Item(filename).Close
End Function
Function saveData(d As DataFile, data() As Double, pstart As Double, pstop As Double,
pstep As Double,j As Double,pskip() As Double)
Dim i As Double
Dim c As Double
Dim m As Double
i=0
For c = pstart To pstop Step pstep
        i=i+1
        For m=1 To j
                If c = pskip(m) Then
                GoTo skipPoint
                End If
        Next m
   d.DataAsText= d.DataAsText & c & vbTab & (data(i)) & vbNewLine
```

```
skipPoint:
Next c
End Function
Function getRthermal()As Double
	Dim schem As Schematic
	Dim hfet As Element
	Dim tgan, tsub,lg,Wg,kgan,ksub,s,term1,term2,term3 As Double

	Set schem = Project.Schematics("HB_28")		'access schematic 'DCIV'
	Set hfet = schem.Elements("Lib_HFETNCSUD.X1")		'access
element'Lib_HFETNCSUx_Xx'
	tgan = hfet.Parameters("tgan").ValueAsDouble
	tsub = hfet.Parameters("tsub").ValueAsDouble
	lg   = hfet.Parameters("lg").ValueAsDouble
	Wg   = hfet.Parameters("Wg").ValueAsDouble
	kgan = hfet.Parameters("kgan").ValueAsDouble
	ksub = hfet.Parameters("ksub").ValueAsDouble
	s    = hfet.Parameters("s").ValueAsDouble
	term1=.3183098865*Log(1.273239546*tgan/lg)/(Wg*kgan)
	term2=.3183098865*Log((Sqr(Abs(1.233700548*Wg*ksub/(kgan*tgan)+1))+Sqr(A
bs(1.233700548*Wg*ksub/(kgan*tgan)-1)))*(Sqr(Sqr(Abs(1+(.5)*(Wg^2)/(s^2)-
0.8212785840e-1*(kgan^2)*(tgan^2)/((ksub^2)*(s^2))))+1)-
Sqr(Abs(Sqr(Abs(1+(.5)*(Wg^2)/(s^2)-0.8212785840e-
1*(kgan^2)*(tgan^2)/((ksub^2)*(s^2))))-
1)))/((Sqr(Abs(1.233700548*Wg*ksub/(kgan*tgan)+1))-
Sqr(Abs(1.233700548*Wg*ksub/(kgan*tgan)-1)))*(Sqr(Sqr(Abs(1+(.5)*(Wg^2)/(s^2)-
0.8212785840e-
1*(kgan^2)*(tgan^2)/((ksub^2)*(s^2))))+1)+Sqr(Abs(Sqr(Abs(1+(.5)*(Wg^2)/(s^2)-
0.8212785840e-1*(kgan^2)*(tgan^2)/((ksub^2)*(s^2))))-1)))))/(Wg*ksub)
   term3=(.3183098865/(s*ksub))*Log(Sqr(Abs((Sqr(Abs(.1013211838*Wg^2/tsub^2-
0.6657033469e-
1*kgan^2*tgan^2/(ksub^2*tsub^2)+1))+1)/(Sqr(Abs(.1013211838*Wg^2/tsub^2-
0.6657033469e-1*kgan^2*tgan^2/(ksub^2*tsub^2)+1))-
1)))/Sqr(Abs((Sqr(Abs((.5)*Wg^2/s^2-
.3285114336*kgan^2*tgan^2/(ksub^2*s^2)+1))+1)/(Sqr(Abs((.5)*Wg^2/s^2-
.3285114336*kgan^2*tgan^2/(ksub^2*s^2)+1))-1))))'/(s*ksub)
	getRthermal=term1+term2+term3
End Function
```